University of Algarve
Department of Electrical Engineering and Computer Science
Signal Processing LABoratory

A Time-Frequency approach to Blind Deconvolution in Multipath Underwater Channels

Nelson Martins

University of Algarve, Faro
August 2001

UNIVERSITY OF ALGARVE

FACULTY OF SCIENCE AND TECHNOLOGY

Nelson Martins

Doctor Sérgio Manuel Machado Jesus (Ph.D. in Electronics, Professor in the Department of Electronics and Computer Science from University of Algarve)

Doctor André Quinquis (Ph.D. in Electronics, Professor in the Department of Electronics, Informatics and Automation from ENSIETA)

This work was supported by the research scholarship
PRAXIS XXI (BM/19298/99).

Master of Science Thesis
in Underwater Acoustics

AUGUST 2001

Dissertação realizada sob a orientação do
Professor Doutor Sérgio Manuel Machado de Jesus
Professor Associado da
Área Departamental de Engenharia Electrónica e Computação
Faculdade de Ciências e Tecnologia

Declaro sob compromisso de honra que a presente dissertação
é original (Agosto 2001).

O Mestrando O Orientador

Acknowledgements

I profit this space to thank all the people around me that gave me encouragement to pursue studies on an MSc degree. First, my supervisor Prof. Dr. Sérgio Jesus was fundamental to the development of this work, putting light on the main ideas to be explored and understood. He gave me very important advices in what concerns autonomy and accuracy, in science. Thanks a lot also for having sent me to ENSIETA, Brest, where I found a super-organized team, led by Prof. Dr. André Quinquis, whose accurate directionality and discipline conduced me to a fast understanding of the study subjects, mainly on time-frequency analysis. I would like to have been present in one of the coffee talks between Prof. Dr. André Quinquis, Prof. Dr. Sérgio Jesus and Prof. Dr. Yann Stéphan from the CMO, Brest, where some ideas emerged, that were posteriorly explored in the present work. One of the partners of Prof. Dr. André Quinquis, Prof. Dr. Cédric Gervaise, was always on my side, to discuss many, many ideas, and the work's progress, everyday. Thanks also to all the people at ENSIETA that gave me the opportunity to spend a good time there. Returning to SiPLAB, led by Prof. Dr. Sérgio Jesus, I won't forget the active listening of Prof. Orlando C. Rodríguez, who, by his huge organization philosophy of life, gave me both labour and life advices. Thanks to all the SiPLAB crew, specially to Cristiano Soares, who has been like an older brother, taking part on many discussions about signal processing and programming, and Cristiano Lopes (the second older brother), whose "engineering spirit" helped me in difficult technical questions. I would like to thank my parents, for all the support and belief put on me. Finally, I overappreciate Marta's comprehension, specially in the more difficult moments that pulled me intensively into work.

Abstract

Blind deconvolution is studied in the underwater acoustic channel context, by time-frequency (TF) processing. The acoustic propagation environment is modelled by ray tracing and mathematically described by a multipath propagation channel. Representation of the received signal by means of a signal-dependent TF distribution (radially Gaussian kernel distribution) allowed to visualize the resolved replicas of the emitted signal, while significantly attenuating the inherent interferences of classic quadratic TF distributions. The source signal instantaneous frequency estimation was the starting point for both source and channel estimation. Source signature estimation was performed by either TF inversion, based on the Wigner-Ville distribution of the received signal, or a subspace-based method. The channel estimate was obtained either via a TF formulation of the conventional matched-filter, or via matched-filtering with the previously obtained source estimate. A shallow water realistic scenario is considered, comprising a 135-m depth water column and an acoustic source located at 90-m depth and 5.6-km range from the receiver. For the corresponding noiseless simulated data, the quality of the best estimates was 0.856 for the source signal, and 0.9664 and 0.9996 for the amplitudes and time-delays of the impulse response, respectively. Application of the proposed deconvolution method to real data of the INTIMATE '96 sea trial conduced to source and channel estimates with the quality of 0.530 and 0.843, respectively. TF processing has proved to remove the typical ill-conditioning of single sensor deterministic deconvolution techniques.

Resumo

Neste trabalho, é abordado o problema de desconvolução cega, no contexto do canal acústico submarino, através de processamento no domínio tempo-frequência (TF). O ambiente de propagação acústica é modelado por traçamento de raios e matematicamente descrito por um canal de propagação de múltiplos caminhos. A representação do sinal recebido por uma distribuição TF dependente do sinal (distribuição de núcleo radialmente Gaussiano) permitiu a visualização das réplicas resolvidas do sinal emitido, simultaneamente atenuando de forma significativa as interferências inerentes às distribuições TF quadráticas clássicas. A estimação da frequência instantânea do sinal da fonte foi o ponto de partida para as estimações da fonte e do canal. A estimação do sinal emitido foi feita, quer através de inversão TF baseada na distribuição de Wigner-Ville do sinal recebido, quer através dum método baseado em sub-espaços. A estimativa do canal foi obtida, quer através duma formulação TF do filtro adaptado (*matched-filter*) convencional, quer através de filtragem adaptada com a estimativa da fonte obtida previamente. Um cenário realístico de águas pouco profundas é considerado, compreendendo uma coluna de água com 135 m de profundidade, e uma fonte acústica localizada a 90 m de profundidade e a 5.6 km de distância do receptor. Para os correspondentes dados simulados sem ruído, a qualidade das melhores estimativas foi de 0.856 para o sinal da fonte, e de 0.9664 e 0.9996 para as amplitudes e tempos de atraso da resposta impulsiva, respectivamente. A aplicação do método de desconvolução proposto a dados reais da experiência acuśtica INTIMATE ’96 conduziu a estimativas da fonte e do canal com a qualidade de 0.530 e 0.843, respectivamente. O processamento TF provou poder eliminar o mau condicionamento típico das técnicas de desconvolução determinística com um único sensor.

Contents

Acknowledgements **i**

Abstract **iii**

Resumo **v**

List of Figures **ix**

List of Tables **xiii**

1 Introduction **1**

2 Background in Underwater Acoustics: Data Model **7**

3 Problem Formulation and State-of-the-Art **15**
- 3.1 Objectives 15
- 3.2 State-of-the-Art 16
  - 3.2.1 Source Signature Estimation 17
  - 3.2.2 Channel Estimation 17
  - 3.2.3 Blind Deconvolution 19

4 Time-Frequency Distributions **23**
- 4.1 Stationarity 24
- 4.2 Quadratic Time-Frequency Distributions 25
  - 4.2.1 Wigner-Ville Distribution and Ambiguity Function 27
  - 4.2.2 The Cohen Class 32
- 4.3 Signal-Dependent Time-Frequency Distributions 35
  - 4.3.1 Chirp-Adapted Distribution 36
  - 4.3.2 Radially Gaussian Kernel Distribution 39

5 Problem Solving in Simulated Data **43**
- 5.1 Instantaneous Frequency Estimation 49
- 5.2 Source Signature Estimation 55
  - 5.2.1 Wigner-Ville Inversion 56
  - 5.2.2 The Basis Method 60
- 5.3 Channel Estimation 68
  - 5.3.1 Matched-Filter 68
  - 5.3.2 Time-Frequency Formulation of the Matched-Filter 70
  - 5.3.3 Matched-Filtering with the Source Estimate 74

6 Performance in Noise **77**

7 Experimental Data: the INTIMATE '96 Sea Trial **81**

8 Conclusions and Perspectives **91**

Bibliography **95**

A The Hilbert Transform **105**

B The Analytic Signal **107**

C Auto-Correlation Function of an LFM Signal **109**

List of Figures

1.1 LTI system with input and output signals. 2

2.1 Generic underwater acoustic scenario, modelled as a 3-layer waveguide. 7
2.2 Multi-channel system as a representation of the signals involved in underwater acoustic propagation, where a propagated emitted signal is received by a set of L hydrophones, with additive noise. 9
2.3 Illustration of propagation ray tracing modelling: some synthetic ray trajectories. The left-hand figure shows the sound speed profile considered for the generation of the rays. 10
2.4 Typical shallow water IR modulus. 11

3.1 Channel and source signature estimation problem. 16

4.1 WV of the sum of two LFM sweeps with amplitudes 1 and .5, respectively. 28

5.1 Complete estimation procedure in the TF approach to blind deconvolution of LFM signals. 43
5.2 Channel estimation based on the source estimate referred in Fig. 5.1, for signals with both FM and AM components. 44
5.3 Canonical scenario used in simulations. 44
5.4 Sound speed profile of the propagation scenario in Fig. 5.3. 45
5.5 Reference IR $h(t)$ of the canonical simulated scenario. The dashed line separates unresolved from resolved impulses, explained later. 45
5.6 Time differences between all adjacent time-delays. Data correspond to the synthetic scenario. The dashed line gives an idea of the resolution of the MF. 46
5.7 Source emitted LFM signal –real part of $s(t)$–, of duration 0.0625 s, and sweeping the [300, 800]-Hz IF range, used in simulations. 47
5.8 IF $f_i(t)$ of the LFM source signal considered in the simulation. 47
5.9 WV of the LFM source signal, $WV_s(t, f)$, respecting to synthetic data. 47
5.10 Received signal $r_r(t)$ used in simulations, for an LFM source signal. 48
5.11 IFs of the received signal's components (weighted replicas of the emitted signal), in simulated data. 48
5.12 WV of the received synthetic signal, $WV_r(t, f)$ (a), and contour plot of the corresponding ambiguity function $AF_r(\nu, \tau)$ (b). The diagonal lines in the up-side of (a) indicate each replica's IF direction. 49
5.13 IF estimate obtained by global maximization of $WV_s(t, f)$, with respect to time. The dashed line indicates the true IF. 52
5.14 Chirp-adapted distribution of the received signal, $CA_r(t, f)$. For illustration purposes, the emitted LFM signal true frequency modulation rate α has been used in the calculation of the distribution. The temporal support and IF range of $r(t)$ are marked. 53
5.15 Source IF estimate, obtained via $CA_r(t, f)$'s maximization with respect to time. Time is relative to the first instant of maxima, 0.323 s. 53

5.16 One of the functions that were maximized with respect to t, $CA_r(t, 550)$, to estimate the IF of the synthetic source signal. 54
5.17 RGK signal-dependent distribution of the received synthetic signal, $RGK_r(t, f)$ (a), and contour plot of the corresponding optimal kernel $\Phi_{opt}(\nu, \tau)$ (b). 54
5.18 Source IF estimate, obtained via $RGK_r(t, f)$'s maximization with respect to time. Time is relative to the first instant of maxima, 0.322 s. 55
5.19 Reference source estimate, obtained by WV inversion of $M(t, f)WV_s(t, f)$. 57
5.20 Model function $\tilde{WV}_s(t, f)$ considered for first arrivals-based source estimation. 58
5.21 First group of arrivals-based source estimate –real part of $\hat{s}_{WI,f}(t)$–, by WV inversion. 58
5.22 WV of the first arrivals-based estimated source signal $\hat{s}_1(t)$, by WV inversion. 59
5.23 Source estimate quality as a function of τ_s in $M(t - \tau_s, f)$. The estimate was obtained via WV inversion, in simulated data. Red lines indicate the instants of the arrivals. 59
5.24 Scheme illustrating bilinear signal synthesis of $\hat{s}_{BM}(t)$, departing from $r(t)$. 60
5.25 Source estimate –real part of $\hat{s}_{BM}(t)$–, in synthetic data. This estimate was obtained via the basis method, taking as input the model function in Fig. 5.20. 67
5.26 WV of $\hat{s}_{BM}(t)$. 67
5.27 Evolution of the correlation coefficient between the real parts of $s(t)$ and $\hat{s}_{BM}(t)$, as a function of φ, in simulated data. The dashed line indicates the correlation between $s(t)$ and $\hat{s}_{BM}(t)$. 68
5.28 Channel estimate obtained by classic matched-filtering: normalized envelope of the cross-correlation function between emitted and received signals (the well-known *arrival pattern*). Data correspond to the simulated scenario. 70
5.29 Comparison of the LFM auto-correlation envelope (blue line), with the function obtained via coherent integration on the WV of the LFM, for the simulated data. Here, $\alpha = 8000$ Hz/s and T=0.0625 s. 72
5.30 Comparison of the LFM auto-correlation envelope (blue line), with the function obtained via coherent integration on the WV of the LFM, for the case α=320 Hz/s and T=0.0625 s. 72
5.31 Channel estimate, obtained by coherent integration of $WV_r(t, f)$, in synthetic data. 73
5.32 Simulation channel IR estimate obtained by $RGK_r(t, f)$'s coherent integration. 73
5.33 Channel estimate obtained by matched-filtering of $r(t)$ with the estimate $\hat{s}_{BM}(t)$. 75

6.1 Average $RGK_r(t, f)$ (β=1), for SNR=-5 dB and 100 trials. 79
6.2 IF estimate, in -5 dB noisy data, for 100 trials. The dashed line represents the true IF. 79
6.3 Source estimate, obtained via the basis method, with SNR=-5dB, for 100 trials. 79
6.4 Channel estimate, obtained by $\overline{WV}_r(t, f)$ integration, with SNR=-5dB, for 100 trials. 79
6.5 Source estimation performance in noise. 80
6.6 Channel estimation performance in noise. 80

7.1 INTIMATE '96 real data environment scenario considered in this chapter. 82
7.2 Electro-acoustic transducer amplitude spectrum (a) and IR (b), in the INTIMATE '96 sea trial. 82
7.3 Model of the true source signal –real part of $s(t)$– in the INTIMATE '96 sea trial. 83
7.4 IA $a_i(t)$ of the source signal model, in the INTIMATE '96 sea trial. 83
7.5 IF of $s(t)$, in the INTIMATE '96 sea trial. 83
7.6 One of the received snapshots, at 5.5-km range, on the 115-m depth hydrophone, in the INTIMATE '96 sea trial. 84
7.7 Portion of the average distribution $\overline{RGK}_r(t, f)$, in the INTIMATE '96 sea trial. 84
7.8 IF estimate $\hat{f}_i(t)$ of the source signal, obtained by maximization of $\overline{RGK}_r(t, f)$, in the INTIMATE '96 sea trial. 85
7.9 WV of $s(t)$. 85

7.10 Reference source estimate, obtained by application of the basis method, in the INTIMATE '96 sea trial. 85
7.11 Portion of the average distribution $\overline{WV}_r(t,f)$, in the INTIMATE '96 sea trial. . . 86
7.12 Source estimate –real part of $\hat{s}_{BM}(t)$–, in the INTIMATE '96 sea trial, with $\varphi = 0$. 86
7.13 Normalized correlation coefficient between the real parts of $s(t)$ and $\hat{s}_{BM}(t)$, for different values of φ. 87
7.14 WV of $\hat{s}_{BM}(t)$, in the INTIMATE '96 sea trial. 87
7.15 Instantaneous frequency of $\hat{s}_{BM}(t)$, in the INTIMATE '96 sea trial. 87
7.16 IA of $\hat{s}_{BM}(t)$, in the INTIMATE '96 sea trial. This is to be compared with the true IA $a_i(t)$ in Fig. 7.4. 87
7.17 Reference channel estimate, defined as the average output of the MF, in the INTIMATE '96 sea trial. 88
7.18 Channel estimate $\hat{h}_{IF}(t)$ in the INTIMATE '96 sea trial, by $\overline{WV}_r(t,f)$ coherent integration, assuming the knowledge of the IF of $s(t)$. 88
7.19 Channel estimate in the INTIMATE '96 sea trial, by $\overline{WV}_r(t,f)$ coherent integration, departing from $\hat{f}_i(t)$. 89
7.20 Average channel estimate obtained by cross-correlation between $\hat{s}_{BM}(t)$ and $r(t)$, in the INTIMATE '96 sea trial. 89

List of Tables

4.1 Some examples of TFDs. 25
4.2 Some desirable mathematical properties of the WV. 29

5.1 Amplitude estimators comparison in noiseless simulated data. The amplitudes respect to the resolved last 37 Dirac functions of the IR. 75
5.2 Time-delay estimators comparison in noiseless simulated data. The time-delays respect to the resolved last 37 Dirac functions of the IR. 76

Chapter 1

Introduction

Two fundamental problems arising in many signal processing applications are channel and source signature estimation. Both problems are often referred in the literature as deconvolution. The need for deconvolution arises in a number of important practical areas such as data transmission, reverberation cancellation, seismic signal processing, image restoration, etc. High-speed data transmission over a communication channel (*e.g.*, telephone channel) relies on the use of adaptive equalization. In its traditional form, adaptive equalization requires the transmission of a training sequence, the exact form of which is known at the receiver. In seismic deconvolution, the usual procedure is to assume a layered Earth model, and the requirement is to use the received signal to estimate the sequence of reflection coefficients corresponding to the various layers of the model. The received signal is itself made up of echoes produced at the different layers of the model in response to the excitation which has ordinarily the form of a short-duration pulse. In this case, the deconvolution problem is complicated by the fact that the exact waveform of the excitation responsible for the generation of the received signal is usually unknown. A similar problem arises in image restoration. In this application, blurring effects caused by photographic or electronic imperfections are represented by an unknown system. An original image or scene of interest constitutes the system input. The system output is a blurred version of the original image.

Given the blurred image, the requirement is to restore the original image.

Consider Fig. 1.1, which depicts a linear time-invariant (LTI) system (or channel, in communications' terminology) with input and output signals. The output signal $r(t)$, which in many cases is some *received signal*, is defined as the convolution of the input signal $s(t)$ and the *impulse response* (IR) $h(t)$ of the system, where it is assumed that the system is causal and its output is accessible. *Deconvolution* refers to the problem of determining the IR of the system and/or the input signal[24]. Deconvolution may assume two forms, depending on the complexity of the problem. In the first form, either the system is unknown, but its input is accessible (this is the problem of system identification), or a reliable model of the system is available, and the requirement is to estimate the unknown input signal –since convolution is commutative, these two deconvolution problems are mathematically equivalent, within the single-channel framework. In the second form, the system is unknown and its input is inaccessible; in this latter situation, deconvolution is referred to as *blind deconvolution*. Although the term *deconvolution* is used indifferently in the literature to refer to either channel or input signal estimation, these two problems will be named herein by *channel estimation* and *source signature estimation*, respectively, when dealing with underwater acoustic signals. It is well known that the first form of deconvolution is an ill-posed problem, *i.e.*, its solution is non unique and the inversion is unstable with respect to numerical errors and/or noise. For example, when the requirement is to estimate the input signal, difficulties are related to the filtering characteristics of the IR, which can suppress some frequency components of

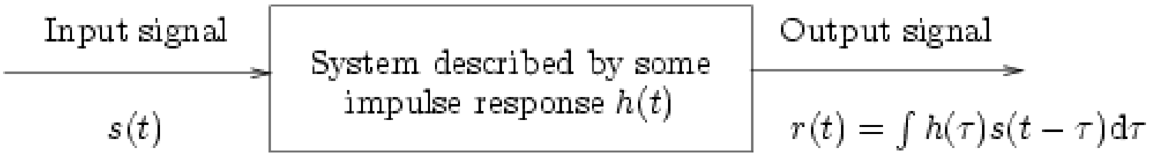
Input signal
$s(t)$
System described by some impulse response $h(t)$
Output signal
$r(t) = \int h(\tau)s(t-\tau)d\tau$

Figure 1.1: LTI system with input and output signals.

the input signal spectrum, thus allowing for a multitude of possible values for the unknown spectrum in the corresponding null or almost null frequency components of the IR. The introduction of *a priori* information, for example through the use of a smoothness constraint or enforcement of positive definiteness when appropriate, can stabilize the inversion, though there is no general rule for choosing a suitable regularization parameter[42]. Moreover, when the input signal is non-stationary (a very common case), and in the presence of noise, there is usually a need for obtaining a reasonable number of random output signal statistical realizations (snapshots), to estimate second-order statistical quantities of the input signal, noise and the received signal[46]. Ideally, one would like to estimate the source signal when only one snapshot of the received signal random process is available, whatever the stationary character of the emitted or received signals. However, even within a theoretical framework, it is expected that such an estimate is biased or suffers from a large variance. In blind deconvolution, usually statistical information about the system transfer function or input is available[24]. Basically, blind deconvolution involves the use of a nonlinear adaptive filtering algorithm, designed to extract higher-order statistical information from the received signal.

The large variety of contexts where deconvolution finds application includes ocean acoustics, where a fundamental problem is the passive characterization of acoustic transients in/and the ocean environment. For example, *classification* is a promising area, where the objective is the determination of the nature of the transient sound source. Another increasing interest consists of determining the physical properties of the propagation medium, mainly water temperature and currents of oceanographic interest.

This work aims to give an approach to solve the problem of blind deconvolution in underwater acoustics, *i.e.*, obtain at once estimates of the emitted signal and the medium IR representative of its physical properties. The received signal will be modelled as a weighted sum of time-delayed replicas of the emitted signal. The non-stationarity of the source signal gave the motivation to explore time-frequency representations' capabilities, to solve the problem. In fact, their 2 degrees of freedom (associated to simultaneous time and frequency information) allowed to treat both the input signal and the IR as an unknown, with assumptions about their structure. Analysis of the received signal allowed to identify a time-frequency representation of one or some replicas of the emitted signal. Inversion of this time-frequency representation to the time domain gave the source signature estimate. An equivalent formulation of the matched-filter in the time-frequency domain allowed the estimation of the channel IR, for signals with no amplitude modulation component. For a more general class of signals, the source signal estimate was incorporated in channel estimation.

In terms of applications, the IR (which synthesizes the physical parameters of interest) estimate obtained by the proposed blind deconvolution time-frequency approach could then be matched to a family of candidate IRs to posteriorly recover the physical parameters, constituting an inversion process which could find some application in ocean acoustic tomography. The treatment of the source position as an unknown parameter could be used in source localization, following the method proposed in [56].

This report is structured as follows. Next chapter justifies and presents the data model. The mathematical problem formulation, followed by an overview of the state-of-the-art, is presented in Chap. 3. Chap. 4 reviews the fundamental concepts of time-frequency distributions. An illustrative example of the problem solution, for a linear frequency modulation source, is given in Chap. 5. Deconvolution robustness to noise is shown in Chap. 6. Application of the deconvolution approach to data from the INTIMATE '96 sea trial is mentioned in Chap. 7, followed by the conclusions and perspectives, in Chap. 8.

Chapter 2

Background in Underwater Acoustics: Data Model

To get into the problem at hand, let's consider an underwater scenario, in which a source is positioned at range 0 and depth z_0, and a vertical array of L acoustic sensors (hydrophones) is positioned at range r_0 and depths z_l, $l = 1, ..., L$ –Fig. 2.1. In a practical scenario, it is assumed that the array is one of the components of a complex receiving system. At some instant τ_0, the source starts to emit an acoustic signal propagating in the media defined

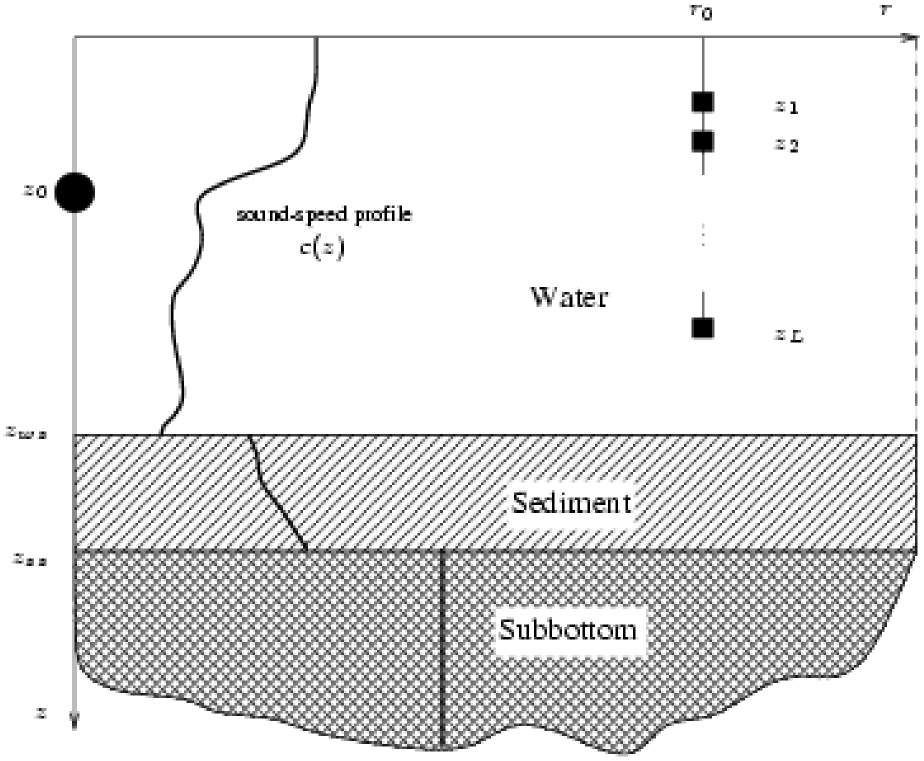
r_0
r
z_1
z_2
z_0
sound-speed profile
$c(z)$
Water
z_L
z_{wb}
Sediment
z_{sb}
Subbottom
z

Figure 2.1: Generic underwater acoustic scenario, modelled as a 3-layer waveguide.

by the ocean with its physical limits. Upon emission by the source, an acoustic field is created, which is partially received by the hydrophone array, after propagation. For each spatial location in the water column, the created field is dependent on the source signal and the medium characteristics. The field can be represented by the acoustic pressure $p \equiv p(r_0, z_0, r, z, t-\tau_0)$, where (r_0, z_0) and (r, z) denote the source position (usually, $r_0 = 0$) and arbitrary spatial location (cylindrical) coordinates, respectively. In this context, the acoustic pressure depends on three independent variables (range r, depth z and time t), and satisfies the wave equation below, describing propagation of an unit impulse source to an arbitrary location in the waveguide:

$$\nabla^2 p - \frac{1}{c^2(z)}\frac{\partial^2}{\partial t^2}p - \frac{1}{\rho(z)}\nabla\rho(z)\cdot\nabla p \quad = \quad -\delta\left(r-r_0\right)\delta\left(z-z_0\right)\delta(t-\tau_0), \tag{2.1}$$

subject to appropriate boundary and initial conditions[65, 46, 36]. In (2.1), $c(z)$ and $\rho(z)$ designate the depth-dependent sound-speed profile and density, respectively. For the space and time scales considered in this work, these quantities are modelled as time-invariant, and the emitter can be approximated by a spatially stationary point source, *i.e.*, the source is assumed to not move until end of emission. Also, the emitted signal is assumed to have small amplitude, and the ocean is modelled as a stratified medium –Fig. 2.1. Physically speaking, and if the emitted signal is well approximated by a pulse, this one is subject to a distortion which is principally the combined effect of multipath, absorption, frequency dispersion and scattering. All these effects emerge mainly as a consequence of the boundary conditions (water surface, water-sediment interface, geologic strata) and the variations in sound-speed throughout depth.

Prediction of the acoustic field due to a source in the ocean, is not a trivial problem, taking into account the wave equation (2.1). However, a good approximation to the problem

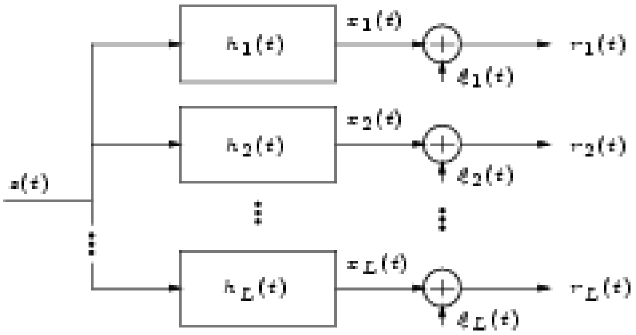

Figure 2.2: Multi-channel system as a representation of the signals involved in underwater acoustic propagation, where a propagated emitted signal is received by a set of L hydrophones, with additive noise.

solution can be obtained, by considering the linear part of the acoustic field[65]. This allows to regard the ocean as a filter, with a given IR $h(t)$. The modelled invariance of the physical parameters and boundary conditions, together with the model $h(t)$, lead naturally to the representation of the propagation scenario as an LTI multi-channel system, from a signal processing point of view –Fig. 2.2. Following this model, the emitted signal $s(t)$ is convolved with L LTI single-channel systems $h_l(t)$, giving rise to L received signals $r_l(t)$ with additive noise $\xi_l(t),\ l = 1,\ ...,\ L$.

There are different types of models (computer solutions to the wave equation) to describe sound propagation in the sea[36], from which, ray tracing will be adopted in this work. The ray tracing model originally emerged from optics, where it was used to understand the propagation of light. In the underwater acoustics context, the model considers that sound propagates through privileged trajectories (rays) which are perpendicular to level curves or wavefronts –Fig. 2.3. Ray tracing considers that an infinitude of rays depart from the source, each associated with a specified angle, the *launching angle*. The trajectories of the rays are governed by Snell's law:

$$\frac{\cos\left[\theta(z)\right]}{c(z)} = \text{constant}, \tag{2.2}$$

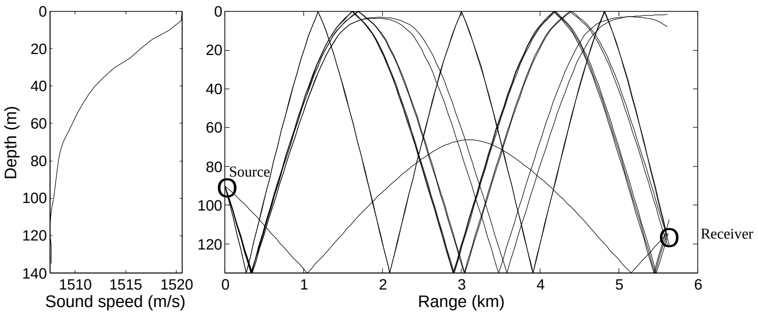

(Perfectly rigid bottom)

Figure 2.3: Illustration of propagation ray tracing modelling: some synthetic ray trajectories. The left-hand figure shows the sound speed profile considered for the generation of the rays.

where $\theta(z)$ represents the angle between the trajectory's tangent and the horizontal, at depth z[36]. For each pair of points in the waveguide that are connected by a certain number of rays, these rays are called the *eigenrays* for that points. Eigenrays take a special meaning when the two points are the locations of the source and an hydrophone, respectively. Sound-speed variations with depth give rise to refraction of acoustic rays, which drives the energy through the sound channel axis (depth of minimum sound-speed). Let's consider a point s_r (in ray coordinates[36]) that is the location of an hydrophone. For this point, each eigenray (departing from the source) will be characterized by an *arrival time*, written as

$$\tau(s_r) \quad = \quad \tau_0 + \int_0^{s_r} \frac{\mathrm{d}{s_r}'}{c({s_r}')}, \tag{2.3}$$

where τ_0 is the emission instant, $c(s'_r)$ is the sound speed at the ray coordinate s'_r, and the last term is the *travel-time*, defined by an integral along the eigenray path. The other important parameter (in this work) that characterizes each eigenray is the *amplitude*, determined by the conservation of energy flux through the variable cross section of ray tubes (tubes formed by pairs of adjacent rays)[65]. The received signal in each hydrophone is described as the sum of each of the eigenrays' pressure contributions, or *arrivals*. As each eigenray contains the information of the emitted signal, it is acceptable to model the received signal as a sum of various weighted and delayed source signal replicas. Correspondingly, the medium can be represented by a series of weighted impulses –Fig. 2.4. Hence, the main information given

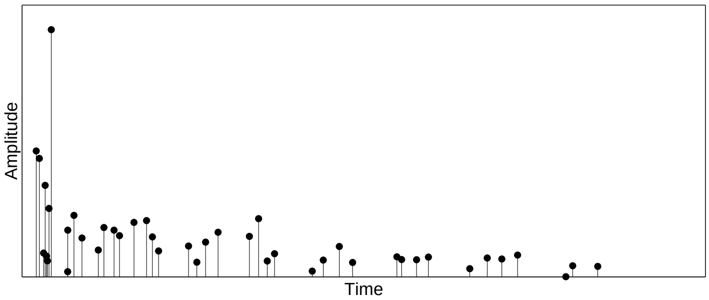

Figure 2.4: Typical shallow water IR modulus.

by the ray tracing model concerns travel-times, amplitudes and directions of the wavefronts. The model is derived under the assumption that the wavelengths are much less than the water depth and much less than the distance between the source and the receiver[1] (however, at high frequencies, a detailed environmental knowledge is necessary for accurate predictions). Another condition of validity is that the change of sound-speed is negligible over several wavelengths, once sound is partially reflected at sharp changes of the sound-speed. Hence, in an environment defined by some sound-speed profile, it is possible to determine the propagation characteristics (number of paths, amplitudes, travel-times, etc.) by ray tracing models. All the above considerations imply that, when a sound pulse travels through the ocean, specially in shallow water, it reflects back and forth between the sea surface and the ocean bottom. Typically, in shallow water, for different source and receiver depths, the first arrivals are very close in time, while late arrivals are more separated and “clustered” in quadruplets[60], as shown in Fig. 2.4. From ray-tracing predictions, it can be shown that most of the initial arrivals correspond to refracted and bottom reflected eigenrays, while the quadruplets correspond to surface and bottom reflected eigenrays.

The connection between ray tracing and this work consists in modelling the IR as a multiple time-delay attenuation channel, where the time-delays and attenuations are respectively the eigenrays' travel-times and amplitudes.

---

[1] For the cases considered in this work, the ratios between the water depth and maximum wavelength, and between source-receiver distance and maximum wavelength, are of orders 10 and 10^3, respectively.

Ocean Acoustic Tomography

The knowledge of the underwater medium, while acoustic wave propagation medium, is fundamental. In fact, it interests oceanographers, for the physical study of the ocean, since sound-speed, in water, is dependent on some intrinsic parameters like the temperature, salinity, pressure and density; it concerns the geophysicists who analyze the geologic structure of the underwater bottom, for seismic sounds (where the petroleum prospection is an important application); it is primordial to sailor-men, for detection systems (sonars) and underwater communication. There has been increasing interest in developing techniques to obtain such a knowledge of the underwater medium, what conduces naturally to a brief explanation of the tomography concept. Issued essentially from seismology and medicine, tomography always involves some kind of medium mapping, with a measured quantity as input, which is directly related to physical propagation through the mapped medium[49]. Examples of tomography are the Earth's interior mapping by the use of travel-times, or the body mapping, by means of X-ray propagation. Tomography is an inverse problem, since it demands indirect estimation of certain properties.

In 1979, Munk and Wunsch extended the classical tomography concept to ocean mapping, proposing what is called ocean acoustic tomography[48]. Ocean acoustic tomography takes advantage of two relevant facts: first, travel-time and other measurable acoustic parameters, like the direction of incoming rays, or the phase of narrowband signals, are functions of temperature, sound-speed and other parameters of oceanographic interest, and can be interpreted to provide information about the ocean, using inverse methods; second, the ocean is nearly transparent to low-frequency sound, so that signals can be transmitted over distances of many thousands of kilometers. Ocean tomography is usually classified in active or passive, respectively when the source signal is known, or when that knowledge is not available.

Let us restrict to travel-time-based tomography[60]. In the active form, the emitted signal consists typically of a pulse, whose emission can be repeated (in the case of a controlled source), giving rise to a set of snapshots in the received signal. The emitted signal has generally a large bandwidth, to allow for the resolution of individual arrivals. Thus, it is possible to estimate the IR, and comparison of this estimate with candidate synthetic IRs constitutes an effective tomographic measure. In passive tomography, if the emitted signal is a time-stationary long-duration signal, the received signal can be divided into several snapshots, allowing the estimation of statistical properties of both emitted and received signals. Otherwise, if the emitted signal is non-stationary, it is erroneous to resort to an ergodic hypothesis to obtain statistically reliable temporal averages on the received snapshots. It is thus likely advantageous to treat the problem by means of signal representations that take non-stationary properties into account.

Data Model

Following the ray tracing model described in pp. 9 and ff., the medium between the source and each hydrophone is considered to behave as a multiple time-delay attenuation channel, and all the IRs $h_l(t),\ l = 1,\ \dots,\ L$ in Fig. 2.2 can be represented by the system:

$$\left\{\begin{array}{lcl} h_1(t) & = & \sum_{m=1}^{M_1} a_{1m}\delta\left(t-\tau_{1m}\right) \\ h_2(t) & = & \sum_{m=1}^{M_2} a_{2m}\delta\left(t-\tau_{2m}\right) \\ & \vdots & \\ h_L(t) & = & \sum_{m=1}^{M_L} a_{Lm}\delta\left(t-\tau_{Lm}\right) \end{array}\right. , \tag{2.4}$$

where $\{a_{lm},\ \tau_{lm};\ l = 1,\ \dots,\ L;\ m = 1,\ \dots,\ M\}$ are respectively the attenuations and time-delays, along the M_l acoustic paths[37]. The attenuations a_{lm} designate the modulus of the true amplitudes (whose sign indicates the polarity of the arrivals). This simplification is justified because only the modulus is considered for many practical purposes[45]. The IRs $h_l(t)$ can be grouped into the vector

$$\mathbf{h}(t) \;=\; \left[h_1(t),\ h_2(t),\ ...,\ h_L(t)\right]^T. \tag{2.5}$$

For a single hydrophone, $L = 1$ and (2.4) turns into the single-channel model (with obviously dropped indices)

$$h(t) \;=\; \sum_{m=1}^{M} a_m \delta\left(t - \tau_m\right). \tag{2.6}$$

The amplitudes and time-delays of $h(t)$ can be grouped into 2 vectors, respectively:

$$\mathbf{a} = [a_1, a_2, ..., a_M]^T; \quad \boldsymbol{\tau} = [\tau_1, \tau_2, ..., \tau_M]^T. \tag{2.7}$$

In the presence of additive noise, (2.6) implies that the received signal is a linear combination of the source $s(t)$, plus the noise $\xi(t)$:

$$\begin{aligned} r(t) &= \sum_{m=1}^{M} a_m s(t - \tau_m) + \xi(t) \\ &= x(t) + \xi(t). \end{aligned} \tag{2.8}$$

The noise is assumed temporally white, zero-mean and uncorrelated with the signal. Wherever appropriate, discrete or continuous time n or t, respectively, will be used. For simplicity, some physical units will be omitted.

Chapter 3

Problem Formulation and State-of-the-Art

3.1 Objectives

This work concerns the blind deconvolution problem, where the system and input signal in Fig. 1.1 are here respectively representations of the acoustic propagation channel and source emitted waveform. The system is considered LTI during the period comprising emission and propagation. The emitted signal is a deterministic non-stationary signal, and the noise is a white (stationary) random process.

Briefly, the received signal on one hydrophone, consisting of one data snapshot, will be processed, in order to give the emitted signal estimate $\hat{s}(t)$ and the IR estimate $\hat{h}(t)$, as illustrated by the scheme in Fig. 3.1. Two hypothesis will be presented to accomplish blind deconvolution: the first, represented by the first branch in Fig. 3.1, will be used when the emitted signal consists of an LFM sweep; the second (second branch in Fig. 3.1) respects to a more general class of signals. In the former approach, a source estimator will produce $\hat{s}(t)$, and the first type of channel estimator will produce the channel estimate $\hat{h}_1(t)$. For the more general class of emitted signals, the channel estimate $\hat{h}_2(t)$ will be conditioned on $\hat{s}(t)$, by the use of a second type of channel estimator.

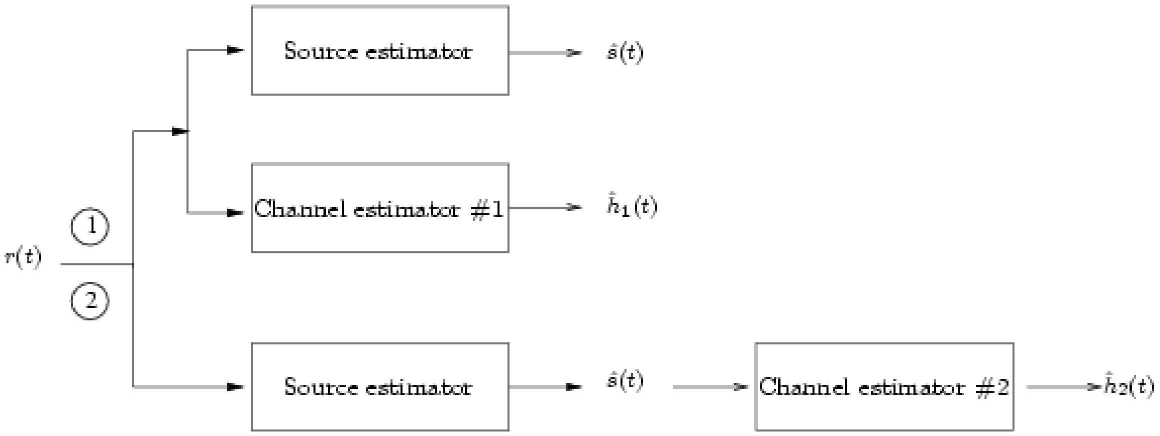

Figure 3.1: Channel and source signature estimation problem.

In a complete formulation of the channel estimation problem, the 3 deterministic parameters M, $\mathbf{a}$ and $\boldsymbol{\tau}$ are to be estimated, since they are necessary and sufficient to describe the channel IR $h(t)$. The estimates of the above true parameters are represented by $\hat{M}$, $\hat{\mathbf{a}}$ and $\hat{\boldsymbol{\tau}}$, respectively. The combined effect of the temporal proximity between the IR's adjacent Dirac functions (mainly the first) and the emitted signal band will determine the discrimination ability of the channel estimators. Hence, in general, the estimated number of (observed) arrivals $\hat{M}$ will be less than M, corresponding to the reduced dimension estimates

$$\hat{\mathbf{a}}_{red} = [\hat{a}_J,\ \hat{a}_{J+1},\ ...,\ \hat{a}_M]^T;\quad \hat{\boldsymbol{\tau}}_{red} = [\hat{\tau}_J,\ \hat{\tau}_{J+1},\ ...,\ \hat{\tau}_M]^T,\quad 1 \le J \le M \tag{3.1}$$

of the (reduced) true quantities

$$\mathbf{a}_{red} = [a_J,\ a_{J+1},\ ...,\ a_M]^T;\quad \boldsymbol{\tau}_{red} = [\tau_J,\ \tau_{J+1},\ ...,\ \tau_M]^T,\quad 1 \le J \le M. \tag{3.2}$$

Also, as the receiving system has no knowledge about the transmission instant τ_0, the estimate $\hat{\boldsymbol{\tau}}_{red}$ will be relative to the minimum time-delay estimate $\hat{\tau}_J$.

3.2 State-of-the-Art

Various methods have been proposed regarding the subject of deconvolution, in view of its large application. Here, the state-of-the-art will be divided in the topics of source signature estimation, channel estimation and finally the more difficult and interesting problem of blind deconvolution, describing applications in underwater acoustics as well as other research areas.

3.2.1 Source Signature Estimation

In terms of source signature estimation, which falls into the first form of deconvolution mentioned in the Introduction, many works have been done [7, 8, 18, 46, 62, 64]. The LTI Wiener deconvolution filter is a classical example of Fourier-domain regularized deconvolution[33]. It provides the minimum mean-squared-error-optimal regularized LTI solution to the deconvolution problem. A hybrid approach to deconvolution for image restoration in ill-conditioned systems, has comprised Fourier-domain (Wiener-like) system inversion followed by wavelet-domain noise suppression[51].

In underwater acoustics, the ill-poseness of the single-sensor deconvolution problem led to the use of multiple sensors corresponding to different propagation channels, whose combined information about the source signature limits the solution space of the ill-posed problem. This is referred to as multi-channel deconvolution, and has been solved by *maximum a posteriori* estimation, in [46]. In the multi-channel framework, another approach was presented, in which source estimation was solved by simulated annealing[64]. However, this method requires a significant computational cost, and careful must be taken in the choice of some user-defined parameters, like the initial temperature.

3.2.2 Channel Estimation

In terms of channel estimation, when the source signal is known, emphasis is given in the literature, to multiple time-delay attenuation channels, due to their abundance in the fields of, *e.g.*, sonar, radar and geophysics[1, 9, 17, 30, 41].

A classical method for channel estimation, known as matched-filtering, is by correlating the received waveform with the transmitted signal[9]. The peaks in the correlator output give the estimates of the amplitudes and time-delays. It can be shown that if the true time-delays differ by more than the duration of the signal autocorrelation function, and in the presence of white Gaussian noise, the correlator is equivalent to the maximum likelihood estimator[17]. Usually, the core of multiple time-delay attenuation channel estimation remains at estimating the time-delays, since their estimates do not depend on the amplitudes, whereas they depend on the source signal. These estimates are then used for amplitude estimation. A frequency-domain approach was proposed by Kirsteins[41]. Since a delay in the time domain is equivalent to multiplication by an exponential in the frequency domain, the corresponding frequency domain problem is one of fitting weighted complex exponentials to the spectrum of the received signal. Utilizing an iterative method, this approach provides a way of estimating the time-delays. However, the algorithm does not work if the spectrum of the source signal has small sample values or zeros in the regions of its support, causing serious numerical ill-conditioning of the algorithm, or even impossibility of application. More importantly, the delay estimates obtained via this method are biased and do not correspond to the true parameter estimates. In addition, contiguous frequency samples have to be considered, which might not be desirable, since it is difficult to obtain a good signal-to-noise-ratio at every frequency sample, in practice. Vaccaro *et al.* developed another frequency domain algorithm that finds least-squares-based unbiased estimates of the time-delays[68]. In [1], time-delay estimation is done by adaptive filtering, for a linear time-varying channel driven by white noise.

3.2.3 Blind Deconvolution

In terms of the non-linear problem of blind deconvolution, use of higher-order statistics and random search methods have been made in many situations, as stated below. Use of higher-order statistics is motivated by the fact that convolution increases the similarity between the probability density function of the output of a linear system, and a Gaussian function, with respect to the one of the input[70]. This amounts to a decrease in kurtosis. Deconvolution intends to reverse this effect by producing a filter that drives the output of the system towards higher kurtosis. This procedure can also be viewed as moving the output towards lower entropy. In [50], some algorithms based on third-order cumulants have been studied for the identification of (minimum or nonminimum phase) FIR systems, from only the noisy output, which has been contaminated by additive zero-mean white (Gaussian) noise of unknown variance. In communication systems involving the use of modulation for information transmission, the received signal exhibits interesting cyclostationary properties. Gardner has proposed a novel scheme for channel identification based on the second-order cyclic autocorrelation function[22]. Gardner's scheme involves the use of a training period during which the unobserved channel input is transmitted at a slow rate. This mode of transmission has the beneficial effect of making the inter-symbol interference negligible, and therefore offers the potential of an almost distortionless data transmission for training. Tong, Xu and Kailath[66], and Ding and Li[16] have proposed extensions of Gardner's scheme for channel identification. The approach taken in the latter two papers is different from Gardner's original approach in that it shows that, for certain channel models, channel identification is attainable without the need for a pilot tone or training period. A common feature of blind deconvolution algorithms is the presence of local minima. This problem may be overcome through the use of simulated annealing. In [31], such a technique is incorporated into a higher-order cumulant-based procedure for the blind identification/equalization of a linear moving average channel model. Unfortunately, the computational burden imposed by the use of simulated annealing is too heavy. Blind deconvolution may be viewed as a self-organized learning process, self-organized in the sense that the deconvolution is performed in the absence of a supervisor (*i.e.*, training sequence). In this context, much can be gained from neural networks, in particular, that part of the subject that deals with self-organization, as shown in [23]. In [24], four classes of blind deconvolution/equalization procedures are described, that differ from each other in the way in which the nonlinear adaptive filtering is performed. The first class of blind deconvolution algorithms is the class of Bussgang algorithms. They are so called because the statistics of the deconvolved signal are approximately Bussgang. This class of blind deconvolution algorithms includes the famous Sato algorithm and the Godard algorithm as special cases. The structure used for Bussgang algorithms consists of a linear combiner with adjustable coefficients, followed by some form of a zero-memory nonlinear device. Such a structure represents a natural extension of conventional linear adaptive filters. The second class of blind deconvolution/equalization algorithms is based on the idea that, in order to solve the problem, it is sufficient to equalize the variance and any other nonzero higher-order statistic (cumulant) of a sample in the received signal to that of a sample in the unobserved signal applied to the unknown system input. This idea is used to formulate several deconvolution criteria, the maximization of which yields the desired solution to the blind deconvolution problem. The criteria described herein are universal in the sense that they do not impose any restrictions on the statistics of the input signal, so long as it is non-Gaussian. Also, it appears that the criteria do not lead to spurious local minima. The third class of blind equalization algorithms is based on higher-order statistics of the received signal. The parameters of particular interest are the higher-order cumulants or their Fourier transforms known as polyspectra. The attractive feature of polyspectra is that they have the inherent ability to identify a nonminimum-phase channel from the channel output and do it without a training sequence. The fourth class of blind equalization algorithms concerns unknown communication channels, involving a joint data and channel estimation. In principle, this joint estimation is accomplished by finding the least-squares channel estimate between the received signal and every possible input signal that may have been transmitted, and selecting that particular estimated pair of transmitted signal and channel response, with the least-squares error. In essence, this is a maximum likelihood decoding rule for solving the blind equalization problem, the natural tool for which is the Viterbi algorithm. However, a major limitation of this approach is the explosive growth in computational complexity with the number of data symbols transmitted. A number of sub-optimal search procedures based on the use of a trellis are described in [24], for solving the blind joint data and channel estimation problem, which would be justified when the received signal-to-noise ratio is high.

Focusing now the underwater acoustics context, an approach to solve the blind deconvolution problem is to back propagate the received signal, *i.e.*, to time reverse the received time series and (back) propagate an array of time-reversed signals[32]. The back-propagated signals should converge in principle at the true source location and produce a waveform which should be a good replica of the original signal. This method could be implemented in practice using the sound channel for (back) propagation, if the signal is not severely attenuated by the two-way propagation; an alternative is to deduce analytically or numerically the back-propagated signal, using propagation codes. In [68], the algorithm for channel estimation (with a known source) was extended to the case in which the source signal is not known precisely, but is assumed to belong to a parametric class of signals, in that case, sinusoids of unknown frequency, duration and starting time. An extension of the optimization method for source signature estimation, in [64], by simulated annealing, is proposed in the same paper, treating the channel transfer function also as an unknown parameter, what allows for the simultaneous estimation of both source spectrum and transfer function. However, careful must be taken in the choice of the tradeoff between source and channel estimates accuracy. Motivated by the use of higher-order statistics, a work has been done, in which, the transfer function is statistically characterized, and the output of deconvolution are both the deterministic source signature and the statistical parameters of the IR. The IR is interchanged with the source signal, turning the source signature estimation problem into a linear deterministic system identification problem, with random input. The estimation proceeds by maximization of the deconvolved signal's normalized cumulant[6].

Chapter 4

Time-Frequency Distributions

It is now clear, from Chap. 2, that the underlying physical scenario transforms the emitted signal into a set of replicas arriving at the receiver, at multiple time instants. Obviously, from a simple analysis of the received signal spectrum or time series, the extraction of the emitted signal, and of the time-delays and amplitudes of the channel is not trivial. This difficulty led to the investigation of other signal representations, namely *time-frequency distributions* (TFDs), due to their two degrees of freedom. It will be seen in subsequent sections, that such representations show simultaneously the arrival structure of the received signal (time information), and the replicated and weighted source spectral content (frequency information).

Consider some signal as an information support. The time and frequency energy densities of the signal are not sufficient to describe the (usually) implicit physical situation, because they do not fully describe what is happening. In particular, the frequency energy density is inherently a statistic of the frequencies present in the signal, but not revealing the manner in which the signal's spectral behaviour evolves as a function of time. TFDs are bidimensional (2D) functions of time t and frequency f, that contain effectively both the temporal and spectral information of the signal being analyzed, indicating its joint *time-frequency* (TF) energy content. They provide a multitude of information such as frequency response, power, instantaneous frequency, group delay, etc. The importance of TFDs is reinforced when the signal to be analyzed is non-stationary, what entails naturally a definition of the stationarity concept, in next section.

4.1 Stationarity

It is important to define here the concept of stationarity, to distinguish between the non--stationary signals and stationary random processes treated in this work, and to motivate TF processing.

A random process $X_x(t)$ is said to be *stationary of order* K, if the joint probability density function of the sets $[X_x(t_1),\ X_x(t_2),\ ...,\ X_x(t_K)]$ and $[X_x(t_1+u), X_x(t_2+u), ..., X_x(t_K+u)]$ is the same for all choices of $t_1,\ t_2,\ ...,\ t_K$ and u[7]. The random process that will be used in simulated data has its elements composed of independent samples of an underlying generating random variable –the well known white noise. It follows that white noise is stationary of all orders[7]. For deterministic signals (that can always be interpreted as non-stationary stochastic processes), the classification into stationary implies that their definition parameters –like the instantaneous amplitude (IA), frequency, auto-regressive parameters or respective order, temporal average, etc.– be time-invariant[58]. This can be synthesized in the definition of a stationay deterministic signal as a sum of components with constant IAs and frequencies. For both random processes and deterministic signals, non-stationarity is defined by opposition to stationarity.

4.2 Quadratic Time-Frequency Distributions

The basic objective of TF analysis is to devise a function –a TFD– that will describe the energy density of a signal simultaneously in time and frequency, and that can be used and manipulated in the same manner as any probability density function[14]. There are many examples of such representations, some of which mentioned in Tab. 4.1. One of the most popular TFDs is the short-time Fourier transform. It is well-known that this distribution has the noteworthy drawback that a good time resolution requires short-duration windows whereas a good frequency resolution necessitates long-duration windows. Although linearity of a TFD is a desirable property, the quadratic structure of a TFD is an intuitively reasonable assumption when a TFD is to be interpreted as a TF energy distribution (or "instantaneous power spectrum"[54]), since energy is a quadratic signal representation. An "energetic" *quadratic TFD* (QTFD) $T_x(t,f)$ seeks to combine the concepts of the instantaneous power $p_{x,t}(t) = |x(t)|^2$ and the spectral energy density $p_{x,f}(f) = |X(f)|^2$. Ideally, this energetic

Linear
Short-time Fourier transform Wavelet transform (TF version)
Bilinear (quadratic)
Choi-Williams distribution Cone-kernel distribution Flandrin distribution Generalized exponential distribution Generalized Wigner distribution Modal distribution Rihaczek distribution Scalogram Spectrogram Wigner-Ville distribution
Nonlinear and nonquadratic
Cohen nonnegative distribution

Table 4.1: Some examples of TFDs.

interpretation is expressed by the marginal properties

$$\int T_x(t,f)\mathrm{d}f = p_{x,t}(t) = |x(t)|^2; \tag{4.1a}$$

$$\int T_x(t,f)\mathrm{d}t = p_{x,f}(f) = |X(f)|^2, \tag{4.1b}$$

which state that the one-dimensional (1D) energy densities $p_{x,t}(t)$ and $p_{x,f}(f)$ are "marginal densities" of the TFD $T_x(t,f)$[72] (when not explicitly mentioned, all integrations are from $-\infty$ to ∞). As a consequence, the signal energy $E_x = \int |x(t)|^2 \,\mathrm{d}t = \int |X(f)|^2 \,\mathrm{d}f$ can be derived by integrating $T_x(t,f)$ over the entire TF plane. The variables t and f are treated as if they were random variables, allowing the definition of concepts as average time, average frequency, standard deviation, etc. Hence, the TFD can be loosely interpreted as a 2D distribution of signal energy over the TF plane. However, it cannot be interpreted as a pointwise TF energy density, since it may locally assume negative values, as is the case of the Wigner-Ville distribution (see Sec. 4.2.1).

Apart from the "energetic" interpretation of QTFDs, there exists a dual interpretation in terms of correlation functions[12]. A "correlative" TFD $T_x(\nu,\tau)$ seeks to combine the temporal correlation $\Gamma_{x,t}(\tau)$ and the spectral correlation $\Gamma_{x,f}(\nu)$ defined below, both of which are again quadratic signal representations. Ideally, this is expressed by the "correlative marginal properties"

$$T_x(0,\tau) = \Gamma_{x,t}(\tau) = \int x(t+\tau)x^*(t)\ \mathrm{d}t; \tag{4.2a}$$

$$T_x(\nu,0) = \Gamma_{x,f}(\nu) = \int X(f+\nu)X^*(f)\ \mathrm{d}f, \tag{4.2b}$$

where the variables τ and ν are the *time-lag* and *frequency-lag*, respectively, and the superscript * denotes complex conjugation.

Depending on the number of well delineated regions in the TF plane, a signal can be classified as *monocomponent* or *multicomponent*, when the signal is represented by one or multiple regions, respectively.

The Quadratic Superposition Principle

Any QTFD $T_x(t,f)$ satisfies the *quadratic superposition principle*

$$\begin{aligned} x(t) &= c_1x_1(t)+c_2x_2(t) \Rightarrow \\ \Rightarrow T_x(t,f) &= |c_1|^2\,T_{x_1}(t,f)+|c_2|^2\,T_{x_2}(t,f)+c_1c_2^*T_{x_1,x_2}(t,f)+c_2c_1^*T_{x_2,x_1}(t,f), \end{aligned} \quad (4.3)$$

where $T_x(t,f)$ is the *auto-TFD* of the signal $x(t)$, and $T_{x_1,x_2}(t,f)$ is the *cross-TFD* of the two signals $x_1(t)$ and $x_2(t)$, with $T_{x,x}(t,f)=T_x(t,f)$[27]. The cross-TFD $T_{x_1,x_2}(t,f)$ is quadratic (bilinear) in the signals $x_1(t)$ and $x_2(t)$. Generalizing the quadratic superposition principle to an M-component signal $x(t)=\sum_{m=1}^{M}c_mx_m(t)$, the following rules are obtained[19]:

- To each signal component $c_mx_m(t)$, there corresponds a *signal term* $|c_m|^2T_{x_m}(t,f)$;
- To each pair of signal components $c_mx_m(t)$ and $c_nx_n(t)$ (with $m\neq n$), there corresponds a cross-component or *interference term* (IT) $c_mc_n^*T_{x_m,x_n}(t,f)+c_nc_m^*T_{x_n,x_m}(t,f)$.

Thus, for an M-component signal $x(t)$, $T_x(t,f)$ will have M signal terms and $M(M-1)/2$ ITs. The ITs may have higher amplitude than the signal terms, what causes some difficulty in the visual analysis of the TFDs of multicomponent signals. Fig. 4.1 illustrates the WV of the sum of two LFM sweeps with amplitudes 1 and 0.5, respectively, where it can be seen the relative amplitudes of the signal terms and the ITs, for this particular case.

4.2.1 Wigner-Ville Distribution and Ambiguity Function

Motivated by a quantum correction calculus, Wigner introduced a joint distribution that gave, as marginals, the quantum mechanical distributions of position and momentum[72].

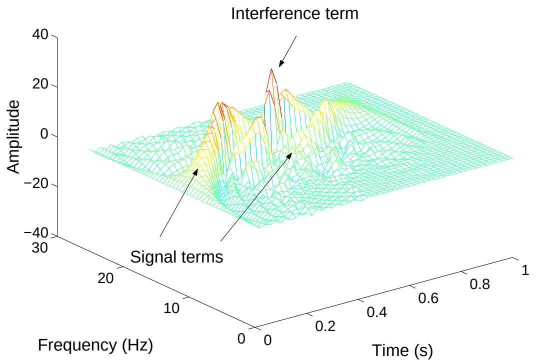

Figure 4.1: WV of the sum of two LFM sweeps with amplitudes 1 and .5, respectively.

The distribution of Wigner was introduced into signal analysis by Ville[69], and is nowadays known as the *Wigner-Ville distribution* (WV). The WV is a QTFD that overcomes the drawback of low-resolution (unlike the well-known spectrogram). The cross-WV of 2 continuous-time signals $x(t)$ and $y(t)$ is a complex-valued function defined by[1]:

$$WV_{x,y}(t,f) \triangleq \int_{-\infty}^{\infty} x\left(t+\frac{\tau}{2}\right) y^*\left(t-\frac{\tau}{2}\right) \mathrm{e}^{-\mathrm{j}2\pi f\tau}\mathrm{d}\tau. \qquad (4.4)$$

If $x(t) \equiv y(t)$, then the WV of $x(t)$ is a real-valued function, defined, for a given time, as the Fourier transform with respect to τ, of the signal's local auto-correlation function

$$\Gamma_{x,t,\tau}(t,\tau) \triangleq x\left(t+\frac{\tau}{2}\right) x^*\left(t-\frac{\tau}{2}\right). \qquad (4.5)$$

The WV of $x(t)$ is thus defined by

$$WV_x(t,f) = \int_{-\infty}^{\infty} x\left(t+\frac{\tau}{2}\right) x^*\left(t-\frac{\tau}{2}\right) \mathrm{e}^{-\mathrm{j}2\pi f\tau}\mathrm{d}\tau. \qquad (4.6)$$

The WV has naturally a definition, for discrete-time signals $x(n)$ and $y(n)$[58]:

$$WV_{x,y}(n,f) = 2\sum_k \mathrm{e}^{-\mathrm{j}2\pi kf} x(n+k)y^*(n-k). \qquad (4.7)$$

This definition encompasses a periodicity of $1/2$ with respect to the continuous variable f. For this reason, the TF-represented signals in this work are the analytic counterparts of the real physical signals (see App. B), thus avoiding aliasing effects and oversampling[58].

---

[1] It can be viewed as the Fourier transform of a different concept of cross-correlation defined not as an inner product, but as a pointwise product.

A dual distribution of the WV is the *ambiguity function* (AF), defined as

$$AF_{x,y}(\nu,\tau) \triangleq \int x\left(t+\frac{\tau}{2}\right) y^*\left(t-\frac{\tau}{2}\right) \mathrm{e}^{-\mathrm{j}2\pi\nu t}\mathrm{d}t. \tag{4.8}$$

The AF can be interpreted as a joint TF correlation function. Specifically, it satisfies the "correlative marginal properties" (4.2). In addition, the maximum value of an auto-AF occurs at the origin, and equals the signal's energy, *i.e.*, $|AF_x(\nu,\tau)| \leq AF_x(0,0) = \int |x(t)|^2 \, \mathrm{d}t$. The WV and the AF are duals in the sense that they are a Fourier transform pair[69]:

$$AF_{x,y}(\nu,\tau) = \iint WV_{x,y}(t,f)\mathrm{e}^{-\mathrm{j}2\pi(\nu t-\tau f)}\mathrm{d}t\ \mathrm{d}f. \tag{4.9}$$

Property name	**Mathematical definition**
▶ Instantaneous frequency	$\frac{\int f\ WV_x(t,f)\mathrm{d}f}{\int WV_x(t,f)\mathrm{d}f} = f_{i,x}(t) = \frac{1}{2\pi}\frac{\mathrm{d}}{\mathrm{d}t}\mathrm{arg}\left[x(t)\right];$
▶ Finite time support	$x(t) = 0$, for $t \notin [t_1,t_2] \Rightarrow WV_x(t,f) = 0$, for $t \notin [t_1,t_2]$
▶ Convolution	$\tilde{x}(t) = \int h(t-t')x(t')\ \mathrm{d}t' \Rightarrow$ $\Rightarrow WV_{\tilde{x}}(t,f) = \int WV_h(t-t',f)WV_x(t',f)\mathrm{d}t'$
▶ Multiplication	$\tilde{x}(t) = h(t)x(t) \Rightarrow$ $\Rightarrow WV_{\tilde{x}}(t,f) = \int WV_h(t,f-f')WV_x(t,f')\mathrm{d}f'$
▶ Moyal's formula (unitarity)	$\langle WV_{x1,y1} \vert WV_{x2,y2}\rangle = \langle x_1 \vert x_2\rangle \langle y_1 \vert y_2\rangle^*$
▶ Chirp convolution	$\tilde{x}(t) = x(t) * \sqrt{\lvert c\rvert}\mathrm{e}^{\mathrm{j}2\pi\frac{c}{2}t^2} \Rightarrow WV_{\tilde{x}}(t,f) = WV_x\left(t-\frac{f}{c},f\right)$
▶ Chirp multiplication	$\tilde{x}(t) = x(t)\mathrm{e}^{\mathrm{j}2\pi\frac{c}{2}t^2} \Rightarrow WV_{\tilde{x}}(t,f) = WV_x\left(t,f-ct\right)$

Table 4.2: Some desirable mathematical properties of the WV.

Among all QTFDs with "energetic" interpretation, the WV can be regarded as theoretically optimal in that it features optimal TF resolution[69] and satisfies a maximum[58] number of "desirable" mathematical properties[72], some of which are indicated in Tab. 4.2.

For example, the WV preserves the time or frequency support of the signal. This is different from the spectrogram and scalogram, which generally introduce some broadening with respect to time and frequency, often not allowing an effective resolution of the components. This optimality of the WV is however accompained by substantial ITs.

Wigner-Ville's Resolution for Finite-Duration Signals

An important issue regarding the WV analysis of finite signals is the resolution of the distribution. Whereas the WV presents in general good concentration along the instantaneous frequency (IF), for infinite-duration signals[14], this concentration is relaxed, for finite signals, due to WV's Fourier-based definition. Consider a signal $x(t)$ with finite time support $\mathcal{T} = t_2 - t_1$ (often imposed by the time observation window), which is zero, for $t \notin [t_1, t_2]$. It is easily seen that the signal's local auto-correlation function (4.5), as a function of τ, is a finite-length signal, whose duration, parameterized by t, varies between 0 and $2\mathcal{T}$. For practical purposes referred in Chap. 5, it can be considered that most of signal's energy is concentrated along the IF (this encompasses a large variety of signals[14]), in a support dictated by $\mathcal{T}$. It is well known that the Fourier transform of an unitary $2\mathcal{T}$-length window is a cardinal sinusoid (sinc), with a main lobe width of $1/\mathcal{T}$. Based on the maximum length of the local auto-correlation function, one can consider that $WV_x(t, f)$ will be concentrated along $[t, f_i(t)]$, and the domain $[f_{i,x}(t) - 1/(2\mathcal{T}),\ f_{i,x}(t) + 1/(2\mathcal{T})],\ t \in [t_1, t_2]$ (according also to temporal support's conservation in Tab. 4.2) will contain most of the energy of $x(t)$.

Interference Geometry

As said above, improved TF concentration and an extensive list of desirable mathematical properties are attractive features of the WV. On the other hand, certain characteristics of the WV's ITs often cause problems in practical applications. Whereas the ITs of the spectrogram or the scalogram will be zero if the corresponding signal terms do not overlap, the ITs of the WV will be nonzero regardless of the TF distance between any two signal terms, as follows.

Two signal components occuring around TF points (t_1, f_1) and (t_2, f_2) give rise to two signal terms and one IT in both the WV and the AF. For the following discussion, let's define the center point (t_{12}, f_{12}) and the lags τ_{12}, ν_{12}, as $t_{12} = (t_1 + t_2)/2,\ f_{12} = (f_1 + f_2)/2;\ \tau_{12} = t_1 - t_2,\ \nu_{12} = f_1 - f_2$. In the WV, the signal terms are located around (t_1, f_1) and (t_2, f_2), respectively. The IT is located around the center point (t_{12}, f_{12}). It oscillates with respect to time with oscillation period $1/|\nu_{12}|$, and with respect to frequency with oscillation period $1/|\tau_{12}|$. Correspondingly, in the AF, the signal terms are located around the origin of the (ν, τ)-plane. The IT consists of two subterms located around the lag points (ν_{12}, τ_{12}) and $(-\nu_{12}, \tau_{12})$, respectively. In general, ITs occur also in the case of monocomponent signals. The signal's energy is concentrated along the curved instantaneous frequency; this also defines the WV's signal term. Oscillatory ITs are seen to exist midway between any two points on the signal term.

The ITs of the WV can be identified by their oscillatory nature, while the ITs of the AF are characterized by their locations away from the origin of the (ν, τ)-plane[35]. From a practical viewpoint, ITs are troublesome, since they may overlap with auto-terms (signal terms), and thus make it difficult to visually interpret a WV or AF plot. Nevertheless, ITs are necessary for a TFD's unitarity[29] or, equivalently, for Moyal's formula[47] to hold. Moyal's formula is critical for the TF formulation of optimum detection and estimation methods[20, 39], what will be important for channel estimation in the present work (see Sec. 5.3.2), and for a closed-form solution to the signal synthesis problem[5, 29], what was explored for source signature estimation (cf. Sec. 5.2.2).

4.2.2 The Cohen Class

For a given time, the WV weighs equally all times of the past and future. Similarly, for a given frequency, it weighs equally all frequencies below and above that frequency. There are three reasons for modifying this basic property of the WV. First, in practice, it may not be possible to integrate from minus to plus infinity, and so one should study the effects of limitting the range. Second, in calculating the distribution for a time t, one may want to emphasize the properties near the time of interest compared to the far past and future times. Third, practical application of the WV is often restricted by the occurence of ITs, and it is natural to seek modified versions of the WV that attenuate to some extent these ITs. As will be seen, this last issue corresponds to looking for a TFD that presents good auto-component concentration and interference attenuation, in other words, that it be concentrated and approximately linear.

Taking into account the definition (4.6), to emphasize the signal around time t, the local auto-correlation function (4.5) can be multiplied by a function (window) whose peak is located around $\tau = 0$, prior to the integration in (4.6), defining a distribution named *pseudo-WV*[14]. The WV is highly nonlocal, and the effect of windowing is to increase locality. One of the consequences of this is that the pseudo-WV supresses, to some extent, the cross-terms for multicomponent signals. In counterpart, the marginals and instantaneous frequency properties no longer hold. Similarly, the signal spectrum around frequency f can also be emphasized, and the conjugation of these two modifications of the WV gave origin to the *smoothed pseudo-WV*. The smoothed pseudo-WV is defined by a separable *smoothing* kernel $\phi(t, f) = g(t)H(f)$, in which $g(t)$ and $H(f)$ are two windows whose effective lengths independently determine the time and frequency smoothing spreads, respectively[27]:

$$SPWV_x^{g,H}(t,f) \quad = \quad \iint g(t-t')H(f-f')WV_x(t',f')\mathrm{d}t'\ \mathrm{d}f'. \tag{4.10}$$

This distribution extends the spectrogram in that it allows an independent control of the time and frequency resolutions. An even more general modification of the WV, the *local WV*, has been proposed in [53], making use of a local kernel, *i.e.*, depending on the considered TF point. This approach associates to each pair (t,f) a specific pair of functions $g(u,t,f)$ and $H(v,t,f)$.

The above ideas were progressively developed and applied mainly to suppress ITs of the WV, giving rise to a generalized family of TFDs –the *Cohen class* (denoted C_E)–, introduced by Cohen, in 1966. This class along with the affine class, contain all possible QTFDs[27]. Any function $C_x\left(t,f;\Phi\right)$ of C_E is defined as

$$C_x\left(t,f;\Phi\right) = \frac{1}{2\pi}\int_{-\infty}^{\infty}\int_{-\infty}^{\infty}\int_{-\infty}^{\infty} x\left(u+\frac{\tau}{2}\right)x^*\left(u-\frac{\tau}{2}\right)\Phi(\nu,\tau)\ \mathrm{e}^{-\mathrm{j}2\pi(\nu t+\tau f-\nu u)}\mathrm{d}u\ \mathrm{d}\tau\ \mathrm{d}\nu, \tag{4.11}$$

where $x(t)$ is the signal being analyzed, and $\Phi(\nu,\tau)$ is a 2D function called the *kernel* of the distribution, that completely characterizes the particular TFD, giving rise to widely different types of distributions[14]. Examples of TFDs of C_E are the WV presented in the above subsection, spectrogram (squared-magnitude of the short-time Fourier transform), Choi-Williams distribution[10] and cone-kernel distribution[75]. The TFDs of C_E satisfy the basic property of TF shift-invariance: if a signal $x(t)$ is shifted in time and/or in frequency, then its TFD will be shifted by the same time-delay and/or modulation frequency:

$$\tilde{x}(t) = x(t-t_0)\mathrm{e}^{\mathrm{j}2\pi f_0 t} \quad \Rightarrow \quad C_{\tilde{x}}(t,f) = C_x(t-t_0,f-f_0). \tag{4.12}$$

Every member of C_E may be interpreted as a 2D filtered WV. In fact, it can be shown that a TFD $T_{x,y}(t,f)$ is a member of C_E if and only if it can be derived from the cross-WV of the signals $x(t)$ and $y(t)$ via a TF (2D) convolution[11]:

$$T_{x,y}(t,f) \in C_E \quad \Leftrightarrow \quad T_{x,y}(t,f) = \iint \phi\left(t-t', f-f'\right) WV_{x,y}\left(t', f'\right) \mathrm{d}t' \, \mathrm{d}f', \tag{4.13}$$

where $\phi(t,f)$ is an arbitrary function. Clearly, the above convolution transforms into a simple multiplication in the Fourier transform domain. Each member $C_x(t,f)$ of C_E is associated with an unique signal-independent kernel function $\phi(t,f)$ (or 2D filter).

To every shift-invariant TFD $C_x(t,f) \in C_E$, corresponds a "dual correlative TFD" $C_{x,dual}(\nu,\tau)$ as the 2D FT[19]

$$C_{x,dual}(\nu,\tau) \quad \triangleq \quad \iint C_x(t,f)\mathrm{e}^{-\mathrm{j}2\pi(\nu t-\tau f)}\mathrm{d}t \, \mathrm{d}f. \tag{4.14}$$

The class of dual correlative TFDs, denoted C_C, consists of all TFDs satisfying the "correlative shift-invariance"[26]

$$\tilde{x}(t) = x(t-t_0)e^{\mathrm{j}2\pi f_0 t} \quad \Rightarrow \quad C_{\tilde{x},dual}(\nu,\tau) = C_{x,dual}(\nu,\tau)e^{\mathrm{j}2\pi(f_0\tau - t_0\nu)}, \tag{4.15}$$

which is the dual expression of (4.12), and motivated by the shift properties

$$\Gamma_{\tilde{x},t}(\tau) = \Gamma_{x,t}(\tau)e^{\mathrm{j}2\pi f_0\tau}, \quad \Gamma_{\tilde{x},f}(\nu) = \Gamma_{x,f}(\nu)\mathrm{e}^{-\mathrm{j}2\pi t_0\nu} \tag{4.16}$$

of the 1D correlations $\Gamma_{x,t}(\tau)$ and $\Gamma_{x,f}(\nu)$. Most importantly, any TFD $C_{x,dual}(\nu,\tau)$ which is a member of the correlative class can be derived from the AF of the signal $x(t)$, by means of a multiplication[19]:

$$C_{x,dual}(\nu,\tau) \in C_C \quad \Leftrightarrow \quad C_{x,dual}(\nu,\tau) = \Phi(\nu,\tau)AF_x(\nu,\tau). \tag{4.17}$$

The kernel $\Phi(\nu,\tau)$ of $C_{x,dual}(\nu,\tau)$ in the above equation and the kernel $\phi(t,f)$ of $C_x(t,f)$ in (4.13) are a Fourier transform pair, just as $C_{x,dual}(\nu,\tau)$ and $C_x(t,f)$. A prominent example of a pair of dual TFDs is given by the WV and the AF, related by the Fourier transform (4.14) [cf. (4.9), for the cross-distributions]. Finally, inverting (4.14) and taking (4.17) into account, a distribution $C_x(t,f)$ from C_E can be interpreted as the 2D Fourier transform of a weighted version of the AF of the signal[4]:

$$C_x(t,f) \;=\; \frac{1}{2\pi}\int_{-\infty}^{\infty}\int_{-\infty}^{\infty}\Phi(\nu,\tau)AF_x\left(\nu,\tau\right)\mathrm{e}^{-\mathrm{j}2\pi(\nu t+\tau f)}\mathrm{d}\nu\;\mathrm{d}\tau. \tag{4.18}$$

Because WV's ITs are oscillatory, they may be attenuated by means of a smoothing operation (*i.e.*, 2D low-pass filtering)[19]. The Cohen class above defined provides a convenient framework for WV smoothing. TFDs of Cohen class are thus often called *smoothed WVs*, and the kernel $\phi(t,f)$ is called a *smoothing function*. Unfortunately, this attenuation of ITs comes at the cost of a loss of TF concentration, since a smoothing generally causes a broadening of the WV's signal terms[28]. In the dual correlative domain, this broadening transforms to a truncation of the AF's signal terms caused by the weighting operation (4.17). Another disadvantage of smoothing is the potential loss of desirable mathematical properties. One can conclude that there exists a fundamental tradeoff between good interference attenuation, and good TF concentration and desirable mathematical properties. A broad WV-domain smoothing function $\phi(t,f)$ [corresponding to a narrow lowpass-type AF-domain weighting function $\Phi(\nu,\tau)$] yields good interference attenuation but poor TF concentration, and conversely.

4.3 Signal-Dependent Time-Frequency Distributions

Fixed kernel TFDs seen in previous section have a fundamental limitation: they offer good performance (they achieve a high degree of both cross-component supression and auto-component concentration, providing an accurate representation of the TF content of the signal) only for certain configurations of AF's auto- and cross-components, thus only for a limited class of signals. This is because the locations of the auto- and cross-components depend on the signal to be analyzed. The lack of a single distribution that is "best" for a broad class of signals has resulted in a proliferation of TFDs, each corresponding to a different fixed mapping from signals to the TF plane. A significant performance gain may often be obtained, by adapting the smoothing characteristics of a smoothed WV to the signal to be analyzed, *i.e.*, designing a kernel function which varies with the signal[2]. A signal-dependent kernel can provide a good TFD, by adjusting its shape to pass auto-components and supress cross-components, regardless of their shape and orientation. Of course, the resulting *signal-dependent* (or -*adaptive*) TFD is then no longer quadratic. The following two subsections are devoted to the description of two signal-dependent TFDs with direct application in the present work: the chirp-adapted distribution and the radially Gaussian kernel distribution.

4.3.1 Chirp-Adapted Distribution

In view of the limitations caused by the ITs in the WV of multicomponent chirp signals, Ma *et al.*[43] developed a TFD specially adapted to this type of signals (directly applicable to the signals involved in this work): the *chirp-adapted distribution* (CA), whose description is summarized in this subsection.

Let $x_c(t)$ be an infinite-duration linear frequency modulation (LFM or *chirp*) signal, defined by:

$$x_c(t) = a\ \mathrm{e}^{\mathrm{j}2\pi\left(\alpha\frac{t^2}{2}+f_0 t\right)},\quad a \in \mathbb{R}, \tag{4.19}$$

where α is the frequency modulation rate, and f_0 is the IF at $t = 0$. It is readily verified that the IF of $x_c(t)$ is the linear function

$$f_{i,x_c}(t) = \alpha t + f_0. \tag{4.20}$$

According to (4.6), the WV of $x_c(t)$ is given by

$$WV_{x_c}(t,f) = a^2\delta\left[f-(\alpha t+f_0)\right]. \tag{4.21}$$

This shows that the WV of $x_c(t)$ is infinitely concentrated along its IF. One can verify that the signal's AF is composed by only one signal term: a 2D Dirac function that crosses the origin. When the signal to be analyzed consists of a weighted sum of (finite or infinite) LFM signals instead, the corresponding AF possesses a signal term composed, this time, roughly by a sum of cisoids (respectively, finitely or infinitely concentrated) across the origin, and a certain number of cross-terms away from the origin. Due to these properties of the AF of multicomponent chirp signals, the kernel function of the CA is defined as:

$$\Phi(\nu,\tau) = \mathrm{rect}\left(\frac{\nu-\alpha\tau}{w}\right), \tag{4.22}$$

where $\mathrm{rect}\left(\frac{\cdot}{w}\right)$ is the unitary window function of length w, centered at the origin. The kernel, hence, has a rectangular support along the direction $\nu = \alpha\tau$. The resulting CA with the associated kernel function is

$$CA_x(t,f) = \int_{-\infty}^{\infty}\int_{-\infty}^{\infty} w\,\mathrm{sinc}\left[w(t-u)\right]e^{\mathrm{j}2\pi\alpha\tau(t-u)}x\left(u+\frac{\tau}{2}\right)x^*\left(u-\frac{\tau}{2}\right)\mathrm{e}^{-\mathrm{j}2\pi f\tau}\mathrm{d}u\,\mathrm{d}\tau, \tag{4.23}$$

where $x(t)$ is the multi-component chirp signal to be analyzed. The kernel function (4.22) satisfies the condition $\Phi(\nu,\tau) = \Phi^*(-\nu,-\tau)$, what implies that (4.23) be a real distribution. This representation is a smoothed signal-dependent version of the WV, whose smoothing function is composed of 2 (non-multiplicative) parts: a low-pass filter $h(t) = w\ \mathrm{sinc}(wt)$ and a frequency modulation $\delta(f - \alpha\tau)$. As mentioned in Sec. 4.2.2, for any type of smoothing, the low-pass filtering implies a loss of concentration of the signal terms.

As seen in (4.23), the CA is completely defined by two parameters: the frequency modulation rate α and the kernel width w. Due to the above mentioned AF properties of multicomponent chirp signals, the smoothing parameters necessary to the calculation of the CA can be optimally estimated regarding the criteria of interference attenuation. These parameters will control the performance of the distribution, and are determined by the following equations, in the ambiguity domain:

$$U(\alpha, w) = \iint \operatorname{rect}\left(\frac{\nu - \alpha\tau}{w}\right) |AF_x(\nu, \tau)| \, \mathrm{d}\nu \, \mathrm{d}\tau; \tag{4.24}$$

$$\alpha_{opt} = \hat{\alpha} = \arg\max_{\alpha} U(\alpha, w_0); \tag{4.25a}$$

$$w_{opt} = \arg\min_{w} \frac{\partial}{\partial w} U(\alpha_{opt}, w). \tag{4.25b}$$

(4.24) calculates the volume of the signal's ambiguity function under the kernel functions with different α and w. In order to estimate the two parameters from this volume, at first, parameter w is fixed at w_0. The optimal value for α will correspond to the global maximum of $U(\alpha, w_0)$ –(4.25a). It is expected that $U(\alpha, w_0)$ be very sensible to variations of α, due to the directional structure of $AF_x(\nu, \tau)$. After the estimation of α, w is unfixed, and the first minimum of the first derivative of $U(\alpha_{opt}, w)$ with respect to w, gives the optimal value for w –(4.25b). This is because $U(\alpha_{opt}, w)$ is a monotonic increasing function of w, including first the volume due to the auto-terms, and then the volume due to ITs which (hopefully) are distinct in the AF.

4.3.2 Radially Gaussian Kernel Distribution

This section summarizes one of the most successful approaches to signal-dependent kernel design, presented by Baraniuk and Jones[3, 4] who have shown that the optimal kernel for interference reduction depends on the analyzed signal, and also formulated the kernel design problem as a constrained optimization problem.

The optimal kernel consists of a radially-Gaussian weighting function $\Phi_{opt}(\nu, \tau)$, where the Gaussian spread in each radial direction in the (ν, τ)-plane is optimally adapted to the signal. Hence, given a signal, it is automatically designed a kernel that is optimal with respect to a set of performance criteria that attempt to capture, mathematically, the kernel properties that lead to a high degree of ITs reduction and auto-component concentration.

Optimal Kernel Design

The signal-dependent kernel design procedure is an optimization problem whose formulation requires a class of 2D kernel functions from which the optimal kernel is chosen, and a performance index that measures the quality of the TFD with respect to criteria deemed important by the designer. The class of kernels is specified by a set of constraints, and the performance measure is chosen to yield a tractable optimization problem that can be solved efficiently. It is the kernel maximizing the value of the performance measure that is selected as the optimal kernel for the signal.

Radially Gaussian Kernels

It is desirable that the kernel possess the following properties: it should be lowpass to suppress cross-components and noise in the TFD, it should be smooth to reduce ringing artifacts, and it should take a functional form for which an optimization problem can be easily solved. A functional form that satisfies all of the above requirements is a radially Gaussian kernel. A radially Gaussian kernel is a 2D function that is Gaussian along any radial profile:

$$\Phi(\nu, \tau) \quad = \quad \mathrm{e}^{-\left(\nu^2+\tau^2\right)/\left[2\sigma^2(\psi)\right]}, \tag{4.26}$$

where the angle ψ is measured between the radial line through the point (ν, τ) and the ν axis,

$$\psi \quad = \quad \arctan \frac{\tau}{\nu}, \tag{4.27}$$

and the function $\sigma(\psi)$, called the *spread function*, controls the 'spread' of the Gaussian at angle ψ. If $\sigma(\psi)$ is smooth, then $\Phi(\nu, \tau)$ is also smooth. A radially Gaussian kernel is a generalization of a 2D lowpass Gaussian kernel. It is natural to express radially Gaussian kernels in polar coordinates, using $r = \sqrt{\nu^2 + \tau^2}$ as the radius variable:

$$\Phi(r, \psi) \quad = \quad \mathrm{e}^{-r^2/\left[2\sigma^2(\psi)\right]}. \tag{4.28}$$

Continuous-Time Optimization Formulation

Since the shape of a radially Gaussian kernel is completely parameterized by the 1D function $\sigma(\psi)$, finding the optimal radially Gaussian kernel for a signal is equivalent to finding the optimal spread function $\sigma_{opt}(\psi)$ for the signal. Therefore, given a signal, the optimal kernel $\Phi_{opt}\left(r, \psi\right)$ is defined as the radially Gaussian function whose spread function $\sigma_{opt}(\psi)$ solves the following optimization problem:

$$\max_{\psi} \int_0^{2\pi} \int_0^{\infty} \left|\Phi\left(r, \psi\right) AF\left(r, \psi\right)\right|^2 r \ \mathrm{d}r \ \mathrm{d}\psi, \tag{4.29}$$

subject to

$$\Phi(r, \psi) = \mathrm{e}^{-r^2/\left[2\sigma^2(\psi)\right]}, \tag{4.30a}$$

$$\frac{1}{2\pi}\int_0^{2\pi}\int_0^{\infty}|\Phi(r,\psi)|^2\, r\ \mathrm{d}r\ \mathrm{d}\psi \leq \beta, \qquad \beta \geq 0, \tag{4.30b}$$

where $AF\,(r,\psi)$ is the AF of the signal, in polar coordinates. The constraint (4.30b) limits the volume of the optimal kernel. The special structure of radially Gaussian kernels permits a simplification of (4.30b) to the equivalent volume constraint

$$\frac{1}{2\pi}\int_0^{\pi}\sigma^2(\psi)\mathrm{d}\psi \ \ \leq \ \ \beta. \tag{4.31}$$

Also, since the AF is symmetric about the origin, that is,

$$|AF\,(r,\psi)|^2 \ \ = \ \ |AF\,(r,\psi+\pi)|^2\,, \tag{4.32}$$

$\sigma_{opt}(\psi)$ is completely determined on the interval $0 \leq \psi < \pi$. The constraint (4.31) forces the optimal kernel to be a lowpass filter of fixed volume β. The shape of the passband of the optimal radially Gaussian kernel is determined by maximizing the performance measure (4.29). Clearly, in order to maximize the performance measure, $\Phi\,(r,\psi)$ should be large where $AF\,(r,\psi)$ is large, regardless of whether the peaks correspond to auto- or cross-components. However, assuming that the auto- and cross-components are somewhat separated in the ambiguity plane, the radially Gaussian constraint (4.30a) imposes a penalty on kernels whose passbands extend over cross-components. Kernels having large spread in the direction of cross-components must waste precious kernel volume over the regions between the auto- and cross-components, where $|AF\,(r,\psi)|^2$ and thus also the $|\Phi(r,\psi)AF\,(r,\psi)|^2$ contribution to the performance measure is small.

Kernel Volume Selection

By controlling the volume under the optimal kernel, the parameter β controls the tradeoff between cross-component supression and smearing of the auto-components. The exact value of β is application-dependent, though two bounds for β are suggested in [4], as follows.

A reasonable lower bound for β is the volume of a spectrogram kernel, since there appear to be few benefits gained from more smoothing[38]. Since the spectrogram kernel is the AF of the analysis window, and assuming that the window has unit energy, the kernel has unitary volume, and a lower bound for β is therefore

$$\beta \geq 1. \tag{4.33}$$

An heuristic upper bound for β can be determined by computing the amount of smearing in the TFD for a simple Gaussian mono-component signal

$$x(t) = \frac{1}{\sqrt[4]{\pi}} \mathrm{e}^{-t^2/2}. \tag{4.34}$$

The proposed upper bound for β is

$$\beta \leq 5. \tag{4.35}$$

Optimal Kernel Solution

The reader is referred to [4] for a complete description of the constrained optimization problem (4.29)–(4.31) solution. A discretized version of the problem is solved by a modified constrained form of the well-known step-project ascent algorithm. The modification of this iterative algorithm for solving unconstrained optimization problems, consists in rescaling the vector corresponding to the spread function $\sigma(\psi)$, every iteration, thus taking into account the constraint (4.31).

Chapter 5

Problem Solving in Simulated Data

This chapter explains the TF-based approach to blind deconvolution studied in this work, which obeys to the schemes in Figs. 5.1 and 5.2, explained as follows. Departing from the received signal $r_r(t)$ [the real part of the corresponding analytic signal $r(t)$], and for an emitted LFM signal, the first step is to calculate a signal-dependent TFD of the received signal. Then, the source signal IF is estimated. The IF estimate allows the definition of a TF function, whose inversion gives the source signal estimate. Simultaneously, the IF

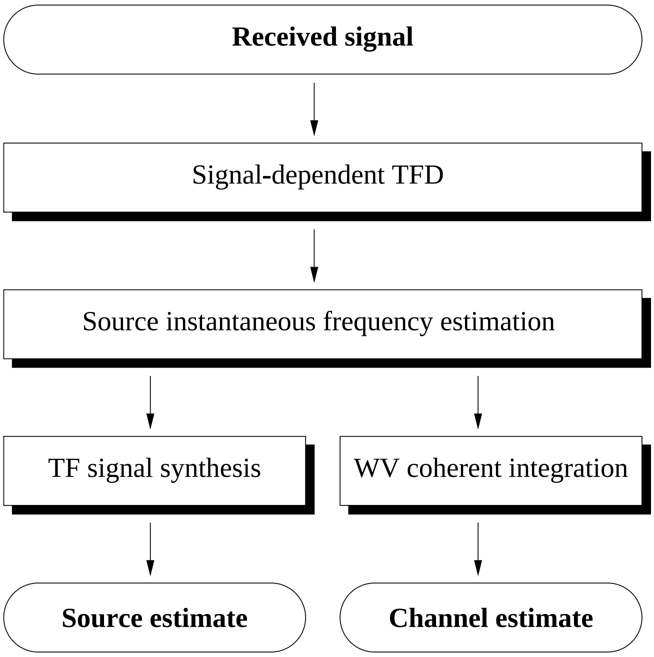
Received signal
Signal-dependent TFD
Source instantaneous frequency estimation
TF signal synthesis
WV coherent integration
Source estimate
Channel estimate

Figure 5.1: Complete estimation procedure in the TF approach to blind deconvolution of LFM signals.

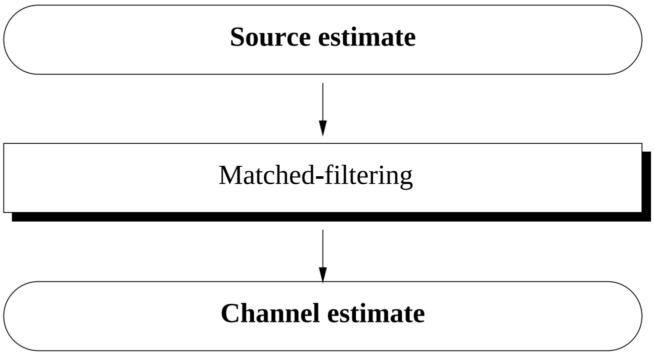

Figure 5.2: Channel estimation based on the source estimate referred in Fig. 5.1, for signals with both FM and AM components.

estimate defines an integration domain for the WV of the received signal, which allows the application of a TF formulation of the matched-filter. This leads to the channel IR estimate. Alternatively, as schematized in Fig. 5.2, the channel estimate can be obtained by matched-filtering with the previously obtained source signal estimate. The presentation of the deconvolution approach is supported by application to synthetic data.

The simulated data set corresponds to a canonical two-layered shallow water waveguide whose environment is very similar to the real data acquisition scenario of the INTIMATE '96 sea trial[15]. The acoustic source is positioned at 90-m depth, and one hydrophone, at 5.6-km range and 115-m depth, receives a distorted version of the emitted signal, as illustrated in Fig. 5.3. The 135-m water column is superimposed to a perfectly rigid bottom. The considered sound speed profile is shown in Fig. 5.4. Application of the ray/beam propagation model BELLHOP[55], taking as input the environment in Fig. 5.3, allowed to obtain the reference

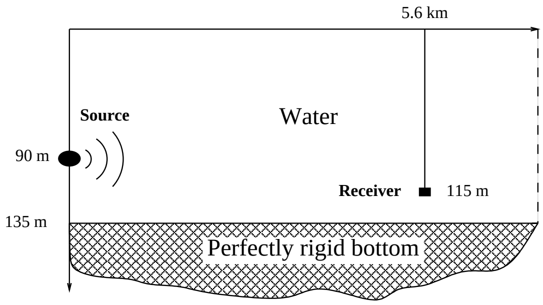

Figure 5.3: Canonical scenario used in simulations.

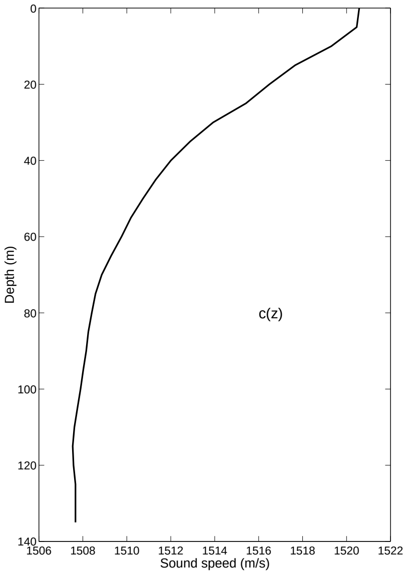

Figure 5.4: Sound speed profile of the propagation scenario in Fig. 5.3.

channel IR $h(t)$ and the (real) received signal $r_r(t)$. Launching angles were taken from the interval $[-30, \ +30]^\circ$, discretized in $7.50 \times 10^{-3}\ ^\circ$ intervals. In what follows, analysis will concern the $[3.4, \ \ 5.45]$-s interval of $r_r(t)$, and time will be relative to the absolute time 3.4 s. A total number of $M = 45$ arrivals have been predicted by the model, spanning the time interval $[0.31, 0.86]$ s, synthesized in the true IR $h(t)$ in Fig. 5.5. According to the

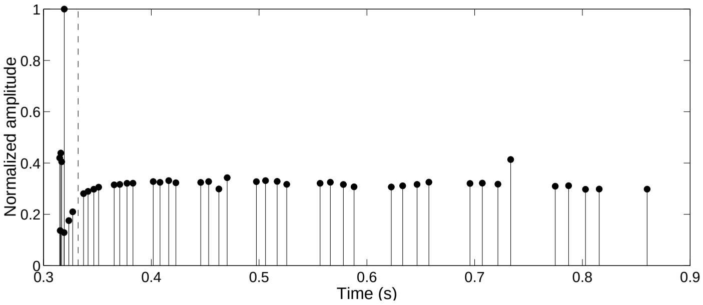

Figure 5.5: Reference IR $h(t)$ of the canonical simulated scenario. The dashed line separates unresolved from resolved impulses, explained later.

ray tracing model, the channel's IR $h(t)$ consists of a series of weighted and delayed Dirac functions, and is expressed as

$$h(t) \;=\; \sum_{m=1}^{45} a_m \delta(t - \tau_m), \tag{5.1}$$

where the amplitudes a_m and time-delays τ_m are the channel parameters to estimate, grouped into the vectors $\mathbf{a}$ and $\boldsymbol{\tau}$, respectively. The last 37 amplitudes and time-delays of $h(t)$ are mentioned in Tabs. 5.1 and 5.2, respectively. Time differences between all adjacent time-delays are depicted in Fig. 5.6, with the pair indexes sorted by increasing time. The dashed line indicates what can be crudely considered as the resolution of the matched-filter, as will be discussed in Sec. 5.3.1. The minimum time difference is 0.176 ms, verified between 5th and 6th arrivals. For reasons that will become evident in Sec. 5.3, the IR is split into 2 packets of arrivals (cf. Fig. 5.5): one packet contains the first 8 arrivals, designated as *unresolved* arrivals; the other contains the remaining 37 arrivals, designated as *resolved* arrivals.

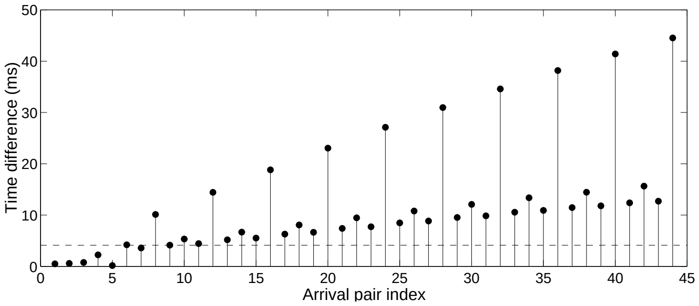

Figure 5.6: Time differences between all adjacent time-delays. Data correspond to the synthetic scenario. The dashed line gives an idea of the resolution of the MF.

Source signal consists of a $\mathcal{T} = 0.0625$-s duration LFM pulse, spanning the $[300, 800]$-Hz IF range (Fig. 5.7), whose analytic version is given by

$$s(t) \quad = \quad \mathrm{e}^{\mathrm{j}2\pi\left(4000t^2+300t\right)}\mathrm{rect}\left(\frac{t-0.03125}{0.0625}\right). \tag{5.2}$$

The IF of $s(t)$ is obviously the linear function

$$f_i(t) \quad = \quad (8000t+300)\mathrm{rect}\left(\frac{t-0.03125}{0.0625}\right), \tag{5.3}$$

representing a modulation rate of $\alpha = 8000$ Hz/s –Fig. 5.8. The WV of the source signal, $WV_s(t,f)$, is shown in Fig. 5.9, and given by

$$\begin{aligned} WV_s(t,f) \quad = \quad & 4t\,\mathrm{sinc}\left\{4\pi t\left(\alpha t+f_0-f\right)\right\}\mathrm{rect}\left(\tfrac{t-\mathcal{T}/4}{\mathcal{T}/2}\right)+ \\ & +\left(\mathcal{T}-t\right)\mathrm{sinc}\left\{4\pi(\mathcal{T}-t)\left(\alpha t+f_0-f\right)\right\}\mathrm{rect}\left(\tfrac{t-\mathcal{T}/2}{\mathcal{T}/2}\right). \end{aligned} \tag{5.4}$$

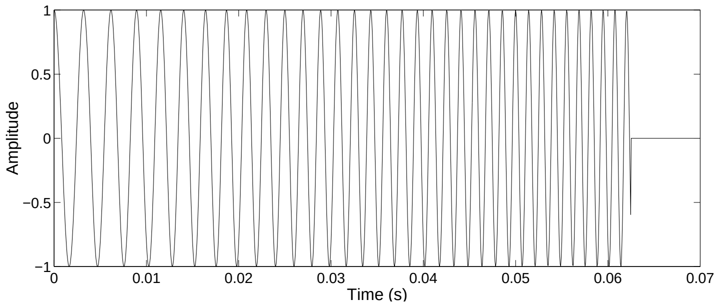

Figure 5.7: Source emitted LFM signal –real part of $s(t)$–, of duration 0.0625 s, and sweeping the [300, 800]-Hz IF range, used in simulations.

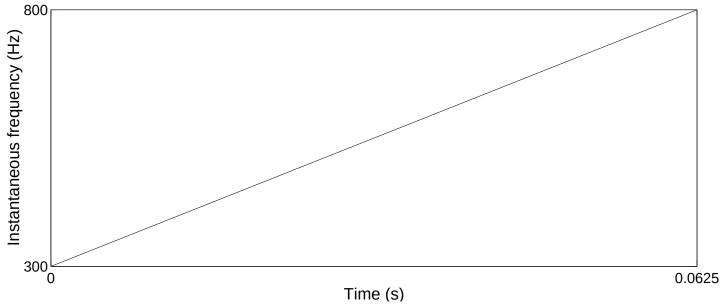

Figure 5.8: IF $f_i(t)$ of the LFM source signal considered in the simulation.

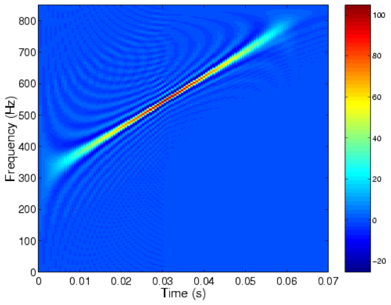

Figure 5.9: WV of the LFM source signal, $WV_s(t,f)$, respecting to synthetic data.

The analytic received signal $r(t)$ associated with $r_r(t)$ is simply the convolution of $s(t)$ with $h(t)$ (due to the filtering property of analytic signals[44]), thus obviously defined by

$$r(t) \;=\; \sum_{m=1}^{45} a_m e^{j2\pi\left[4000(t-\tau_m)^2+300(t-\tau_m)\right]} \mathrm{rect}\left(\frac{t-\tau_m-0.03125}{0.0625}\right), \tag{5.5}$$

whose real part $r_r(t)$ is represented in Fig. 5.10. Data is sampled at $f_s = 1700$ Hz, and importance has been given to a band of interest $\mathcal{B} = [300,\ 800]$ Hz, coincident with the LFM's IF range, for simplicity. Obviously, the multi-component received signal spans a time

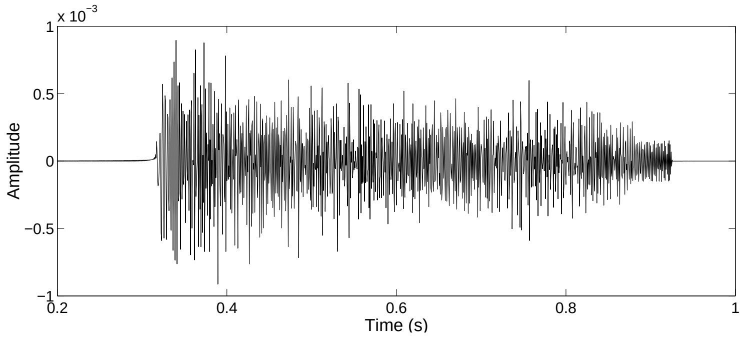

Figure 5.10: Received signal $r_r(t)$ used in simulations, for an LFM source signal.

interval equal to source signal duration plus the channel time dispersion, (0.0625 + 0.5450) s = 0.6075 s, being associated to 45 individual IF lines, as seen in Fig. 5.11 [refer to $h(t)$ in Fig. 5.5]. The WV of $r(t)$ is given by

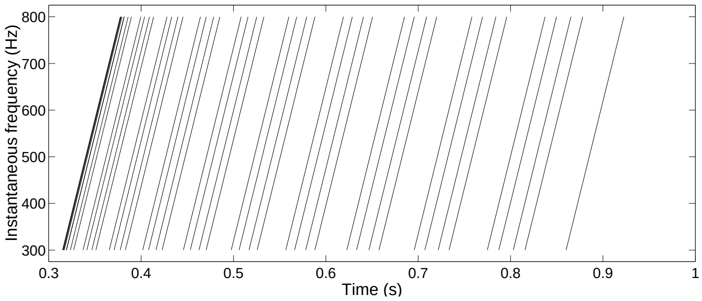

Figure 5.11: IFs of the received signal's components (weighted replicas of the emitted signal), in simulated data.

$$WV_r(t,f) \quad = \quad \sum_{m=1}^{45} WV_{s_m}(t,f) + 2\sum_{m=1}^{44}\sum_{n=m+1}^{45} \mathrm{Re}\left[WV_{s_m,s_n}(t,f)\right], \tag{5.6}$$

where $WV_{s_m}(t,f)$ and $WV_{s_m,s_n}(t,f)$ designate the auto-WV and cross-WV of each source replica, and source replicas pair, respectively. The simple-sum and double-sum terms correspond hence to the 45 signal terms and 1980 cross-terms, respectively, giving rise to a somewhat complicated illustration of the received signal's structure, as shown in Fig. 5.12(a).

Next three sections will describe the estimation of the three quantities IF $f_i(t)$, source signal $s(t)$ and channel IR $h(t)$, respectively. It will be seen that the proposed approach

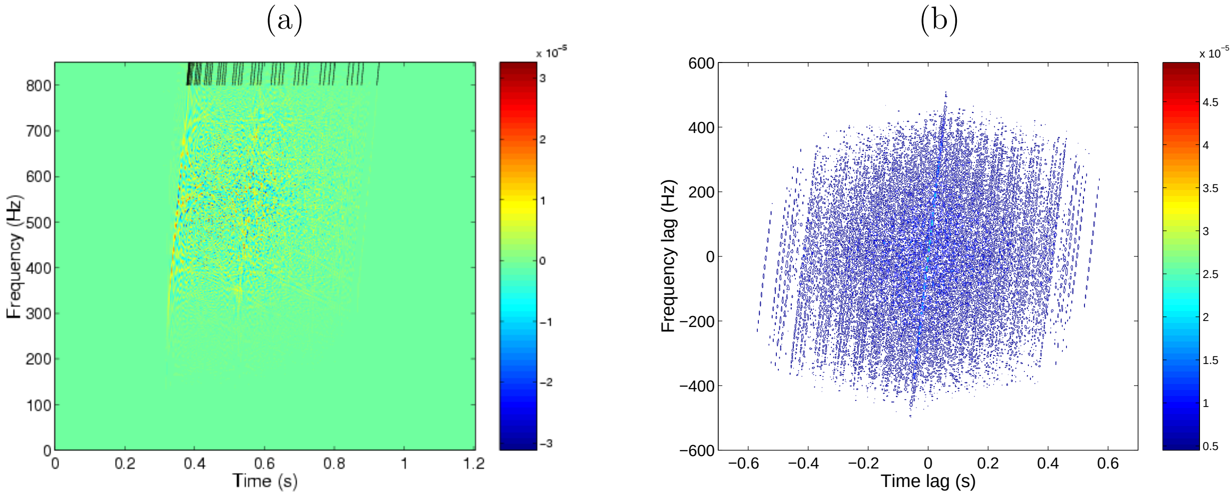

Figure 5.12: WV of the received synthetic signal, $WV_r(t, f)$ (a), and contour plot of the corresponding ambiguity function $AF_r(\nu, \tau)$ (b). The diagonal lines in the up-side of (a) indicate each replica's IF direction.

doesn't suffer from the typical ill-conditioning of single-sensor deterministic deconvolution methods.

5.1 Instantaneous Frequency Estimation

The information of the synthesized emitted signal, which obeys to the form

$$s(t) \quad = \quad \mathrm{e}^{\mathrm{j}\varphi_i(t)} \tag{5.7}$$

[where $\varphi_i(t)$ is the instantaneous phase], is contained in $f_i(t)$, apart from a phase term, since the signal's *amplitude modulation* (AM) component is constant [$a_i(t) = 1$, in (B.5)]. For a large variety of signals of the class represented by (5.7), almost the whole signal energy concentrates around the line defined by the points $[t,\ f_i(t)]$, in the TF space[14]. Upon this characteristic, the line $[t,\ f_i(t)]$ can be used in blind deconvolution, in the following manner:

- it provides a TF support that conduces, by inversion, to the source signature estimate;
- it defines an integration domain for $WV_r(t, f)$, which leads to the channel IR estimate.

As the true IF $f_i(t)$ is not available, one must first obtain an estimate $\hat{f}_i(t)$ to be used in the above steps. It is expected that a good estimate of $f_i(t)$ will yield an also good estimate of $s(t)$ and $h(t)$.

To estimate $f_i(t)$, one measure of the received signal's IF, using (B.6), would not be a good procedure to adopt, since the multi-component structure would imply an erroneous measure which, at each time t, would take into account all the present components. Some methods have been proposed for IF estimation, in the past. For example, in [61], a combined Kalman filtering – high-resolution approach is used to track frequency in a multi-component signal. The performance of this method is dependent on the knowledge of the model and measure errors, often not available. Other approaches have been made by application of random signal theory to the WV[13, 25, 34]. Use of the polynomial WV, a class of TFDs which include and extend the WV to higher polynomial orders, has also been made, where maximization with respect to frequency gave the IF estimate, for monocomponent signals[59]. Of course, for multi-component signals, this method wouldn't give yet a meaningful estimate of $f_i(t)$.

In this work, the estimation of $f_i(t)$ will take advantage of signal-dependent distributions, as stated below. Let's designate by $\mathcal{I}(t, f)$ an ideal linear signal-dependent TFD, infinitely concentrated around the IF line, for finite or infinite duration signals with only an FM component. The ideal distribution of the emitted LFM sweep would be[1]

$$\mathcal{I}_s(t, f) = \delta\left[f - (f_0 + \alpha t)\right] \mathrm{rect}\left(\frac{t - \mathcal{T}/2}{\mathcal{T}}\right), \tag{5.8}$$

and, for the received signal,

$$\mathcal{I}_r(t, f) = \sum_{m=1}^{45} a_m^2 \delta\left\{f - \left[f_0 + \alpha\left(t - \tau_m\right)\right]\right\} \mathrm{rect}\left(\frac{t - \tau_m - \mathcal{T}/2}{\mathcal{T}}\right). \tag{5.9}$$

---

[1] The expressions for this ideal distribution are inspired in the WV of an infinite duration LFM signal.

It would be trivial to identify weighted versions of the source distribution $\mathcal{I}_s(t,f)$ in $\mathcal{I}_r(t,f)$, replicated so many times as the number of physical eigenrays. As the first arrivals would be represented in $\mathcal{I}_r(t,f)$ by large amplitudes along the IF of the source signal, maximization of $\mathcal{I}_r(t,f)$ with respect to t, within the band of interest $\mathcal{B}$, would "pick" the strongest arrival, giving an unbiased estimate of $f_i(t)$. Of course, within the available possible non-linear TFDs[2], analysis is constrained by the particular characteristics of the kernel, and by finite data lengths. Nonetheless, it seems reasonable to apply the maximization with respect to t, to a signal-dependent distribution of the received signal, $SD_r(t,f)$, what will give a good estimate of $f_i(t)$, if $SD_r(t,f)$ is a reasonable approximation of $\mathcal{I}_r(t,f)$. Hence, IF estimation was done by maximization of $SD_r(t,f)$ [3] :

$$\left[t,\ \hat{f}_i(t)\right] \ \stackrel{\triangle}{=}\ \{(t,f)\ :\ t=\arg\max_t SD_r\left(t,f\right),\ f\in\mathcal{B}\} \tag{5.10}$$

As stated below, IF estimation was done by use of the signal-dependent distributions CA and RGK, presented in Secs. 4.3.1 and 4.3.2, respectively. Before proceeding to the description of the results, it is important to analyze the characteristics of the estimator of the IF. A signal-dependent distribution is difficult to analyze, due to the variability of the kernel with the signal. However, one can perform a simple analysis on the $WV_s(t,f)$, since $SD_r(t,f)$ is a reasonable approximation of a sum of replicas of $WV_s(t,f)$. According to (5.4), maximization of $WV_s(t,f)$ with respect to time amounts to the resolution of the non-linear equations

$$\begin{aligned} 4\pi\left(\alpha t+f_0-f\right)\left(2\alpha t+f_0-f\right)\cos\left[4\pi t\left(\alpha t+f_0-f\right)\right]-\\ -\alpha\sin\left[4\pi t\left(\alpha t+f_0-f\right)\right]=0, t\in\left[0,0+T/2\right] \end{aligned} \tag{5.11a}$$

$$4\pi\left\{\alpha\left[-2t+T\right]+f-f_0\right\}\left[\alpha t+f_0-f\right]\cos\left[4\pi\left(T-t\right)\left(\alpha t+f_0-f\right)\right]-$$

---

[2] Linear distributions are not mentioned, because they do not present good TF resolution at every frequency[27].

[3] The IF estimate thus obtained is not rigorously a function of t, due to its definition as the 'inverse' of a non-injective function.

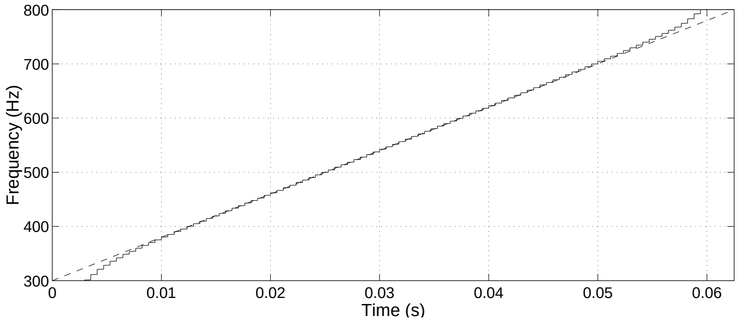

Figure 5.13: IF estimate obtained by global maximization of $WV_s(t,f)$, with respect to time. The dashed line indicates the true IF.

$$-\alpha \sin 4\pi \left(T-t\right)\left[\alpha t+f_0-f\right]=0, t\in\left[T/2,T\right] \tag{5.11b}$$

These non-linear equations are not trivially solved, and possess an infinite number of solutions. However, the solutions that correspond to the global maxima of $WV_s(t,f)$ are represented in Fig. 5.13, as the solutions that conduce to the IF estimate, for the considered synthetic data. It is seen that this IF estimate is systematically biased. However, it is expected that this bias can be attenuated, when maximizing $SD_r(t,f)$, due to the inherent broadening introduced in the signal components.

Beginning with the CA of $r(t)$ –which is a multi-LFM signal–, and for the sake of illustration, the modulation rate α of the emitted LFM signal was supposed to be known; in what concerns kernel's w parameter in (4.22), the unavailability of the information about the time difference between the travel times led to a natural choice of $w \approx 0$, justified by the expected time proximity between the arrivals (characteristic of shallow water environments), as evidenced by the real differences, in Fig. 5.6. Otherwise, if it is known that the emitted signal is an LFM sweep parameterized by α, the procedure (4.25) can be used, for optimal kernel design, with the determination of $\hat{\alpha}$ and w_{opt}. The obtained received signal's CA $CA_r(t,f)$ is depicted in Fig. 5.14. In this reduced-interference TFD, the first 8 arrivals are grouped in a support of large energy. The remaining 37 arrivals, "clustered"

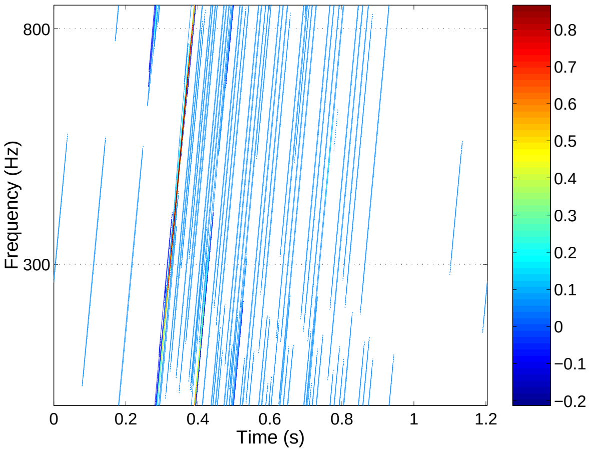

Figure 5.14: Chirp-adapted distribution of the received signal, $CA_r(t, f)$. For illustration purposes, the emitted LFM signal true frequency modulation rate α has been used in the calculation of the distribution. The temporal support and IF range of $r(t)$ are marked.

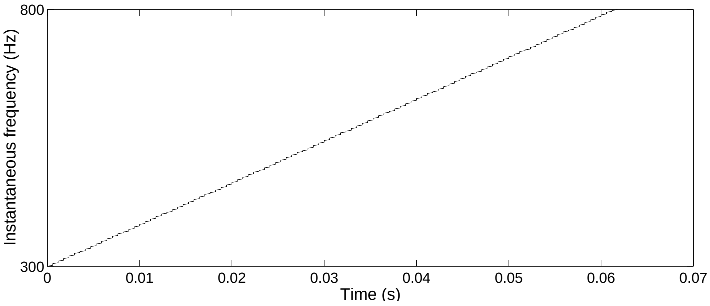

Figure 5.15: Source IF estimate, obtained via $CA_r(t, f)$'s maximization with respect to time. Time is relative to the first instant of maxima, 0.323 s.

in quadruplets, are clearly distinguished. Unavoidingly, the achieved representation of the received signal spans a larger time duration and frequency range than $WV_r(t, f)$ (compare with Fig. 5.12(a)). Unlike the WV, the CA strongly attenuates most of the interferences, while keeping all the important signal components, as discussed in Sec. 4.3.1. The very small value of w implies a loss of concentration of the signal terms, as referred in Sec. 4.3.1. Use of (4.24) and (4.25b) to determine w_{opt} could probably reduce this loss of concentration, by using a larger value for w. However, the loss of concentration has small significance for the instantaneous frequency estimate result, provided that $\mathcal{B}$ is not superior to the LFM's instantaneous frequency range, as will be seen below. Maximization of $CA_r(t, f)$, $f \in \mathcal{B}$, with respect to time, produced the IF estimate shown in Fig. 5.15. Fig. 5.16 shows one of

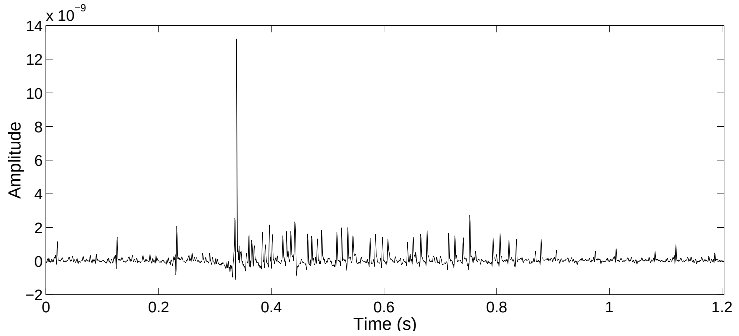

Figure 5.16: One of the functions that were maximized with respect to t, $CA_r(t, 550)$, to estimate the IF of the synthetic source signal.

the maximized functions, $CA_r(t, 550)$. This function clearly exhibits many of the aspects of the channel IR.

The second signal-dependent distribution used for IF estimation was the RGK. For a choice of the kernel volume parameter $\beta = 1$, the RGK of the received signal, $RGK_r(t, f)$, is shown in Fig. 5.17 (a), aside with the corresponding optimal kernel $\Phi_{opt}(\nu, \tau)$ –Fig. 5.17 (b). Global maximization of $RGK_r(t, f)$ with respect to t, gave rise to the IF estimate shown in

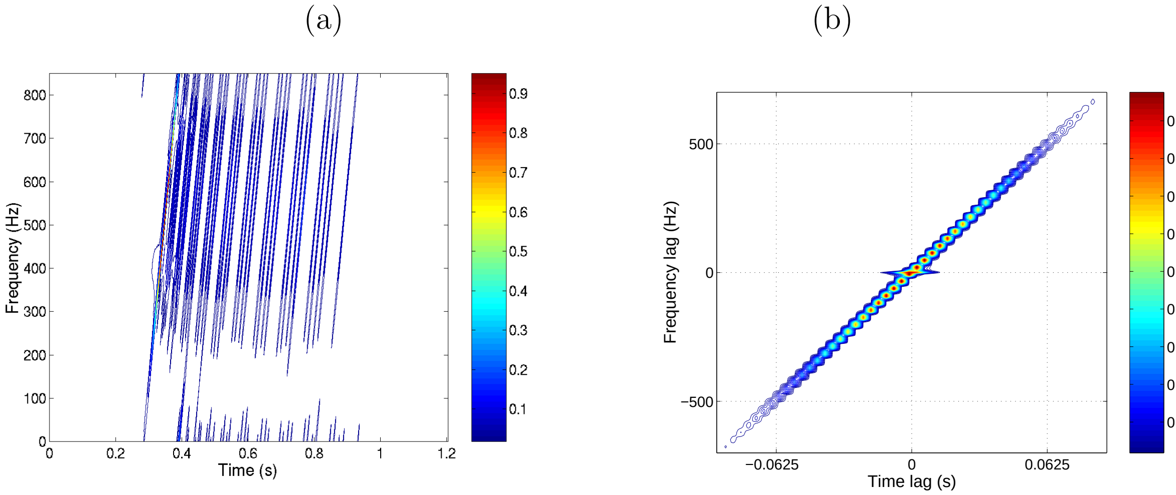

Figure 5.17: RGK signal-dependent distribution of the received synthetic signal, $RGK_r(t, f)$ (a), and contour plot of the corresponding optimal kernel $\Phi_{opt}(\nu, \tau)$ (b).

Fig. 5.18.

As both $CA_r(t, f)$ and $RGK_r(t, f)$ conduced to similar source IF estimates, this last distribution was adopted, since it makes no assumption about the "order" of the modulation,

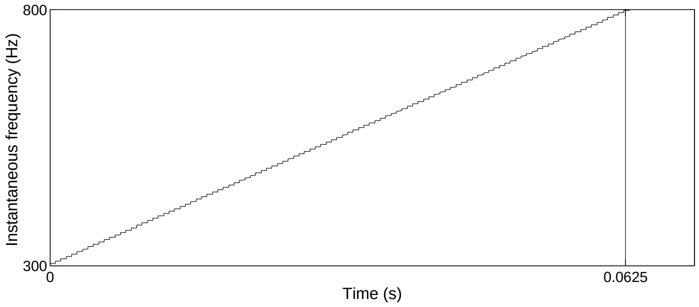

Figure 5.18: Source IF estimate, obtained via $RGK_r(t, f)$'s maximization with respect to time. Time is relative to the first instant of maxima, 0.322 s.

attaining good "performance" in both linear and non-linear modulation cases.

It is likely that the proposed approach will yield a good IF estimate mainly for the class of source signals of the form (5.7), for which $WV_s(t, f)$ is usually concentrated on a continuous region centered on the line defined by the pair $[t,\ f_i(t)]$[14]. However, for non-linear frequency modulation signals, there are always ITs in their auto-WV, what may require a smaller value for the kernel volume β, if some ITs of the auto-WV have greater amplitude than the signal terms. The extension to the case of inconstant amplitude modulation component may be treated the same manner, provided that $a_i(t)$ is a sufficiently smooth function, which weakly increases the spread of the auto-WV along the IF, as will be seen in Chap. 7.

5.2 Source Signature Estimation

This section describes how the source signal can be recovered from a TF representation "extracted" from the WV of the received signal. This synthesis procedure is a transformation from a signal representation in the $t - f$-domain to the t-domain.

WV-based signal synthesis techniques[63] have been developed, which combined smoothing and masking operations to recover signals from noise-contaminated data[27, 71]. The same synthesis techniques have been used to perform multi-component signal separation, in the past[5]. They can isolate a desired component of a multi-component signal, provided that the WV signal term corresponding to the desired signal component does not overlap significantly with other signal terms or ITs. The usual procedure in signal synthesis is to first obtain a modified WV, called a "model function". The solution to the problem is a signal whose WV is closest to the "model function". This obeys to some optimization criteria, from which the least squares approximation[5], the basis function approximation[40] or the outer product approximation[74] are some examples.

Due to the multi-component structure of the received signal, in this work, source signature estimation was performed by multi-component signal separation in the received signal, what allowed to define a "model function" that was transformed to the time domain, first by WV definition inversion, as explained in next subsection, and afterwards by application of a signal synthesis technique named the basis method, explained in the second subsection.

5.2.1 Wigner-Ville Inversion

According to (4.6), the WV is defined as a Fourier transform with respect to τ, of a signal's local auto-correlation function. It is possible to invert this definition, obtaining the following inversion equation:

$$x(t) = \frac{1}{x^*(0)} \int WV_x\left(\frac{t}{2}, f\right) \mathrm{e}^{\mathrm{j}2\pi f t} \mathrm{d}f. \tag{5.12}$$

It is important to remark that if $WV_x(t,f)$ in (5.12) is replaced by some function $T(t,f)$, (5.12) represents WV inversion if and only if $T(t,f)$ is an auto-WV of some time signal (or WV realizable[67]). In a discrete-time setting [see (4.7)], both the values $x(0)$ and $x(1)$ must be known, to exactly recover $x(t)$. If, instead of $WV_x(t,f)$, one reasonable approximation $\tilde{WV}_x(t,f)$ of $WV_x(t,f)$ is available, it is expected that the insertion of $\tilde{WV}_x(t,f)$ into (5.12) will give a reasonable approximation of $x(t)$. This reasoning has given a first motivation to estimate the emitted signal, as explained in the following. Departing from the estimate $\hat{f}_i(t)$, an estimate $\tilde{WV}_s(t,f)$ of $WV_s(t,f)$ was "extracted" from $WV_r(t,f)$, following the definition

$$\tilde{WV}_s(t,f) \quad = \quad M(t-\tau_s,f)WV_r(t,f), \tag{5.13}$$

where $M(t,f)$ is a function concentrated around $\left[t,\ \hat{f}_i(t)\right]$, designated herein by *mask*, that 'extracts' $\tilde{WV}_s(t,f)$. The estimate $\tilde{WV}_s(t,f)$ will be named *model function*. The definition of $M(t,f)$ takes into account WV's resolution, for finite-duration signals (cf. Sec. 4.2.1):

$$M(t,f) = \begin{cases} 1, \ f = f_i(t) \pm \frac{1}{2T} \\ 0, \ f \neq f_i(t) \pm \frac{1}{2T} \end{cases}, \quad t \in [t_1, t_2]\,, \quad f \in [f_1, f_2]\,. \tag{5.14}$$

The source estimate is defined as the result of the inversion of $\tilde{WV}_s(t,f)$ to the time domain, using (5.12). It is expected that if $\tilde{WV}_s(t,f) \approx a\, WV_s(t-\tau_s,f),\ a \in \mathbb{R}$, then a good estimate $\hat{s}(t)$ can be obtained. The TF inversion is constrained essentially by τ_s: if τ_s is the location of some echo well separated from adjacent echoes, it is expected that the TF domain centered in this echo will give a good estimate of the source signal.

A reference estimate $\hat{s}_{ref}(t)$ has been obtained, by inversion of the product of the WV of the true source signal $s(t)$, by $M(t,f)$, *i.e.*, inversion of $M(t,f)WV_s(t,f)$. According to (5.14), the width of $M(t,f)$ in the direction of f was $\frac{1}{T} = \frac{1}{0.0625s} = 16$ Hz. The reference estimate (real part) is depicted in Fig. 5.19. The obtained correlation coefficient between $s(t)$

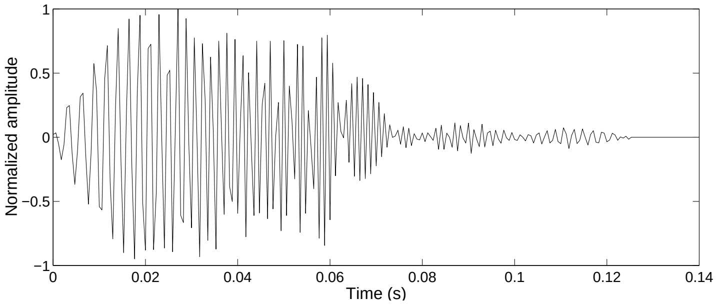

Figure 5.19: Reference source estimate, obtained by WV inversion of $M(t,f)WV_s(t,f)$.

and $\hat{s}_{ref}(t)$ was 0.966. This measure will be taken as a reference for subsequent estimation results, since it corresponds to the best estimate that can be obtained.

Results

First, a source signal estimate was obtained, by TF inversion of a model function $\tilde{WV}_s(t,f)$ centered on the first arrivals, with $M(t,f)$ defined as above, for the calculus of the reference estimate. This model function is depicted in Fig. 5.20. The real part of the estimated source signal $\hat{s}_1(t)$, obtained from inversion of the above function, is shown in Fig. 5.21. The normalized correlation coefficient between $s(t)$ and $\hat{s}_1(t)$ is 0.750. The WV of the estimate $\hat{s}_1(t)$ is seen in Fig. 5.22. The difference between this WV and the non-valid WV model function in Fig. 5.20 is not significant. Alternatively, and if the channel estimate is already available (see Fig. 5.31), one later arrival can be selected, to avoid the superposition of the early arrivals in the model function. The choice of the last arrival, at 0.523 s (relative time) (cf. Tab. 5.2), has given the estimate $\hat{s}_{WI,l}(t)$, whose correlation with $s(t)$ has a

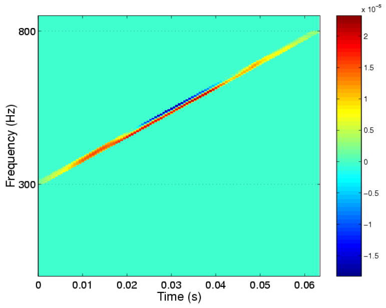

Figure 5.20: Model function $\tilde{WV}_s(t,f)$ considered for first arrivals-based source estimation.

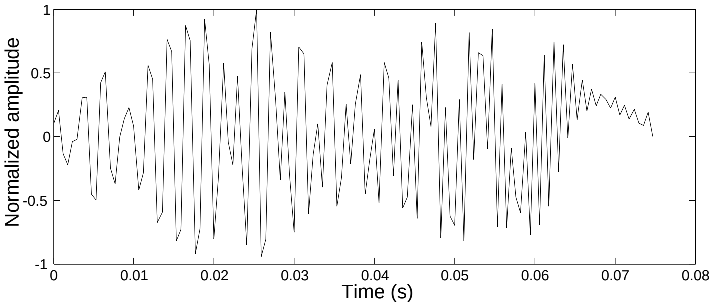

Figure 5.21: First group of arrivals-based source estimate –real part of $\hat{s}_{WI,f}(t)$–, by WV inversion.

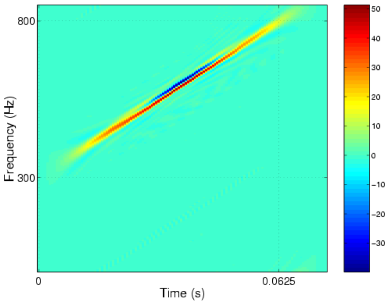

Figure 5.22: WV of the first arrivals-based estimated source signal $\hat{s}_1(t)$, by WV inversion.

maximum value of 0.797. This is an improvement to the value 0.750 corresponding to the first arrivals-based source estimate, but only possible if the channel estimate is available.

Here, one aspect must be pointed out: the quality of the estimate is conditioned on the choice of the TF arrival to invert. The previous results show that the more isolated arrival conduces to a greater quality of the corresponding source estimate. Unfortunately, in noisy real data, it is difficult to determine the instants of later arrivals, as will be seen in Chap. 7, and one finds here a tradeoff in source estimation. The dependence of the quality of the source estimate on the position of $M(t-\tau_s, f)$, *i.e.*, on the value τ_s, is illustrated in Fig. 5.23. There is some evidence that the quality of the estimate increases when τ_s coincides with τ_m, $m = 1, \ldots, M$. Not surprisingly, the maximum value of the estimate quality occurs for the last arrival, at $\tau_s = 0.860$ s (relative to t_0). This is explained by the absence of neighbour arrivals and ITs in the model function, due to the separation of the last peak of

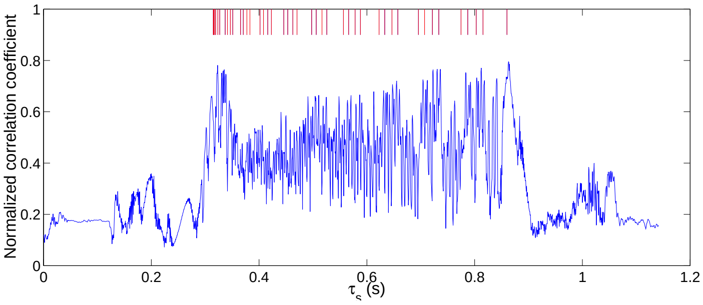

Figure 5.23: Source estimate quality as a function of τ_s in $M(t-\tau_s, f)$. The estimate was obtained via WV inversion, in simulated data. Red lines indicate the instants of the arrivals.

$h(t)$ relatively to the other peaks, as seen in Fig. 5.6.

The source estimate is also conditioned by the width of $M(t, f)$. It is expected that if $M(t, f)$ is centered on a well-resolved arrival, the quality of the estimate will increase with the width of $M(t, f)$. For the case of a non-resolved arrival, it is difficult to find a relation between the mentioned width and the quality of the source estimate.

5.2.2 The Basis Method

This section is devoted to the explanation of the theory and application of the basis method, a bilinear signal synthesis method that makes use of a signal subspace constraint that improves signal synthesis when it depends on the non-valid WV model function presented in the above subsection. The reader is referred to [29], for a more detailed explanation of the method. The basis method was applied in this work, by the following steps(Fig. 5.24):

Step 1: Calculation of $WV_r(t, f)$;

Step 2: Modification of $WV_r(t, f)$ to generate the model function $\tilde{WV}_s(t, f)$;

Step 3: Synthesis of the output signal $\hat{s}_{BM}(t)$ from $\tilde{WV}_s(t, f)$.

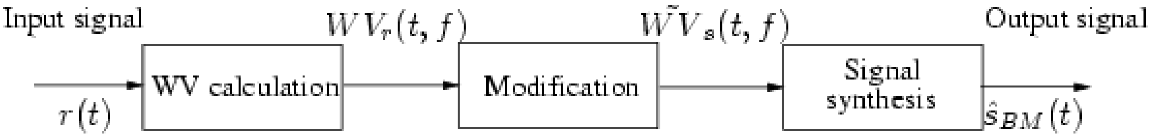

Figure 5.24: Scheme illustrating bilinear signal synthesis of $\hat{s}_{BM}(t)$, departing from $r(t)$.

In [29], QTFDs are considered in a general framework, depending on 2 parameters which may be time t, frequency f, time-lag τ and/or frequency-lag ν. Here, the dependence will relate to time and frequency. Any QTFD can be written as

$$T_{x,y}(t, f) = \int_{t_1} \int_{t_2} u_T (t, f; t_1, t_2) \, q_{x,y} (t_1, t_2) \, \mathrm{d}t_1 \, \mathrm{d}t_2, \tag{5.15}$$

where

$$q_{x,y}\left(t_1,t_2\right) \quad = \quad x\left(t_1\right)y^*\left(t_2\right) \tag{5.16}$$

is the outer product of the signals $x(t)$ and $y(t)$, and $u_T\left(t,f;t_1,t_2\right)$ is the kernel function specifying the QTFD $T_{x,y}(t,f)$[73].

The problem under consideration is the synthesis of a signal $x(t)$, based on the (approximate) specification of its QTFD $T_x(t,f)$. Let $\tilde{T}(t,f)$ be a given *model function* [a model function $\tilde{WV}_s(t,f)$ has already been considered in the previous subsection]. It is intended to find a signal $x(t)$ such that its QTFD $T_x(t,f)$ equals the model function $\tilde{T}(t,f)$. Unfortunately, the model will not, in general, be a valid QTFD of any signal. In this situation, it is natural to look for the signal $x(t)$ whose QTFD $T_x(t,f)$ is closest to the model $\tilde{T}(t,f)$, in the sense that it minimizes the "synthesis error"

$$\epsilon_x \quad = \quad \left|\left|\tilde{T}-T_x\right|\right|. \tag{5.17}$$

By squaring the synthesis error, one must solve the minimization problem

$$\min_x \epsilon_x^2 \quad = \quad \min_x \left|\left|\tilde{T}-T_x\right|\right|^2, \tag{5.18}$$

where

$$\left|\left|\tilde{T}-T_x\right|\right|^2 \quad \triangleq \quad \int_f\int_t \left|\tilde{T}(t,f)-T_x(t,f)\right|^2 \mathrm{d}t\;\mathrm{d}f. \tag{5.19}$$

The minimization (5.18) is termed the *bilinear signal synthesis problem.* A subspace-constrained version of the bilinear signal synthesis problem shall also be formulated, where the signal $x(t)$ is constrained to be an element of a given linear signal subspace $\mathfrak{S}$:

$$\min_{x\in\mathfrak{S}} \epsilon_x \quad = \quad \min_{x\in\mathfrak{S}} \left|\left|\tilde{T}-T_x\right|\right|. \tag{5.20}$$

There are two reasons for including a subspace constraint. First, the subspace constraint can be used for imposing certain properties on the synthesis result $x(t)$: by prescribing a suitable signal space $\mathfrak{S}$, $x(t)$ can be forced to be band-limited, analytic, time-limited, causal, symmetric, etc. Second, in some instances, the structure of the QTFD $T_x(t, f)$ calls for a signal subspace constraint: for example, discrete-time WV suffers from severe aliasing effects unless the signals are restricted to a suitably defined subspace of band-limited signals[11].

The bilinear signal synthesis problem is solved for arbitrary (sub-)space $\mathfrak{S}$ and arbitrary QTFDs possessing an unitary property on the space $\mathfrak{S}$. The space $\mathfrak{S}$ may be defined by an orthonormal basis $\{e_k(t)\}$ spanning $\mathfrak{S}$ such that every $x(t) \in \mathfrak{S}$ can be represented as

$$x(t) = \sum_k \alpha_k e_k(t), \quad \text{with} \quad \alpha_k = \langle x|e_k\rangle = \int_t x(t)e_k^*(t)\mathrm{d}t. \tag{5.21}$$

Orthonormality of the basis signals is expressed by $\langle e_k|e_{k'}\rangle = \delta_{kk'}$, where $\delta_{kk'}$ is the Kronecker delta symbol. An important issue regarding signal spaces is that the linear signal space $\mathfrak{S}$ induces a corresponding linear T-domain space $\mathfrak{S}_T \subseteq L_2\left(\mathrm{I\!R}^2\right)$ which is defined as the linear space of all linear combinations of cross-QTFD outcomes $T_{x,y}(t, f)$, with $x(t),\ y(t) \in \mathfrak{S}$. Now, if a QTFD $T_{x,y}(t, f)$ is $\mathfrak{S}$-unitary, then an orthonormal basis $\{T_{kl}\,(t, f)\}$ of $\mathfrak{S}_T$ is

$$T_{kl}(t, f) \quad = \quad T_{e_k,e_l}(t, f), \tag{5.22}$$

where $\{e_k(t)\}$ is any orthonormal basis of $\mathfrak{S}$.

As shown in [29], the squared version of the minimization problem (5.20) is equivalent to

$$\min_{x\in\mathfrak{S}} \epsilon^2_{\mathfrak{S},x} \quad = \quad \min_{x\in\mathfrak{S}} \left|\left|\tilde{T}_{\mathfrak{S}} - T_x\right|\right|^2, \tag{5.23}$$

where $\epsilon^2_{\mathfrak{S},x}$ and $\tilde{T}_{\mathfrak{S}}$ are the synthesis error and model's projections on $\mathfrak{S}_T$, respectively. According to (5.21), the subspace constraint is incorporated by representing the signal $x(t)$

in terms of the basis $\{e_k(t)\}$ spanning $\mathfrak{S}$:

$$x(t) \;=\; \sum_{k=1}^{N_b} \alpha_k e_k(t), \tag{5.24}$$

where N_b, the dimension of the space $\mathfrak{S}$, may be infinite. This induces a corresponding T-domain representation of $T_x(t,f)$ in terms of the induced T-domain basis $\{T_{kl}(t,f)\}$:

$$T_x(t,f) = \sum_{k=1}^{N_b}\sum_{l=1}^{N_b} \gamma_{kl} T_{kl}(t,f), \quad \text{with} \quad \gamma_{kl} = \alpha_k \alpha_l^*. \tag{5.25}$$

The model projection $\tilde{T}_{\mathfrak{S}}(t,f)$, too, is an element of the induced T-domain space $\mathfrak{S}_T$, and can thus be represented in terms of the induced T-domain basis $\{T_{kl}(t,f)\}$:

$$\tilde{T}_{\mathfrak{S}}(t,f) = \sum_{k=1}^{N_b}\sum_{l=1}^{N_b} \tilde{\gamma}_{kl} T_{kl}(t,f), \quad \text{with} \quad \tilde{\gamma}_{kl} = \left\langle \tilde{T}_{\mathfrak{S}} | T_{kl} \right\rangle, \tag{5.26}$$

where $< \cdot >$ denotes the 2D functional inner product operator. Using (5.25) and (5.26), and the orthonormality of the induced T-domain basis $\{T_{kl}\,(t,f)\}$, the (squared) synthesis error can be developed as

$$\begin{aligned} \epsilon^2_{\mathfrak{S},x} \;&=\; \left|\left|\tilde{T}_{\mathfrak{S}} - T_x\right|\right|^2 = \left|\left|\sum_{k=1}^{N_b}\sum_{l=1}^{N_b} \left(\tilde{\gamma}_{kl} - \alpha_k \alpha_l^*\right) T_{kl}\right|\right|^2 \\ &=\; \sum_{k=1}^{N_b}\sum_{l=1}^{N_b} |\tilde{\gamma}_{kl} - \alpha_k \alpha_l^*|^2 = \left|\left|\tilde{\mathbf{\Gamma}} - \boldsymbol{\alpha}\boldsymbol{\alpha}^H\right|\right|_F^2, \end{aligned} \tag{5.27}$$

with the $(N_b \times N_b)$-dimensional coefficient matrix $\tilde{\mathbf{\Gamma}} = (\tilde{\gamma}_{kl})$ and the N_b-dimensional coefficient vector $\boldsymbol{\alpha} = (\alpha_k)$; $||\cdot||_F$ denotes the Euclidean matrix norm (Frobenius norm), and ^{H} stands for complex transposition. The dyadic-product matrix $\boldsymbol{\alpha}\boldsymbol{\alpha}^H$ is Hermitian and rank 1; the matrix $\tilde{\mathbf{\Gamma}}$, on the other hand, is generally not Hermitian but can be split into a Hermitian component $\tilde{\mathbf{\Gamma}}_H$ and an anti-Hermitian component $\tilde{\mathbf{\Gamma}}_A$. With this, the squared synthesis error can be decomposed as:

$$\begin{aligned} \epsilon^2_{\mathfrak{S},x} \;&=\; \left|\left|\tilde{\mathbf{\Gamma}} - \boldsymbol{\alpha}\boldsymbol{\alpha}^H\right|\right|_F^2 = \left|\left|\left(\tilde{\mathbf{\Gamma}}_H + \tilde{\mathbf{\Gamma}}_A\right) - \boldsymbol{\alpha}\boldsymbol{\alpha}^H\right|\right|_F^2 \\ &=\; \left|\left|\tilde{\mathbf{\Gamma}}_H - \boldsymbol{\alpha}\boldsymbol{\alpha}^H\right|\right|_F^2 + \left|\left|\tilde{\mathbf{\Gamma}}_A\right|\right|_F^2 = \epsilon^2_{\mathfrak{S}H,x} + \epsilon^2_{\mathfrak{S}A}, \end{aligned} \tag{5.28}$$

where the "anti-Hermitian" error component $\epsilon_{\mathfrak{S}A} = \left|\left|\tilde{\mathbf{\Gamma}}_A\right|\right|_F$ does not depend on $x(t)$ (*i.e.*, on $\boldsymbol{\alpha}$), and can hence be disregarded for minimization. Thus, it remains to minimize the "Hermitian" error component

$$\epsilon_{\mathfrak{S}H,x} = \left|\left|\tilde{\mathbf{\Gamma}}_H - \boldsymbol{\alpha}\boldsymbol{\alpha}^H\right|\right|_F \tag{5.29}$$

in the absence of any constraint [note that the constraint $x(t) \in \mathfrak{S}$ has been taken account of by representing $x(t)$ according to (5.24)]. Minimization of (5.29) amounts to the approximation of the Hermitian matrix $\tilde{\mathbf{\Gamma}}_H$ by a dyadic product $\boldsymbol{\alpha}\boldsymbol{\alpha}^H$. With μ_k and $\mathbf{v}_k$ denoting, respectively, the real-valued eigenvalues sorted by decreasing value, and the corresponding orthonormal eigenvectors of the Hermitian matrix $\tilde{\mathbf{\Gamma}}_H$, a derivation presented in [29] yields the solution

$$\boldsymbol{\alpha}_{opt} = \sqrt{\mu_1}\mathrm{e}^{\mathrm{j}\varphi}\mathbf{v}_1, \tag{5.30}$$

where it was assumed that the largest eigenvalue μ_1 is nonnegative, and φ is an arbitrary phase constant. Inserting (5.30) and the spectral decomposition

$$\tilde{\mathbf{\Gamma}}_H = \sum_{k=1}^{N_b} \mu_k \mathbf{v}_k \mathbf{v}_k^H \tag{5.31}$$

into (5.29), the residual synthesis error is obtained as

$$\epsilon^2_{\mathfrak{S}H,\min} = \epsilon^2_{\mathfrak{S}H,x_{opt}} = \left|\left|\textstyle\sum_{k=2}^{N_b} \mu_k \mathbf{v}_k \mathbf{v}_k^H\right|\right|_F^2 = \sum_{k=2}^{N_b} \mu_k^2, \tag{5.32}$$

where the orthonormality of the eigenvectors $\mathbf{v}_k$ has been used.

The basis method can finally be summarized as follows:

Step 1: Calculate the expansion coefficients of the model projection $\tilde{T}_{\mathfrak{S}}(t,f)$:

$$\tilde{\gamma}_{kl} = \left\langle \tilde{T}_{\mathfrak{S}} | T_{kl} \right\rangle = \iint \tilde{T}_{\mathfrak{S}}(t,f)\, T^*_{kl}(t,f)\,\mathrm{d}t\,\mathrm{d}f, \quad 1 \le k,l \le N_b; \tag{5.33}$$

Step 2: Form the matrix $\tilde{\mathbf{\Gamma}} = (\tilde{\gamma}_{kl})$, and take its Hermitian component

$$\tilde{\mathbf{\Gamma}}_H = \frac{1}{2}\left(\tilde{\mathbf{\Gamma}} + \tilde{\mathbf{\Gamma}}^H\right); \tag{5.34}$$

Step 3: Calculate the largest eigenvalue μ_1 and the associated (normalized) eigenvector $\mathbf{v}_1$ of $\tilde{\mathbf{\Gamma}}_H$; if $\mu_1 \geq 0$, then the synthesis solution is given by [cf. (5.24)]

$$x_{opt}(t) \quad = \quad \sum_{k=1}^{N_b} \alpha_{opt,k} e_k(t). \tag{5.35}$$

An open problem is the choice of the best basis $\{e_k(t)\}$ and the number of basis functions N_b. This choice can be based on *a priori* information about the source signal, or, as previously said, on properties that are to be imposed on the synthesis result. In what concerns the number N_b, the discrete-time version of the basis method implemented in the present work has shown that a number N_b of half the number of data points of the synthesis result $x_{opt}(t)$ was sufficient to decompose $x_{opt}(t)$ in the basis $\{e_k(t)\}$, with a good approximation.

Ambiguity of the Signal Synthesis Solution

The solution to the signal synthesis problem (5.20) is not uniquely defined. Let us assume that the QTFD $T_x(t,f)$ is invariant with respect to some signal transformation $\mathfrak{T}$ such that $T_{\mathfrak{T}x}(t,f) = T_x(t,f)$ for all $x(t) \in \mathfrak{S}$. Let's suppose also that $x(t) \in \mathfrak{S}$ entails $(\mathfrak{T}x)(t) \in \mathfrak{S}$. Then, if $x_0(t) \in \mathfrak{S}$ is a solution to (5.20), $(\mathfrak{T}x_0)$ is a solution as well since it is also an element of $\mathfrak{S}$ and achieves the same minimal synthesis error. It is thus seen that any invariance of the QTFD with respect to a space-preserving signal transformation entails a corresponding ambiguity of the signal synthesis solution. Now, in the case of an $\mathfrak{S}$-unitary QTFD, only a very trivial and comparatively harmless invariance exists. In fact, it can be shown that

$$T_{x_1}(t,f) \quad = \quad T_{x_2}(t,f), \tag{5.36}$$

with $x_1(t),\ x_2(t) \in \mathfrak{S}$ then implies

$$x_2(t) \quad = \quad x_1(t)\mathrm{e}^{\mathrm{j}\varphi}, \tag{5.37}$$

with φ being an arbitrary phase constant.

A second ambiguity may exist, if the basis $\{e_k(t)\}$ that defines $\mathfrak{S}$ is not unique. In this case, it is likely that the synthesis result will not be very sensitive to a change of basis, provided that the number N_b is sufficient to constrain the result $x_{opt}(t)$ to be an element of $\mathfrak{S}$, with good approximation, for each basis $\{e_k(t)\}$.

Results

For application of the basis method, the considered signal space $\mathfrak{S}$ was the subspace $\mathfrak{B}$ of band-limited signals, with the band $[f_1, f_2] = [0, f_s/2]$. This is a natural band limitation, when dealing with discrete-time signals, and as a first study of method's performance. It follows from the sampling theorem[57] that an orthonormal basis $\{e_k(t)\}$ spanning $\mathfrak{B}$ is given by

$$e_k(t) = h(t - k/\upsilon), \quad -\infty < k < \infty, \tag{5.38}$$

where

$$h(t) \quad = \quad \upsilon\ \mathrm{e}^{\mathrm{j}2\pi f_0 t}\mathrm{sinc}(\upsilon t) \tag{5.39}$$

is the impulse response of an ideal bandpass filter with passband $[f_1, f_2]$; here, $f_0 = (f_1 + f_2)/2$ and $\upsilon = f_2 - f_1$ denote the passband's center frequency and bandwidth, respectively. The chosen number N_b of basis functions was half the number of data points, $N_b = 1024$. A discrete-time version of the basis method was implemented, replacing the integrals in the definition of the expansion coefficients (5.33), by sums. The considered model function was the same as in previous section, $\tilde{WV}_s(t, f)$ in Fig. 5.20.

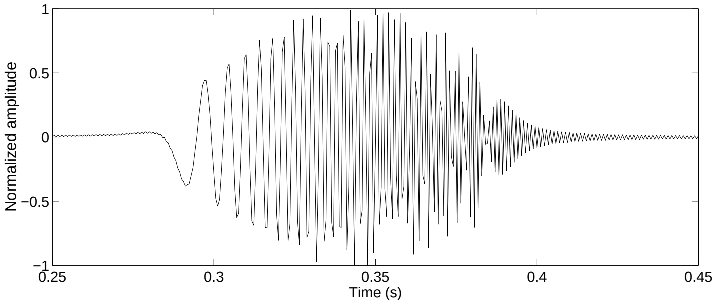

Figure 5.25: Source estimate –real part of $\hat{s}_{BM}(t)$–, in synthetic data. This estimate was obtained via the basis method, taking as input the model function in Fig. 5.20.

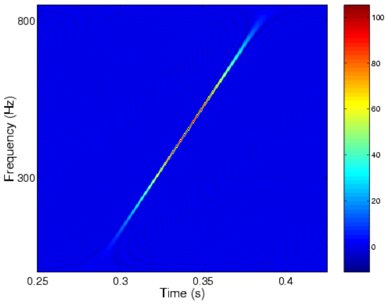

Figure 5.26: WV of $\hat{s}_{BM}(t)$.

The obtained source estimate [the real part of the analytic signal $\hat{s}_{BM}(t)$] is depicted in Fig. 5.25, and corresponds to a cross-correlation coefficient of 0.793 with the true source signal in Fig. 5.7. The maximum of the correlation between $s(t)$ and $\hat{s}_{BM}(t)$ is 0.856 (represented by the dashed line in Fig. 5.27). This value represents a superior quality relative to the "naive" inversion in Sec. 5.2.1, which gave a correlation maximum of 0.750. The WV that best approximates the model function $\tilde{WV}_s(t,f)$, *i.e.*, the WV of the estimate $\hat{s}_{BM}(t)$, is depicted in Fig. 5.26. The band limitation signal constraint is reflected not only in the increased signal duration, as can be seen already in Fig. 5.25, but also in an increase of the IF range, since the limitation to $[0, f_s/2]$ let freedom to the estimate's IF to extend within the whole [0, 850] Hz interval, in order to attain the minimum (5.32). It is difficult to predict what would be the effect of increasing f_s, on the synthesis result.

In view of the ambiguity of the signal synthesis solution afore-mentioned, all the complex signals $\hat{s}_{BM}(t)\mathrm{e}^{\mathrm{j}\varphi}$ are solutions to the signal synthesis problem[cf. (5.36)–(5.37)]. However,

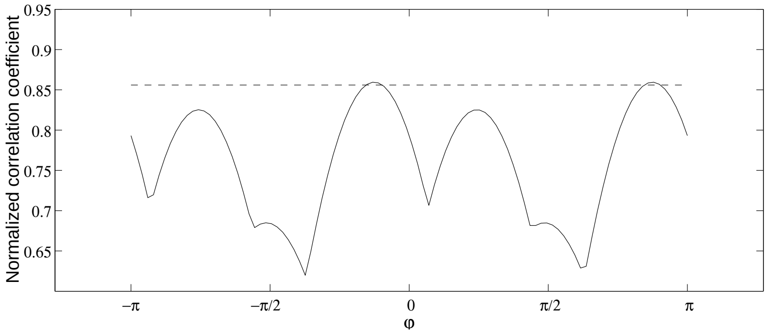

Figure 5.27: Evolution of the correlation coefficient between the real parts of $s(t)$ and $\hat{s}_{BM}(t)$, as a function of φ, in simulated data. The dashed line indicates the correlation between $s(t)$ and $\hat{s}_{BM}(t)$.

it is often necessary to recover the real emitted signal [real part of $s(t)$ in (5.2)], and Fig. 5.27 shows the correlation coefficient between the real parts of $s(t)$ and $\hat{s}_{BM}(t)$ as a function of φ. The maximum value of this function is 0.860.

5.3 Channel Estimation

This section describes the estimation of the parameters $\{a_m,\ \tau_m;\ m = 1,\ ...,\ M\}$ that characterize the channel's IR. In the first subsection, the classical matched-filter is mentioned. Afterwards, the TF channel estimator will be presented as an equivalent TF formulation of the matched-filter. Last subsection treats channel estimation solved by matched-filtering with the source estimate.

5.3.1 Matched-Filter

The matched-filter (MF) is a well-known filter that can be used in the identification of multiple time-delay attenuation channels, when the input and received signals are available[37]. The matched-filter simply calculates the correlation function between the known input signal and the received signal. In a discrete-time setting, the estimation of the amplitude vector **a** is shown to be equivalent to the least squares estimation or, under the Gaussian white noise assumption, to a generalized maximum likelihood problem[37].

Taking the signals involved in this work, the MF output is the correlation function

$$\Gamma_{s_r,r_r,t}(\tau) = \int s_r(t)r_r(t+\tau)\mathrm{d}t. \tag{5.40}$$

For each particular true time-delay value $\tau = \tau_p,\ 1 \leq p \leq M$, the correlation takes the value

$$\Gamma_{s_r,r_r,t}(\tau_p) \quad = \quad a_p E_s + a_m \sum_{\substack{m=1 \\ m \neq p}}^{M} \Gamma_{s_r,t}(\tau_p - \tau_m), \tag{5.41}$$

where E_s is the energy of $s_r(t)$. For values τ_p such that $\Gamma_{s_r,r_r,t}\left(\tau_p - \tau_m\right) = 0,\ \forall m \neq p$, the matched-filter output is thus proportional to the amplitude a_p of the channel, at time-lag τ_p. The condition $\Gamma_{s_r,r_r,t}\left(\tau_p - \tau_m\right) = 0$ is verified if the separation between the time-delays τ_p and τ_m is greater than the duration of the auto-correlation function $\Gamma_{s_r,t}(\tau)$. If this is the case for all the time-delays pairs, the main peaks of $\Gamma_{s_r,r_r,t}(\tau)$ are located in $\tau_m,\ m = 1,\ \ldots,\ M$, and the matched-filter is an optimum estimator of the channel amplitudes a_m and time--delays τ_m[17]. If there are some pairs of time-delays separated by less than the duration of $\Gamma_{s_r,r_r,t}(\tau)$, it is not possible to resolve all the individual signals from the MF output, and the overlap introduces errors into the amplitude and arrival time estimates. The effects of the overlap can be reduced by using a broader bandwidth source[17]. For the data considered in this work, the source bandwidth of ≈ 500 Hz has revealed to be acceptable, for channel estimation. Often, the channel estimate is based on the envelope of the cross-correlation function, since it is a low-pass signal[44].

For the considered simulation case, the channel estimate obtained by matched-filtering is depicted in Fig. 5.28. In practice, to identify the impulses of the IR, in the MF estimate, a threshold can be fixed on the cross-correlation envelope, to then take all peaks greater than the specified threshold as the desired estimates, forming the vectors $\hat{\mathbf{a}}_{red}$ and $\hat{\boldsymbol{\tau}}_{red}$ containing

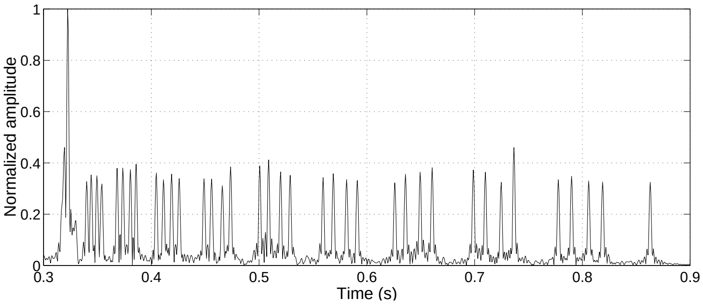

Figure 5.28: Channel estimate obtained by classic matched-filtering: normalized envelope of the cross-correlation function between emitted and received signals (the well-known *arrival pattern*). Data correspond to the simulated scenario.

the resolved amplitudes and time-delays, respectively. This procedure allows to identify, at least, all the arrivals separated in time by more than the imposed resolution, *i.e.*, all but the first peaks. As said before, the resolution depends directly on the source signal's bandwidth, and for the 300-800 Hz LFM, it is found that it is expected to resolve all the peaks separated by more than $\approx$ 2.07 ms (indicated in Fig. 5.6), as given by the first zero (C.6) of the LFM's autocorrelation function. In practice, the first 8 impulses of $h(t)$ are not resolved, and the quality of the channel estimate will refer only to the remaining 37 impulses. The corresponding estimated amplitudes and time-delays are summarized in Tabs. 5.1 and 5.2, respectively. One normalized measure of the quality of the results can be given as

$$\rho_{h,a} = 1 - \frac{||\mathbf{a}_{red} - \hat{\mathbf{a}}_{red}||}{2}; \tag{5.42a}$$

$$\rho_{h,\tau} = 1 - \frac{||\boldsymbol{\tau}_{red} - \hat{\boldsymbol{\tau}}_{red}||}{2}, \tag{5.42b}$$

where the vectors are of unit norm. The performance of the MF was quantified by $\rho_{h,a} = 0.9730$ and $\rho_{h,\tau} = 0.9997$, for amplitude and time-delay estimation, respectively.

5.3.2 Time-Frequency Formulation of the Matched-Filter

This section describes a procedure for channel estimation, for the LFM emitted signal, where the IF estimate obtained in Sec. 5.1 was used in conjunction with a TF formulation of correlation. The channel estimate was obtained either by filtering of $WV_r(t,f)$ or $RGK_r(t,f)$, as will be described in the following.

Wigner-Ville Coherent Integration

As mentioned in Tab. 4.2, the WV obeys to Moyal's formula[20]:

$$\iint_{-\infty}^{\infty} WV_{x_1,x_2}(t,f)WV^*_{x_3,x_4}(t,f)\ \mathrm{d}t\ \mathrm{d}f = \left[\int_{-\infty}^{\infty} x_1(t)x_3^*(t)\ \mathrm{d}t\right]\left[\int_{-\infty}^{\infty} x_2(t)x_4^*(t)\ \mathrm{d}t\right]^* \tag{5.43}$$

For the particular cases $x_1(t) = r(t)$, $x_2(t) = r(t)$, $x_3(t) = s(t+\tau)$ and $x_4(t) = s(t)$, one gets:

$$\iint_{-\infty}^{\infty} WV_r(t,f)WV^*_{s(t+\tau),s(t)}(t,f)\ \mathrm{d}t\ \mathrm{d}f = \left[\int_{-\infty}^{\infty} r(t)s^*(t+\tau)\ \mathrm{d}t\right]\left[\int_{-\infty}^{\infty} r(t)s^*(t)\ \mathrm{d}t\right]^*. \tag{5.44}$$

This shows that correlation can be performed in the TF domain. This constitutes the TF formulation of the MF. Suppose the emitted signal is an infinite-duration LFM signal. In this case, the left-hand side of (5.44) amounts crudely to an integration of $WV_r(t,f)$ along the IF of $s(t)$. Now, in the case of a finite duration LFM signal, that is the case in simulated data, integration of $WV_r(t,f)$ along $f_i(t)$ gives an approximate expression to (5.44). This can be seen by integrating $WV_s(t,f)$, along $f_i(t-\tau_i)$, what can be viewed as a coherent integration:

$$\Gamma_{CI} = \int_{-\infty}^{\infty} WV_s\left[t, f_0 + \alpha\left(t-\tau\right)\right]\mathrm{d}t \quad = \quad \left[\mathcal{T}\operatorname{sinc}\left(\pi\alpha\tau\mathcal{T}\right)\right]^2. \tag{5.45}$$

Taking into account the envelope of the auto-correlation of an LFM signal (C.5), one can see that, for $\tau_i = 0$ and $\tau = 0$, $\Gamma_{CI} = 4a_\Gamma^2(0)$. Moreover, the first zero of (5.45) is

$$b = \frac{1}{\alpha\mathcal{T}}, \tag{5.46}$$

that is an approximation to z_1 in (C.6), when

$$\Delta f \gg \frac{4}{\mathcal{T}}. \tag{5.47}$$

This means that channel estimation performed by TF coherent integration attains essentially the same resolution as the MF, when the condition (5.47) is verified. Fig. 5.29 compares

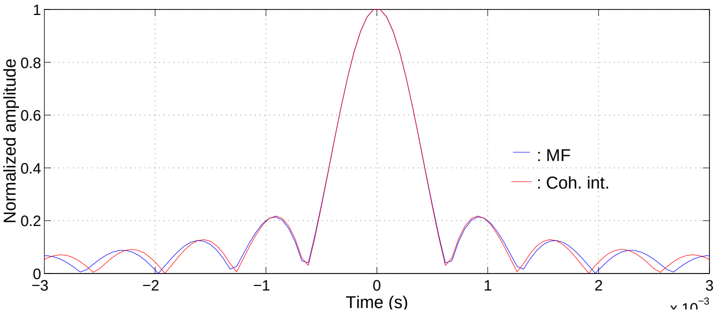

Figure 5.29: Comparison of the LFM auto-correlation envelope (blue line), with the function obtained via coherent integration on the WV of the LFM, for the simulated data. Here, $\alpha = 8000$ Hz/s and T=0.0625 s.

normalized versions of the functions (C.5) and (5.45), where it can be seen the similarity between the two corresponding channel estimators. When the condition (5.47) is not verified, the zeros of (5.45) will be closer than the zeros of (C.5), while the side-lobes of (5.45) will be greater than their homologous in (C.5), as illustrated in Fig. 5.30, for the particular case of $\Delta f = 20$ Hz and $4/\mathcal{T} = 64$ Hz.

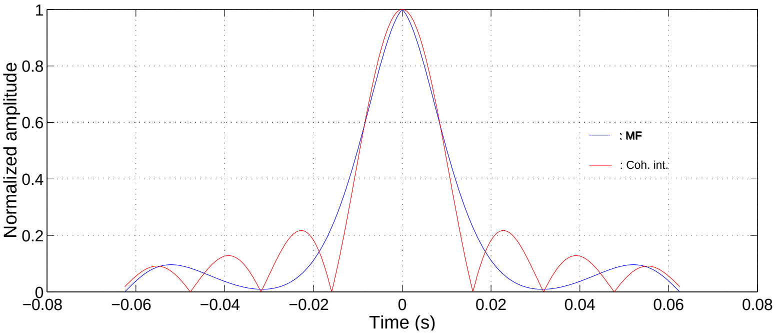

Figure 5.30: Comparison of the LFM auto-correlation envelope (blue line), with the function obtained via coherent integration on the WV of the LFM, for the case α=320 Hz/s and T=0.0625 s.

In view of the above considerations, channel estimation was done by coherent integration of $WV_r(t, f)$, along the path defined by $\hat{f}_i(t)$ in Fig. 5.18. The obtained channel estimate is shown in Fig. 5.31. Applying a threshold value of 0.25, the estimated amplitudes and

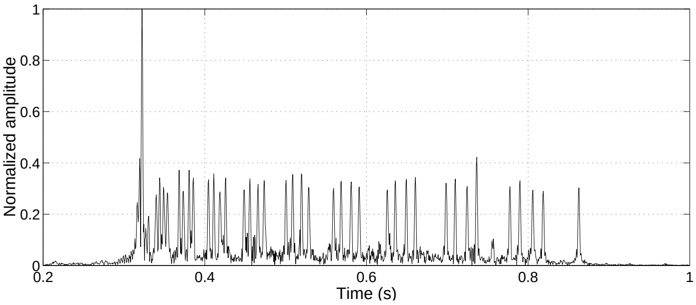

Figure 5.31: Channel estimate, obtained by coherent integration of $WV_r(t, f)$, in synthetic data.

time-delays summarized in Tabs. 5.1 and 5.2, respectively, were obtained. This result is to be compared with the channel estimate obtained by classic matched-filtering, depicted on Fig. 5.28. For the problem at hand, $\Delta f = 500 > 4/\mathcal{T} = 64$, and it can be verified that the obtained resolution is comparable to that of the matched-filter result. The quality of the channel estimate is given by $\rho_{h,a} = 0.9664$ and $\rho_{h,\tau} = 0.9996$, for amplitudes and time-delays, respectively.

Signal-Dependent Distribution Coherent Integration

An interesting alternative to WV coherent integration is to coherently integrate a signal-dependent distribution of $r(t)$, proceeding the same way as with $WV_r(t, f)$. The result of the integration of $RGK_r(t, f)$ was the estimate $\hat{h}_{RGK}(t)$, shown in Fig. 5.32, whose last 37 peaks are mentioned in Tabs. 5.1 and 5.2. The quality of the channel estimate is given

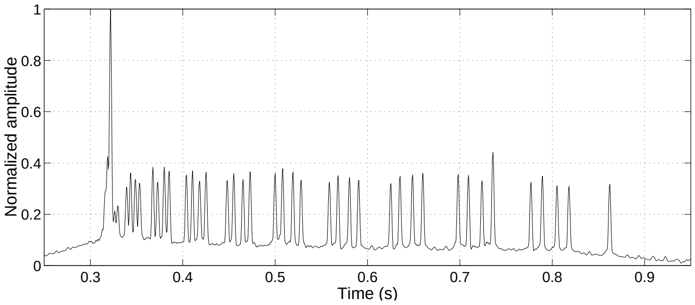

Figure 5.32: Simulation channel IR estimate obtained by $RGK_r(t, f)$'s coherent integration.

by $\rho_a = 0.9760$ and $\rho_\tau = 0.9997$, for the amplitudes and time-delays, respectively. Some interesting issues can readily be seen. First, this estimate is very similar to the previous estimate obtained by $WV_r(t,f)$ integration (cf. Fig. 5.31, and Tabs. 5.1 and 5.2). This is not surprising, since the RGK contains essentially all the important signal terms –the replicas of the emitted signal–, hence conserving the information of these replicas. Second, due to the absence of many negative values in $RGK_r(t,f)$ as opposed to $WV_r(t,f)$, the mean amplitude of $\hat{h}_{RGK}(t)$ is greater than that of $\hat{h}_{WV}(t)$, which constrains a threshold-based peak detection to a greater threshold than in the previous case. A greater threshold may however disregard small peaks, specially at greater times, in $\hat{h}_{RGK}(t)$. Third, the estimate $\hat{h}_{RGK}(t)$ is a smoother function than $\hat{h}_{WV}(t)$, what is possibly explained by the practically complete absence of ITs in $RGK_r(t,f)$. This smoothness may conduce to a less ambiguous extraction of the channel parameters.

5.3.3 Matched-Filtering with the Source Estimate

Alternatively to the procedure of WV coherent integration of the previous subsection, the channel estimate can be obtained by cross-correlation between $\hat{s}(t)$ and $r(t)$, once $\hat{s}(t)$ be available, as schematized in Fig. 5.2. This can give a better channel estimate, if there is some broadening in $WV_s(t,f)$, in which case $f_i(t)$ doesn't contain the whole information of $s(t)$, and hence an integration of $WV_r(t,f)$ along $f_i(t)$ is not sufficient to estimate the channel. This situation occurs when $s(t)$ is composed of both FM and AM components.

Taking the estimate $\hat{s}_{BM}(t)$, the channel estimate obtained by matched-filtering with $\hat{s}_{BM}(t)$ is represented in Fig. 5.33, and the estimated resolved 37 last amplitudes and time-delays are summarized in Tabs. 5.1 and 5.2, respectively. The quality of the channel estimate is given by $\rho_{h,a} = 0.9738$ and $\rho_{h,\tau} = 0.9995$, for the amplitudes and time-delays, respectively.

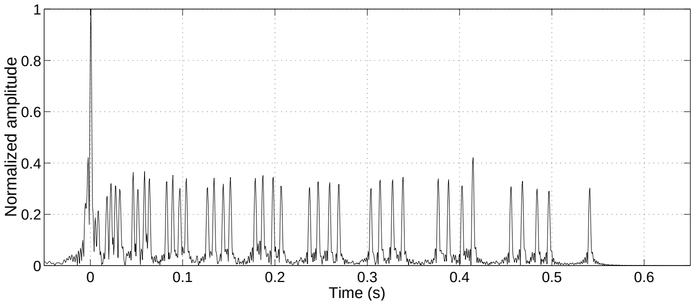

Figure 5.33: Channel estimate obtained by matched-filtering of $r(t)$ with the estimate $\hat{s}_{BM}(t)$.

True	**MF**	**WV coh. int.**	**RGK coh. int.**	**MF with $\hat{s}_{BM}(t)$**
0.2809	0.3275	0.2767	0.3071	0.2703
0.2894	0.3534	0.3415	0.3605	0.3201
0.2977	0.3500	0.3048	0.3365	0.3108
0.3058	0.3179	0.2836	0.3206	0.2978
0.3149	0.3793	0.3722	0.3836	0.3645
0.3167	0.3802	0.2901	0.3254	0.2965
0.3211	0.3745	0.3721	0.3837	0.3669
0.3213	0.3948	0.3419	0.3678	0.3389
0.3278	0.3611	0.3344	0.3534	0.3269
0.3246	0.3343	0.3575	0.3698	0.3527
0.3313	0.3562	0.2871	0.3290	0.3009
0.3230	0.3396	0.3416	0.3634	0.3395
0.3245	0.3384	0.2953	0.3323	0.3039
0.3277	0.3371	0.3393	0.3594	0.3414
0.2988	0.3106	0.3164	0.3352	0.3184
0.3429	0.3843	0.3316	0.3656	0.3441
0.3274	0.3885	0.3325	0.3584	0.3405
0.3315	0.4117	0.3551	0.3778	0.3511
0.3283	0.3650	0.3573	0.3650	0.3453
0.3170	0.3517	0.3044	0.3332	0.3102
0.3211	0.3430	0.3004	0.3261	0.3048
0.3251	0.3579	0.3287	0.3507	0.3273
0.3165	0.3352	0.3261	0.3447	0.3239
0.3073	0.3316	0.3063	0.3327	0.3172
0.3067	0.3223	0.2945	0.3197	0.3007
0.3112	0.3556	0.3312	0.3488	0.3342
0.3167	0.3642	0.3360	0.3535	0.3350
0.3254	0.3815	0.3440	0.3596	0.3447
0.3202	0.3726	0.3210	0.3560	0.3385
0.3219	0.3636	0.3374	0.3525	0.3355
0.3177	0.3244	0.3084	0.3303	0.3115
0.4136	0.4599	0.4220	0.4416	0.4213
0.3095	0.3349	0.3081	0.3258	0.3076
0.3115	0.3482	0.3305	0.3486	0.3292
0.2976	0.3296	0.2943	0.3127	0.2990
0.2985	0.3258	0.2900	0.3094	0.2903
0.2981	0.3242	0.3027	0.3169	0.3026

Table 5.1: Amplitude estimators comparison in noiseless simulated data. The amplitudes respect to the resolved last 37 Dirac functions of the IR.

True	**MF**	**WV coh. int.**	**RGK coh. int.**	**MF with $\hat{s}_{BM}(t)$**
0	0	0	0	0
0.0042	0.0041	0.0041	0.0041	0.0041
0.0095	0.0094	0.0088	0.0094	0.0088
0.0140	0.0141	0.0135	0.0141	0.0135
0.0284	0.0282	0.0282	0.0282	0.0282
0.0336	0.0335	0.0335	0.0335	0.0335
0.0403	0.0406	0.0406	0.0406	0.0406
0.0458	0.0459	0.0459	0.0459	0.0459
0.0646	0.0647	0.0647	0.0647	0.0647
0.0709	0.0712	0.0712	0.0712	0.0712
0.0790	0.0788	0.0788	0.0788	0.0788
0.0857	0.0859	0.0859	0.0859	0.0859
0.1087	0.1088	0.1088	0.1088	0.1088
0.1161	0.1159	0.1159	0.1159	0.1159
0.1256	0.1259	0.1259	0.1259	0.1259
0.1333	0.1335	0.1335	0.1335	0.1335
0.1604	0.1606	0.1606	0.1606	0.1606
0.1689	0.1688	0.1688	0.1688	0.1688
0.1797	0.1800	0.1800	0.1800	0.1800
0.1886	0.1888	0.1888	0.1888	0.1882
0.2195	0.2194	0.2194	0.2194	0.2194
0.2290	0.2288	0.2288	0.2288	0.2288
0.2411	0.2412	0.2412	0.2412	0.2412
0.2510	0.2512	0.2512	0.2512	0.2512
0.2856	0.2859	0.2859	0.2859	0.2859
0.2961	0.2959	0.2959	0.2959	0.2959
0.3095	0.3094	0.3094	0.3094	0.3094
0.3204	0.3206	0.3206	0.3206	0.3206
0.3586	0.3588	0.3588	0.3588	0.3588
0.3701	0.3700	0.3700	0.3700	0.3700
0.3845	0.3847	0.3847	0.3847	0.3847
0.3963	0.3965	0.3965	0.3965	0.3965
0.4377	0.4376	0.4377	0.4377	0.4376
0.4501	0.4500	0.4500	0.4500	0.4500
0.4658	0.4659	0.4659	0.4659	0.4659
0.4785	0.4788	0.4788	0.4788	0.4788
0.5230	0.5229	0.5230	0.5230	0.5229

Table 5.2: Time-delay estimators comparison in noiseless simulated data. The time-delays respect to the resolved last 37 Dirac functions of the IR.

Chapter 6

Performance in Noise

This chapter is devoted to a brief description of deconvolution robustness to noise. When talking about noise, many considerations usually evolve, concerning stationarity, whiteness, etc. In real data, the noise $\xi(t)$ in (2.8) can assume any distribution, and many cases of statistical relations between the implicit random variables are possible. Here, in simulations, analysis will be restricted to white noise (stationary of all orders, as seen in Sec. 4.1).

Let $\xi(t)$ be a stationary complex white random process, present in the received signal following (2.8), uncorrelated with the source signal, such that

$$\mathrm{E}\,\xi(t) = 0; \tag{6.1a}$$

$$\mathrm{E}\left[\xi(t)\xi^*(t-\tau)\right] = \sigma_\xi^2\delta(\tau), \tag{6.1b}$$

where E designates the expectation operator. Since the approach in the present work is based on the analysis and transformation of $WV_r(t,f)$, it is natural to find the expected value of $WV_r(t,f)$, in the presence of noise. Letting $x(t) = s(t) * h(t)$, one finds that

$$\begin{aligned}\mathrm{E}\,WV_r(t,f) &= WV_x(t,f) + \mathrm{E}\,WV_\xi(t,f)\\ &= WV_x(t,f) + \sigma_\xi^2.\end{aligned} \tag{6.2}$$

Two aspects can readily be seen. First, the noise power is the same at each TF location, what is not surprising, since $\xi(t)$ is simultaneously white and stationary. Second, and as a consequence of the above issue, the blind deconvolution method can be performed the same way as in the noiseless data case of Chap. 5, provided that $WV_r(t,f)$ is replaced by its expected value, since the noiseless WV (5.6) will now be added, in average, to a constant. In what concerns $RGK_r(t,f)$, a theoretical analysis is more difficult, since its kernel is dependent on the analyzed signal. However, since the distribution is calculated departing from the AF of the analyzed signal, one can readily verify that

$$\mathrm{E}\ AF_r(\nu,\tau) \quad = \quad AF_x(\nu,\tau) + \sigma_\xi^2 \delta(\nu)\delta(\tau), \tag{6.3}$$

what shows that the AF of the noiseless signal $x(t)$ is added in average to 0, except at the origin of the (ν,τ)-plane, hence not representing a significant change on the calculus of the optimal kernel, relatively to the noiseless case. This can explain the robustness of the RGK in the presence of noise, already mentioned in [4].

The signal-to-noise ratio is here defined as:

$$\mathrm{SNR_{dB}} \quad = \quad 10 \log \frac{\frac{1}{N}\sum_{n=0}^{N-1} s^2(n)}{\sigma_\xi^2}, \tag{6.4}$$

where N is the number of time samples. An illustration of deconvolution behaviour in noisy data is given, which comprises average values corresponding to 100 realizations of the received signal, for SNR = -5 dB. The average function $\overline{RGK}_r(t,f)$, with $\beta = 1$, plotted in Fig. 6.1, is seen to be not much sensitive to noisy data, as discussed in [4]. Maximization of $\overline{RGK}_r(t,f)$ with respect to time produced the IF estimate depicted in Fig. 6.2. The coherent integration of the average WV of the received signal, $\overline{WV}_r(t,f)$ has given the channel estimate of Fig. 6.4. The source estimate obtained by application of the basis method can be seen in Fig. 6.3.

Source estimation's performance in noise is illustrated below. For values of SNR ranging from -20 to 10 dB, source estimation was done by application of the basis method, as

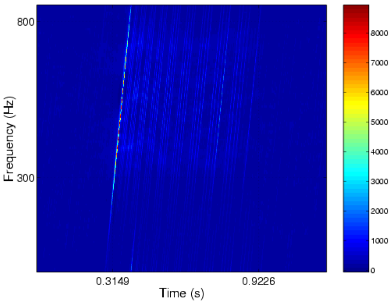

Figure 6.1: Average $RGK_r(t,f)$ (β=1), for SNR=-5 dB and 100 trials.

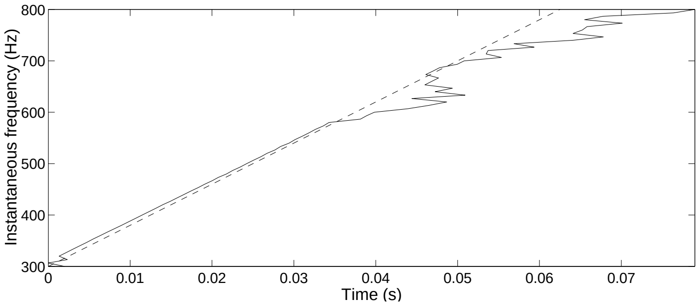

Figure 6.2: IF estimate, in -5 dB noisy data, for 100 trials. The dashed line represents the true IF.

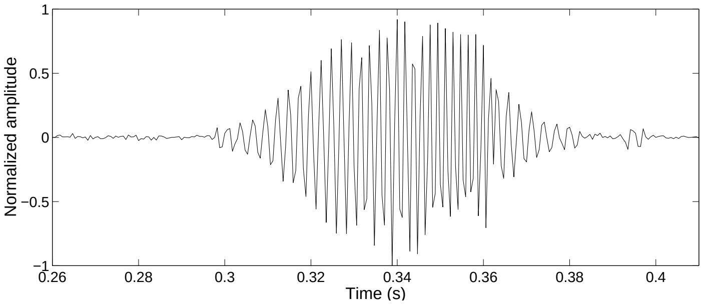

Figure 6.3: Source estimate, obtained via the basis method, with SNR=-5dB, for 100 trials.

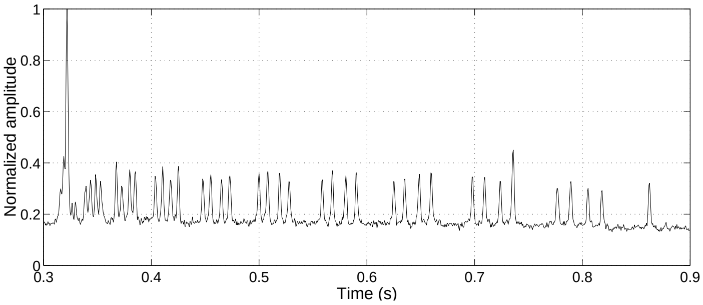

Figure 6.4: Channel estimate, obtained by $\overline{WV}_r(t,f)$ integration, with SNR=-5dB, for 100 trials.

explained in Sec. 5.2.2. The model function was again centered on the strongest arrivals, and the number of basis functions was here also $N_b = 1024$. The performance measure was naturally the correlation coefficient between the true signal $s(t)$ and the estimate $\hat{s}_{BM}(t)$, and is depicted as a function of the SNR, in Fig. 6.5. Each SNR value corresponds to 100 trials.

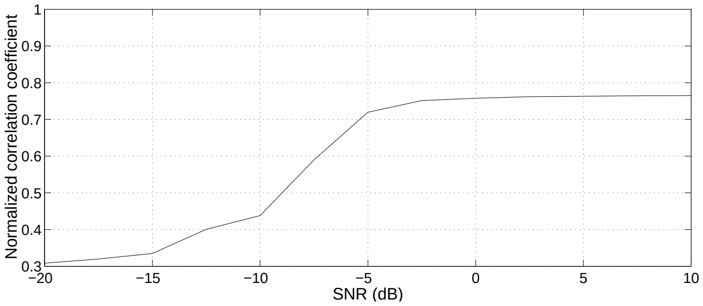

Figure 6.5: Source estimation performance in noise.

Channel estimation's performance in noise was measured by the normalized performance measures (5.42) of the channel estimates obtained by $\overline{WV}_r(t,f)$ coherent integration, for values of SNR ranging from -5 to 10 dB. The same threshold value of 0.25 was used to determine the time locations of the last 37 resolved peaks of the IR estimate, as in Sec. 5.3. For values of SNR below -5 dB, it was not possible to clearly distinguish the 37 resolved peaks, with the specified threshold. The estimated dependence of the performance measures on the SNR is illustrated in Fig. 6.6, again corresponding to 100 trials for each SNR value.

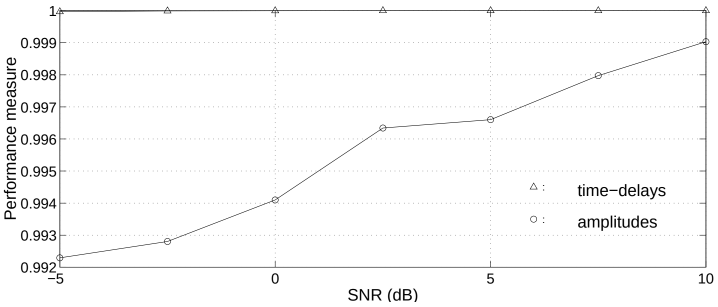

Figure 6.6: Channel estimation performance in noise.

Chapter 7

Experimental Data: the INTIMATE '96 Sea Trial

The INTIMATE '96 sea trial was primarily designed as an acoustic tomography experiment to observe internal tides, and details of the experimental setup have appeared elsewhere[15]. It was conducted in the continental platform near the town of Nazaré, off the west coast of Portugal, during June 1996, and consisted of several phases during which the acoustic source was either spatially stationary or being towed along predetermined paths. The results in this chapter concern ten data snapshots acquired in phase 1 during which the scenario is as shown in Fig. 7.1.

The source signal used in the INTIMATE '96 sea trial was a 300–800 Hz LFM sweep with 2-s duration, repeated every 8 s, and emitted in practice by an electro-acoustic transducer of type Janus-Helmholtz. The transducer presented a main resonance at 650 Hz and a secondary resonance at 350 Hz, as measured on the device, and seen in Fig. 7.2(a). Considering the transducer as a linear filter, an approximation of its IR, for a null spectral phase, is depicted in Fig. 7.2 (b). A model $s(t)$ of the emitted signal is represented in Fig. 7.3. The signal $s(t)$ is well approximated by the product of the 300–800 Hz LFM sweep by the IA $a_i(t)$ [approximately equal to the transducer amplitude spectrum in Fig. 7.2(a), in the LFM's IF range] shown in Fig. 7.4. According to this approximation, the IF $f_i(t)$ of $s(t)$ is

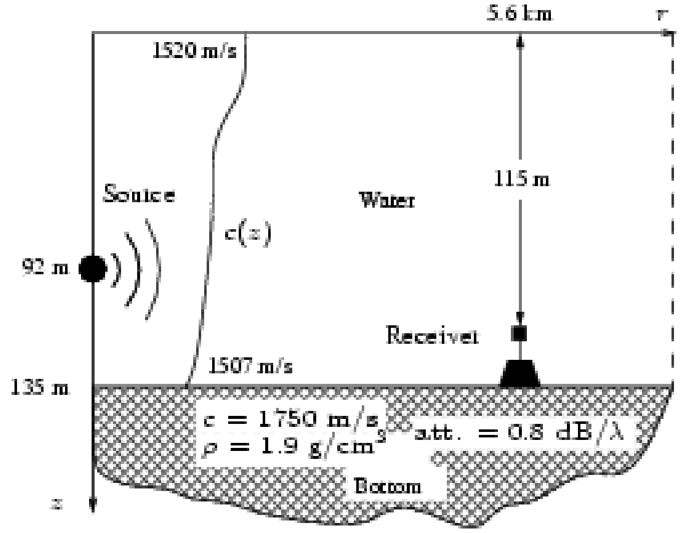
5.6 km
r
1520 m/s
115 m
Source
Water
c(z)
92 m
Receiver
1507 m/s
135 m
c = 1750 m/s
ρ = 1.9 g/cm3
att. = 0.8 dB/λ
Bottom
z

Figure 7.1: INTIMATE '96 real data environment scenario considered in this chapter.

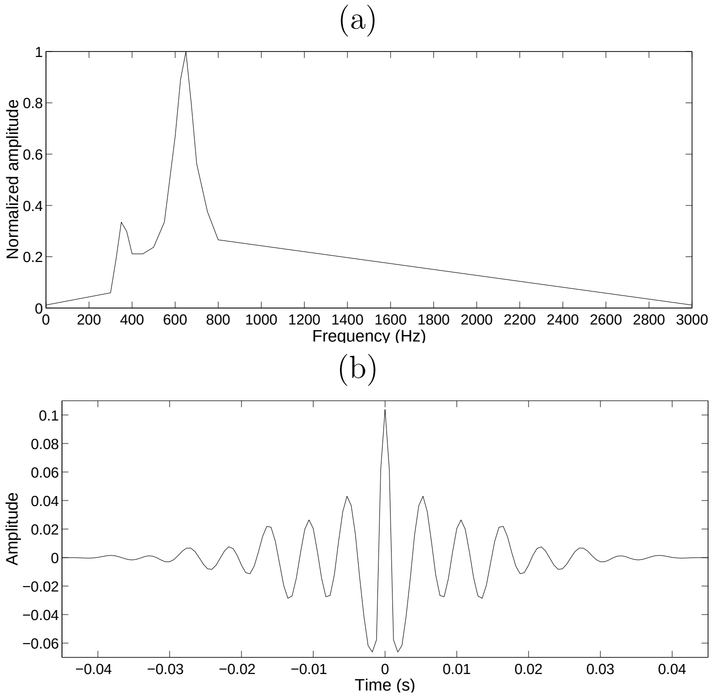

Figure 7.2: Electro-acoustic transducer amplitude spectrum (a) and IR (b), in the INTIMATE '96 sea trial.

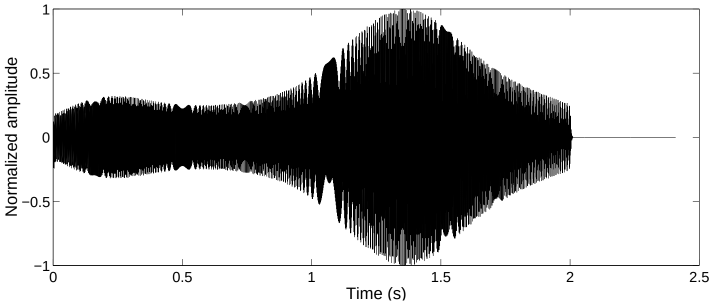

Figure 7.3: Model of the true source signal –real part of $s(t)$– in the INTIMATE '96 sea trial.

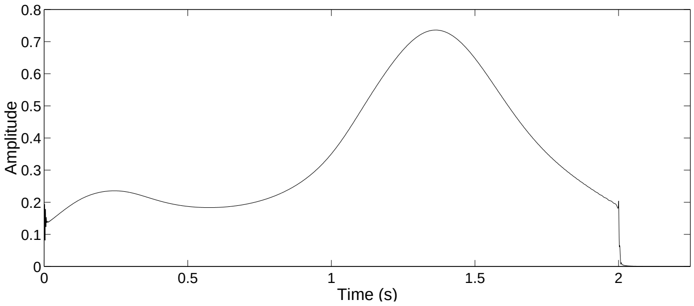

Figure 7.4: IA $a_i(t)$ of the source signal model, in the INTIMATE '96 sea trial.

essentially the same as the IF of the LFM sweep, as seen in the representation of the IF of $s(t)$, determined using (B.6) –Fig. 7.5.

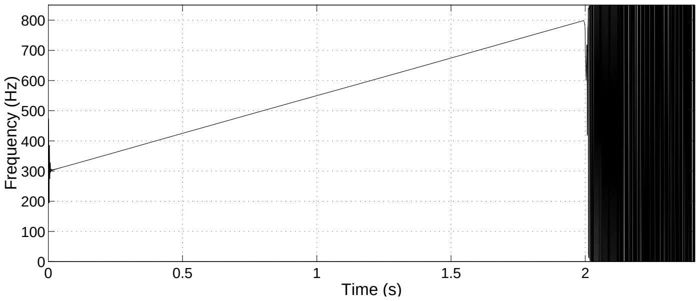

Figure 7.5: IF of $s(t)$, in the INTIMATE '96 sea trial.

One of the snapshots received at 5.5-km range on the 115-m depth hydrophone is shown in Fig. 7.6. The SNR has been estimated to be approximately 10 dB within the frequency band of interest[37].

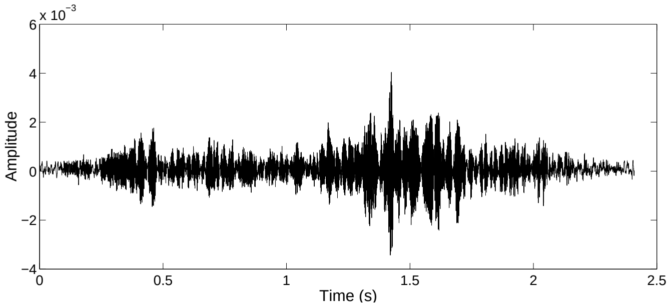

Figure 7.6: One of the received snapshots, at 5.5-km range, on the 115-m depth hydrophone, in the INTIMATE '96 sea trial.

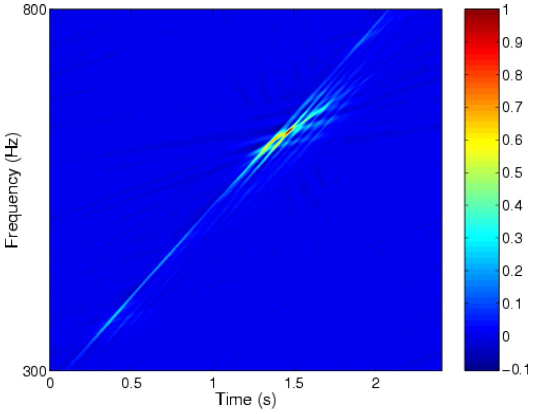

Figure 7.7: Portion of the average distribution $\overline{RGK}_r(t, f)$, in the INTIMATE '96 sea trial.

Instantaneous Frequency Estimation

Taking into account the available ten snapshots, $f_i(t)$ was estimated, by maximization of the average RGK, denoted by $\overline{RGK}_r(t, f)$, obtained by averaging over the snapshots' individual RGK distributions, and represented in Fig. 7.7. The IF estimate $\hat{f}_i(t)$ is shown in Fig. 7.8. By comparison with the true IF $f_i(t)$ in Fig. 7.5, it can be seen that the main difference between $f_i(t)$ and $\hat{f}_i(t)$ occurs around the time interval $[1.2, 1.6]$ s, corresponding to the frequency interval $[600, 700]$ Hz, which contains the main resonance of the transducer spectrum [Fig. 7.2(a)].

Source Signature Estimation

Source signature estimation was done by application of the basis method described in Sec. 5.2.2. Proceeding the same way as in Sec. 5.2.1, in the context of WV inversion, a

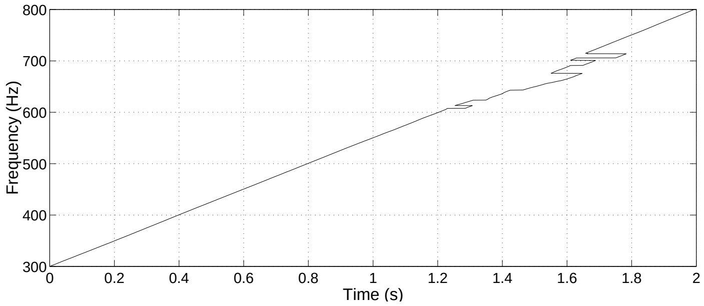

Figure 7.8: IF estimate $\hat{f}_i(t)$ of the source signal, obtained by maximization of $\overline{RGK}_r(t,f)$, in the INTIMATE '96 sea trial.

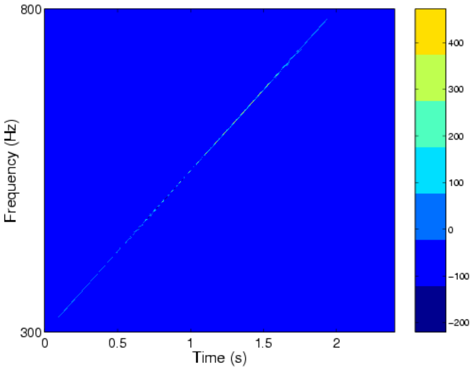

Figure 7.9: WV of $s(t)$.

reference source estimate was obtained by application of the basis method to a model function defined as the multiplication of the WV of $s(t)$ by a function $M(t,f)$ whose width in the direction of f was $\frac{1}{T} = \frac{1}{2\text{ s}} = 0.5$ Hz, centered on $[t, f_i(t)]$. For a number $N_b = 2048$ –half the number of data points– of basis functions, the real part of the obtained reference estimate is depicted in Fig. 7.10.

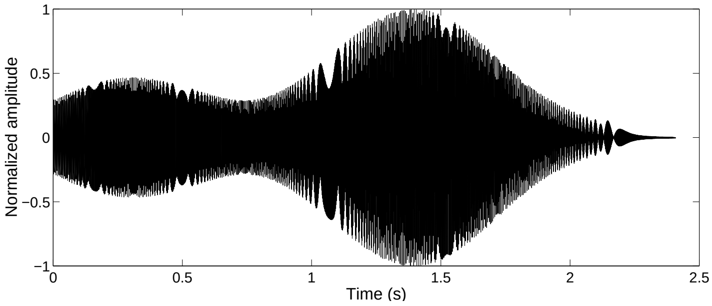

Figure 7.10: Reference source estimate, obtained by application of the basis method, in the INTIMATE '96 sea trial.

In what concerns blind deconvolution, the model function was defined as the multiplication of the average WV, denoted by $\overline{WV}_r(t,f)$ [defined similarly to $\overline{RGK}_r(t,f)$] –Fig. 7.11 –, by a mask $M(t,f)$ centered on $\hat{f}_i(t)$. The real part of the obtained source estimate $\hat{s}_{BM}(t)$ is depicted in Fig. 7.12. The evolution of the correlation coefficient between the real parts of $s(t)$ and $\hat{s}_{BM}(t)$, with φ, is represented in Fig. 7.13. The maximum correlation coefficient is 0.524, occurring for $\varphi = -3.08$ rad, and the maximum of the correlation between the analytic signals is 0.530. The WV of $\hat{s}_{BM}(t)$ is shown in Fig. 7.14. The obtained correlation coefficient is justified by the fact that only the IF of $s(t)$ was reasonably recovered –Fig. 7.15–, as compared to $f_i(t)$ in Fig. 7.5, unlike the AM component –Fig. 7.16, as compared to Fig. 7.4. A possible explanation for the obtained result is the inclusion of many unresolved arrivals in $\tilde{WV}_s(t,f)$, since it is centered on the first arrivals. This is reinforced by the bias of $\hat{f}_i(t)$. Of course, a latter better resolved replica could be chosen, based on the channel

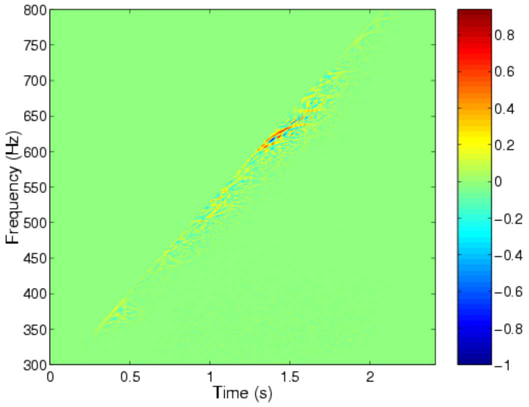

Figure 7.11: Portion of the average distribution $\overline{WV}_r(t,f)$, in the INTIMATE '96 sea trial.

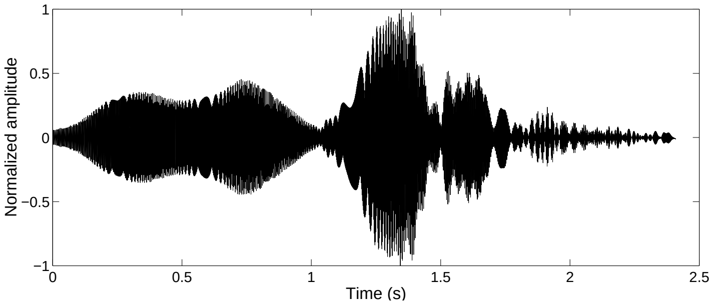

Figure 7.12: Source estimate –real part of $\hat{s}_{BM}(t)$–, in the INTIMATE '96 sea trial, with $\varphi = 0$.

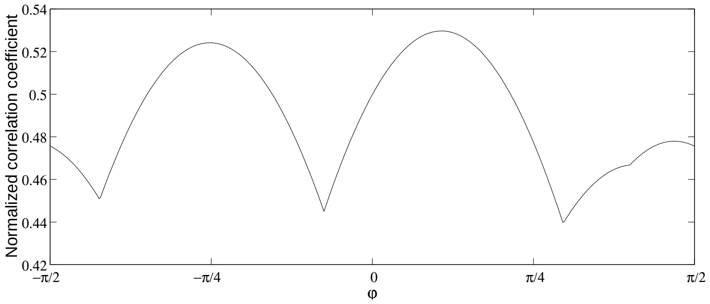

Figure 7.13: Normalized correlation coefficient between the real parts of $s(t)$ and $\hat{s}_{BM}(t)$, for different values of φ.

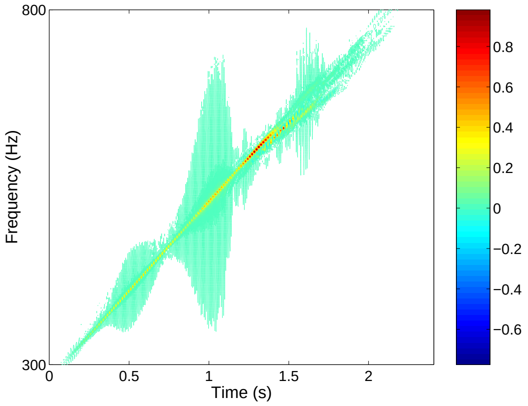

Figure 7.14: WV of $\hat{s}_{BM}(t)$, in the INTIMATE '96 sea trial.

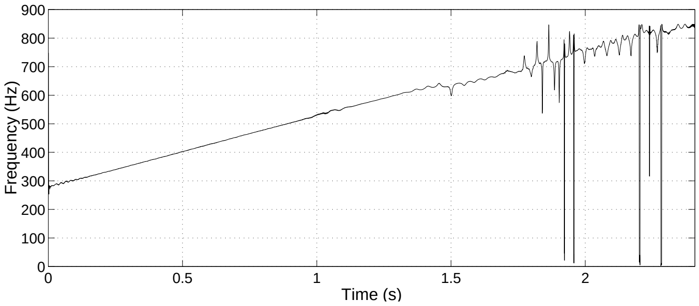

Figure 7.15: Instantaneous frequency of $\hat{s}_{BM}(t)$, in the INTIMATE '96 sea trial.

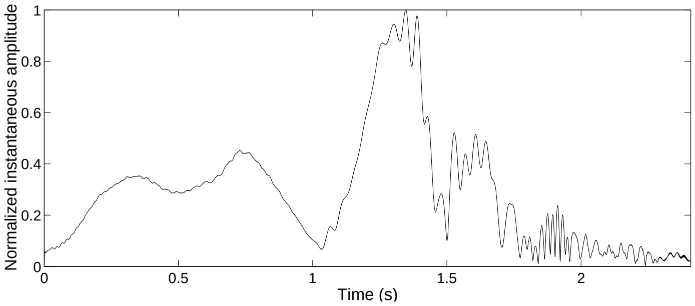

Figure 7.16: IA of $\hat{s}_{BM}(t)$, in the INTIMATE '96 sea trial. This is to be compared with the true IA $a_i(t)$ in Fig. 7.4.

estimate, to construct the model function; however, in noisy real data, this seems difficult, since the arrivals are not so clearly distinguished –cf. Fig. 7.19–, as opposed to the channel estimate in noiseless simulated data –Fig. 5.31.

Channel Estimation

The unavailability of the knowledge of the true IR $h(t)$ led naturally to consider the MF estimate as the reference channel estimate, shown in Fig. 7.17. Also, for the case of coherent integration-based channel estimation, a channel estimate was obtained by coherent integration of $\overline{WV}_r(t,f)$, where $f_i(t)$ in Fig. 7.5 was supposed known, giving rise to the channel estimate $\hat{h}_{IF}(t)$ in Fig. 7.18. The correlation between $\hat{h}_{IF}(t)$ and $\hat{h}_{MF}$ is 0.883. This result proves that the knowledge of the IF of $s(t)$ is not sufficient to obtain a good estimate of the channel IR, with respect to the MF estimate. The obtained channel estimate

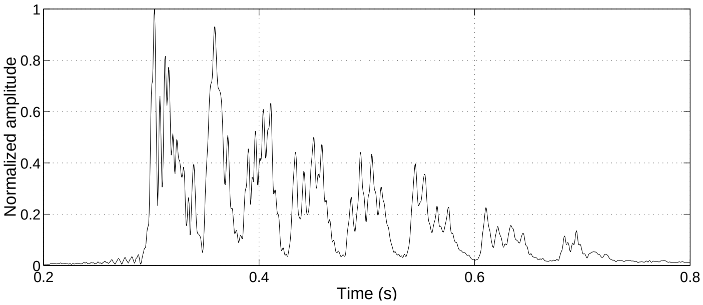

Figure 7.17: Reference channel estimate, defined as the average output of the MF, in the INTIMATE '96 sea trial.

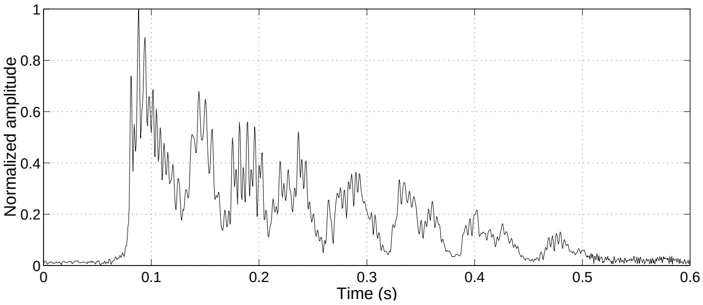

Figure 7.18: Channel estimate $\hat{h}_{IF}(t)$ in the INTIMATE '96 sea trial, by $\overline{WV}_r(t,f)$ coherent integration, assuming the knowledge of the IF of $s(t)$.

$\hat{h}_B(t)$, departing from $\hat{f}_i(t)$ in Fig. 7.8, is shown in Fig. 7.19, with a correlation coefficient of 0.838, with respect to the MF estimate. The channel estimate $\hat{h}_{PMF}(t)$ obtained by the average cross-correlation between $\hat{s}_{BM}(t)$ and $r(t)$, is shown in Fig. 7.20. It can be seen that both $\hat{h}_{MF}(t)$ and $\hat{h}_{PMF}(t)$ contain essentially 8 packets of energy with a time dispersion of approximately 0.45 s. However, there is a difference in the attenuation law, which can be explained by the not high quality of the source IA estimate used in the calculation of $\hat{h}_{PMF}(t)$. The normalized correlation coefficient between $\hat{h}_{MF}(t)$ and $\hat{h}_{PMF}(t)$ is 0.843.

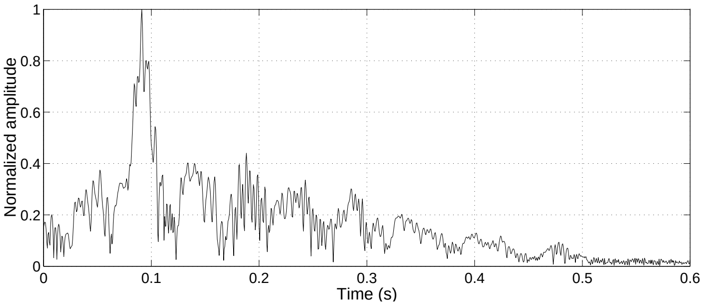

Figure 7.19: Channel estimate in the INTIMATE '96 sea trial, by $\overline{WV}_r(t, f)$ coherent integration, departing from $\hat{f}_i(t)$.

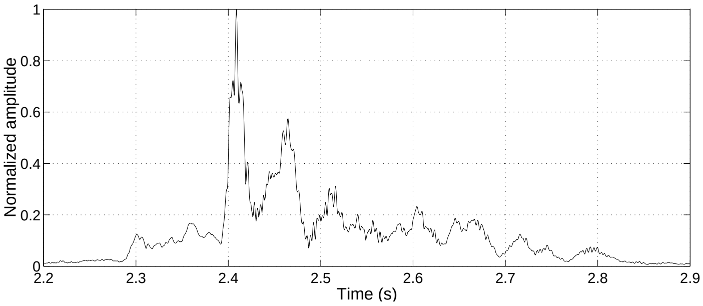

Figure 7.20: Average channel estimate obtained by cross-correlation between $\hat{s}_{BM}(t)$ and $r(t)$, in the INTIMATE '96 sea trial.

Chapter 8

Conclusions and Perspectives

This work has demonstrated the feasibility of single sensor blind deconvolution by TF processing, when the channel behaves as a multiple time delay-attenuation channel, and the source is a deterministic non-stationary signal. The departure point of the blind deconvolution approach was the source signal IF estimation. The fact that the underwater medium impulse response typically contains a set of strong peaks at the beginning allowed the identification of the source signal IF, in the TF plane. This IF estimate was obtained by global maximization with respect to time, of a signal-dependent TFD of the received signal –in this case, the RGK– that allows to distinguish the source resolved replicas. In what concerns source signature estimation, two forms were presented to accomplish this step of blind deconvolution. In the first form, a model function centered around the IF estimate and "extracted" from the WV of the received signal was transformed to the time domain, by inversion of the WV definition equation. In simulated noiseless data, the obtained source signal estimate, when the model function was centered on the first arrivals, had a quality of 0.750. When performing the same reasoning on the last arrival, the quality increased to 0.796, what shows the importance of departing from a well resolved replica of the source signal, in view of its accurate recovery. The non-validity of the model function as a WV led naturally to the application of a synthesis method that, prior to the TF inversion, finds a corresponding valid WV –the basis method, in this work. This constituted the second form of source signature estimation. By means of a signal subspace constraint, this method improved the quality of the first arrivals-based source estimate to a correlation coefficient of 0.856. Channel estimation was accomplished in two ways. The first form was a TF formulation of matched-filtering, where the information contained on the estimated IF of the source was used, to form a domain for integration of the WV of the received signal. The second was simply a matched-filtering with the source estimate obtained previously. The robustness of these correlation-based channel estimation approaches is dependent on the relation between the channel impulses separation and the resolution imposed by the emitted signal band. This fact implied the impossibility of resolving the too close first peaks of the channel IR. In simulated noiseless data, the quality of channel estimates was always superior to 0.966. On simulated noisy data, the blind deconvolution approach proved to be robust, for SNRs greater than -5 dB . Analysis of real data from the INTIMATE '96 experiment has revealed some important issues: although the IF of the source signal was reasonably estimated, there remains a difficulty in obtaining a good estimate of the IA. This can be explained by the use of the non-resolved arrivals packet for source inversion. In what concerns channel estimation, the use of the source estimate produced a slightly better channel estimate, comparatively to the MF estimate. However, if the noise is not white, it is likely that the channel estimate obtained by TF coherent integration can even be a better channel estimate than the MF estimate, when a good IF estimate is available. This idea is motivated by the noise rejection caused by integration exclusively along the (estimated) IF of the source signal. Also, in the presence of more than one data snapshot at reception, it is likely that the proposed channel estimation approach could reduce the minimum number of received signal realizations, necessary to obtain a meaningful channel estimate.

It was verified that the information contained in the TFDs of the single-channel received signal compensates for the lack of complementarity and information redundancy about the emitted waveform, present in multi-channel systems. The blind deconvolution problem has been studied with nonlinear signal analysis, what is not surprising, comparatively to the (not equivalent) nonlinearity of conventional blind deconvolution algorithms.

There are many open problems, one of which is the positioning of the model function, for source signature estimation. One alternative to the use of a single model function would be to take into account the redundancy of source signal information in the received arrivals, defining one model function for each estimated time-delay of the IR, and then combining in some manner the several source estimates obtained from all the model functions, to obtain the final source estimate. The channel estimate resolution could be improved by means of integration of a high-resolution TFD, like the MUSIC-based TFD recently proposed in [52]. Due to the denoising characteristics of the RGK, one alternative to accomplish blind deconvolution of a broad class of signals could be to increase the degrees of freedom, parameterizing the RGK of the received signal as a distribution containing M replicas of the source signal, and parameterizing the structure of the emitted signal as having an IA that is the sum of Gaussian functions, and whose instantaneous phase is a polynomial of degree 3. The procedure would be to estimate all these parameters, for example by the use of random search, as is the case in genetic algorithms. This parameterization of the problem could amount to the estimation of about 100 parameters. A more complicated propagation scenario arises in the presence of low-frequency sources, in which case the physical phenomenon of frequency dispersion is significant and only accounted for by normal mode-based propagation modelling. In this case, frequency dispersion[36] could be first compensated, before replica identification. This procedure would probably require the knowledge of the source position, to define the inherent eigenfunctions in propagation modal modelling.

Bibliography

[1] Abutaleb, A., “Time Delay Estimation and Optimal Control Concepts”, Sig. Proc. **12**, pp. 291–307 (1987).

[2] Andrieux, J.C.; Felix, M.R.; Mourgues, G.; Bertrand, P.; Izrar, B. and Nguyen, V.T., “Optimum Smoothing of the Wigner-Ville Distribution”, IEEE Trans. Acoust. Speech Sig. Proc. **35**, No. 6, pp. 764–9 (1987).

[3] Baraniuk, R.G. and Jones, D.L., “A Radially Gaussian, Signal Dependent Time-Frequency Representation”, IEEE Int. Conf. Acoust., Speech and Sig. Proc. **May**, pp. 3181–4 (1991).

[4] Baraniuk, R.G. and Jones, D.L., “Signal-Dependent Time-Frequency Analysis Using a Radially Gaussian Kernel”, Sig. Proc. **32**, No. 3, pp. 263–84 (1993).

[5] Boudreaux-Bartels, G.F. and Parks, T.W., “Time-Varying Filtering and Signal Estimation Using Wigner Distribution Synthesis Techniques”, IEEE Trans. Acoust. Speech, Sig. Proc. **ASSP-34**, pp. 442–51 (1986).

[6] Broadhead, M.K., “Broadband Source Signature Extraction from Underwater Acoustics Data with Sparse Environmental Information”, J. Acoust. Soc. Am. **97** (2), pp. 1322–5 (1991).

[7] Cadzow, J.A., “Blind Deconvolution via Cumulant Extrema”, IEEE Sig. Proc. Mag. **May**, pp. 24–42 (1996).

[8] Candy, J.V. and Zicker, J.E., “Deconvolution of Noisy Transient Signals: a Kalman Filtering Application”, 21st IEEE Conference on Decision and Control **December** (1982).

[9] Carter, G., “Time Delay Estimation for Passive Sonar Signal Processing”, IEEE Trans. Acoust. Speech Sig. Proc. **ASSP-29**, pp. 463–70 (1981).

[10] Choi, H.-I. and Williams, “Improved Time-Frequency Representation of Multicomponent Signal using Exponential kernels”, IEEE Trans. Acoust. Speech Sig. Proc. **37**, No. 6, pp. 862–71 (1989).

[11] Claasen, T.A.C.M. and Mecklenbräuker, W.F.G., “The Wigner Distribution – a Tool for Time-Frequency Signal Analysis” – Parts I–III, Philips J. Res. **35**, pp. 217–50, 276–300, 372–89 (1980).

[12] Cohen, L. and Posch, T.E., “Generalized Ambiguity Functions”, IEEE Int. Conf. Acoust., Speech and Sig. Proc., pp. 27.6.1–4 (1985).

[13] Cohen, L., “Time-Frequency Distribution and Instantaneous Frequency”, *Adv. Sig. Proc. Alg., Arch. and Impl. II*, Proc. SPIE Conf. **1566** (1991).

[14] Cohen, L., *Time-Frequency Analysis* (Prentice Hall PTR, Englewood Cliffs, 1995).

[15] Démoulin, X.; Stéphan, Y.; Jesus, S.; Coelho, E. and Porter, M.B., “INTIMATE96: a Shallow Water Tomography Experiment Devoted to the Study of Internal Tides”, in Proc. SWAC’97, Beijing, China, Apr. 1997.

[16] Ding, Z. and Li, Y., “Channel Identification Based on Second Order Cyclic Statistics”, Proceedings of the Twenty-Sixth Asilomar Conference on Signals, Systems and Computers, Pacific Grove, CA (1992).

[17] Ehrenberg, J.E., Ewart, T.E. and Morris, R.D., “Signal Processing Techniques for Resolving Individual Pulses in a Multipath Signal”, J. Acoust. Soc. Am. **63**, 1861–5 (1978).

[18] Finette, S.; Mignerey, P.C.; Smith, J.F.; III and Richmond, C.D., “Broadband Source Signature Extraction Using a Vertical Array”, J. Acoust. Soc. Am. **94** (1), 309–18 (1993).

[19] Flandrin, P., “Some Features of Time-Frequency Representations of Multi-Component Signals”, IEEE Int. Conf. Acoust., Speech and Sig. Proc., pp. 41.B.4.1–4 (1984).

[20] Flandrin, P., “A Time-Frequency Formulation of Optimum Detection”, IEEE Trans. Acoust. Speech, Sig. Proc. **36**, No. 9 (1988).

[21] Gabor, D., “Theory of Communication”, Journal of the IEE **93**, pp. 429–57 (1946).

[22] Gardner, W.A., “A New Method of Channel Identification”, IEEE Transactions on Communications **39**, pp. 813–7 (1991).

[23] Haykin, S., “Blind Equalization Formulated as a Self-Organized Learning Process”, Proceedings of the Twenty-Sixth Asilomar Conference on Signals, Systems and Computers, Pacific Grove, CA (1992).

[24] Haykin, S. (ed.), *Blind Deconvolution* (PTR Prentice Hall, Englewood Cliffs, 1994).

[25] Hearon, S. and Amin, M., “Statistical Trade Offs in Modern Time-Frequency Kernel Design”, *Asilomar Conf. on Sig., Syst., Comp.*, pp. 359–63, Pacific Grove, CA **Nov.** (1991).

[26] Hlawatsch, F., “Duality and Classification of Bilinear Time-Frequency Signal Representations”, IEEE Trans. Sig. Proc. **39**, No. 7, pp. 1564–74 (1991).

[27] Hlawatsch, F. and Boudreaux-Bartels, G.F., “Linear and Quadratic Time-Frequency Signal Representations”, IEEE SP Magazine **April**, pp. 21–67 (1992).

[28] Hlawatsch, F. and Flandrin, P., *The Interference Structure of the Wigner Distribution and Related Time-Frequency Signal Representations*, *in* The Wigner Distribution Theory and Applications in Signal Processing (W. Mecklenbräuker, ed., North Holland Elsevier Science Publishers, 1992).

[29] Hlawatsch, F. and Krattenthaler, W., “Bilinear Signal Synthesis”, IEEE Trans. Sig. Proc. **Feb.**, pp. 352–63 (1992).

[30] IEEE Trans. Acoust. Speech, Sig. Proc., Special Issue on Time Delay Estimation, June 1981.

[31] Ilow, J.; Hatzinakos, D. and Venetsanapoulos, A.N., “Blind Deconvolution Based on Cumulant Fitting and Simulated Annealing Optimization”, Proceedings of the Twenty-Sixth Asilomar Conference on Signals, Systems and Computers, Pacific Grove, CA (1992).

[32] Jackson, D.R. and Dowling, D.R., “Phase Conjugation in Underwater Acoustics”, J. Acoust. Soc. Am. **89** (1), pp. 171–81 (1991).

[33] Jain, A.K., *Fundamentals of Digital Image Processing* (Prentice-Hall, 1989).

[34] Janssen, A.J.E.M., *Application of the Wigner Distribution to Harmonic Analysis of Generalised Stochastic Processes*, PhD dissertation (University of Eindhoven, Amsterdam, 1979).

[35] Janssen, A.J.E.M., “On the Locus and Spread of Pseudo-Density Functions in the Time-Frequency Plane”, Philips J. Res. **37**, pp. 79–110 (1982).

[36] Jensen, F.B.; Kuperman, W.A.; Porter, M.B. and Schmidt, H., *Computational Ocean Acoustics* (American Institute of Physics, 1993).

[37] Jesus, S.M.; Porter, M.B.; Stéphan, Y.; Démoulin, X.; Rodríguez, O.C. and Coelho, E.M.M.F., “Single Hydrophone Source Localization”, Journal of Oceanic Engineering **25**, No. 3, pp. 337–46 (2000).

[38] Jones, D.L. and Parks, T.W., “A Resolution Comparison of Several Time-Frequency Representations”, IEEE Trans. Sig. Proc. **40**, No. 2 (1992).

[39] Kumar, B.V.K.V. and Carroll, C.W., “Performance of Wigner Distribution Function Based Detection Methods”, Opt. Eng. **23**, No. 6, pp. 732–7 (1984).

[40] Kumar, B.V.K.V.; Neuman, C.P. and Devos, K.J., “Discrete Wigner Synthesis”, Sig. Proc. **II**, pp. 277–304 (1986).

[41] Kirsteins, I.P., “High Resolution Time Delay Estimation”, in *IEEE Proceedings ICASSP 87* (IEEE, New York, 1987), 451–4.

[42] Lagendijk, R.; Biemond, J. and Boekee, D., "Regularized Iterative Image Restoration With Ringing Reduction", IEEE Trans. Acoust. Speech Sig. Proc. **36**, pp. 1874–88 (1988).

[43] Ma, N.; Vray, D.; Delachartre, P. and Gimenez, G., "Time-Frequency Representation of Multicomponent Chirp Signals", Sig. Proc. **56**, pp. 149–55 (1997).

[44] Maroni, C.-S., *Modulation Linéaire de Fréquence et Compression d'Impulsion. Application au Sondeur de Sédiments.* Rapport de Recherche n^o EIA 974, (ENSIETA, Brest, 1997).

[45] Michalopoulou, Z.-H.; Ma, X.; Picarelli, M. and Ghosh-Dastidar, U., "Fast Matching Methods for Inversion With Underwater Sound", Proceedings of Oceans 2000, Providence (2000).

[46] Mignerey, P. and Finette, S., "Multichannel Deconvolution of an Acoustic Transient in an Oceanic Waveguide", J. Acoust. Soc. Am. **92** (1), 351–64 (1992).

[47] Moyal, J.E., "Quantum Mechanics as a Statistical Theory", Proc. Cambridge Phil. Soc. **45**, pp. 99–124 (1949).

[48] Munk, W. and Wunsch, C., "Ocean Acoustic Tomography: a Scheme for Large Scale Monitoring", Deep-Sea Res. **26**, pp. 123–61 (1979).

[49] Munk, W.; Worcester, P. and Wunsch, C., *Ocean Acoustic Tomography.* (Cambridge University Press, Cambridge, 1995).

[50] Nandi, A., "Blind Identification of FIR Systems Using Third Order Cumulants", Sig. Proc. **39**, pp. 131–47 (1994).

[51] Neelamani, R.; Choi, H. and Baraniuk, R.G., “Wavelet-Based Deconvolution for Ill-Conditioned Systems”, Proceedings of the IEEE Int. Conf. Acoust., Speech and Sig. Proc., Phoenix, AZ, **March** (1999).

[52] Nickel, R. and Williams, W., “High Resolution Frequency Tracking Via Non-Negative Time-Frequency Distributions” (2000).

[53] Oehlmann, H. and Brie, D., “Distribution de Wigner-Ville Locale pour la Réduction des Interférences”, Seizième Colloque Gretsi, 15–9 Septembre, Grenoble, pp. 667–70 (1997).

[54] Page, C.H., “Instantaneous Power Spectra”, J. Appl. Phys. **23**, pp. 103–6 (1952).

[55] Porter, M., *The Kraken Normal Mode Program* (Saclant Undersea Research Centre, San Bartolomeo, 1991).

[56] Porter, M.B.; Jesus, S.M.; Stéphan, Y.; Coelho, E. and Démoulin, X., “Single-Phone Source Tracking in a Variable Environment”, Proceedings of the Fourth European Conference on Underwater Acoustics, pp. 575–80 (1998).

[57] Proakis, J.G.; Manolakis, D.G., *Digital Signal Processing – Principles, Algorithms, and Applications*, 3rd ed. (Prentice Hall, New Jersey, 1996).

[58] Quinquis, A., *Représentations Temps-Fréquence*, 1st ed. (Brest, 1995).

[59] Reid, D.C.; Zoubir, A.M. and Boashash, B., “Aircraft Flight Parameter Estimation based on Passive Acoustic Techniques using the Polynomial Wigner-Ville Distribution”, J. Acoust. Soc. Am. **102** (1), pp. 207–23 (1997).

[60] Rodríguez, O.C. and Jesus, S.M., “Physical Limitations of Travel-Time-Based Shallow Water Tomography”, J. Acoust. Soc. Am. **108** (6), pp. 2816–22 (2000).

[61] Roguet, W.; Martin, N. and Chehikian, A., "Tracking of Frequency in a Time-Frequency Representation", Proc. IEEE Sig. Proc. Intl. Symposium on Time-Frequency and Time-Scale Analysis, Paris, France (1996).

[62] Sacha, J.R. and Johnson, B.L., "A Constrained Iterative Multiple Operator Deconvolution Technique", J. Acoust. Soc. Am. **96** (1), pp. 181–5 (1994).

[63] Saleh, B.E.A. and Subotic, N.S., "Time-Variant Filtering of Signals in the Mixed Time-Frequency Domain", IEEE Trans. Acoust., Speech, Sig. Proc. **33**, pp. 1479–85 (1985).

[64] Smith, J.F.; III and Finette, S., "Simulated Annealing as a Method of Deconvolution for Acoustic Transients Measured on a Vertical Array", J. Acoust. Soc. Am. **94** (4), pp. 2315–25 (1993).

[65] Tolstoy, I. and Clay, C.S., *Ocean Acoustics – Theory and Experiment in Underwater Sound*, 2nd ed. (American Institute of Physics, New York, 1987).

[66] Tong, L.; Xu, G. and Kailath, T., "A New Approach to Blind Identification and Equalization of Multipath Channels", Proceedings of the Twenty-Fifth Asilomar Conference on Signals, Systems and Computers, Pacific Grove, CA (1991).

[67] Topkar, V.; Mullick, S. and Titlebaum, "Invariant Transformation of the $t-\omega$ Plane With Respect to Wigner Distribution", Sig. Proc. **22**, pp. 127–137 (1991).

[68] Vaccaro, R.J., Ramalingam and Tufts, D.W., "Least-Squares Time-Delay Estimation for Transient Signals in a Multipath Environment", J. Acoust. Soc. Am. **92** (1), pp. 210–8 (1991).

[69] Ville, J., "Théorie et Applications de la Notion de Signal Analytique", *Câbles et Transmissions* **2A**, pp. 61–74 (1948), translated into English by I. Selin, (RAND Corp. Report T–92, Santa Monica, CA, 1958).

[70] Walden, A.T., "Non-Gaussian Reflectivity, Entropy, and Deconvolution", Geophysics **50**, pp. 2862–88 (1985).

[71] Wang, C. and Cadzow, J., "Signal Enhancement of Wigner-Ville Time-Frequency Signals", IEEE Proceedings – Southeastcon (1990).

[72] Wigner, E.P., "On the Quantum Correction for Thermo-Dynamic Equilibrium", Physics Review **40**, pp. 749–59 (1932).

[73] Wigner, E.P., "Quantum-Mechanical Distribution Functions Revisited", in *Perspectives in Quantum Theory*, Youngman, W. and Merwe, A. van, Eds. New York: Dover (1971).

[74] Yu, K.B. and Cheng, S., "Signal Synthesis from Pseudo-Wigner Distribution and Applications", IEEE Trans. Acoustic, Speech, and Sig. Proc. **ASSP–35**, No. 9, pp. 1289–302 (1987).

[75] Zhao, Y.; Atlas, L.E. and Marks, R.J., "The Use of Cone-Shape Kernels for Generalized Time-Frequency Representation of Nonstationary Signals", IEEE Trans. Acoust. Speech Sig. Proc. **38, July**, pp. 1084–91 (1990).

Appendix A

The Hilbert Transform

Consider the complex signal $x(t)$ and the quadrature filter $H_Q(f)$ whose transfer function is[44]

$$H_Q(f) \quad = \quad -\mathrm{j}\ \mathrm{sgn}(f). \tag{A.1}$$

The impulse response of $H_Q(f)$ is given by

$$h_Q(t) \quad = \quad \mathrm{pp}\left(\frac{1}{\pi t}\right), \tag{A.2}$$

where pp designates principle part. The Hilbert transform of $x(t)$ is defined by the convolution of $x(t)$ with $h_Q(t)$:

$$\mathrm{H}\left[x(t)\right] \quad \triangleq \quad x(t) * h_Q(t) = \frac{1}{\pi}\int_{-\infty}^{\infty} \frac{x(u)}{t-u}\ \mathrm{d}u, \tag{A.3}$$

where the improper integral is to be understood as an abbreviation of its Cauchy's principal value.

Appendix B

The Analytic Signal

Very advantageous in calculus simplification and mathematical formulation of intuitive notions like a signal's envelope or instantaneous frequency[44], the analytic signal, introduced by Gabor[21], is defined here. Consider a real signal $x(t)$. Since its Fourier transform is of Hermitian symmetry, all the signal information is contained in positive frequencies. The signal $x_a(t)$ obtained by negative frequencies suppression (analytic filtering) is the analytic signal associated to $x(t)$:

$$x_a(t) \quad \overset{\triangle}{=} \quad x(t) + \mathrm{j}\ \mathrm{H}[x(t)], \tag{B.1}$$

where $\mathrm{H}[x(t)]$ is the Hilbert transform of $x(t)$. It's easy to verify that, in the frequency domain:

$$X_a(f) \quad = \mathrm{FT}\left[x_a(t)\right] = X(f) + \mathrm{j}\ \mathrm{FT}\left\{\mathrm{H}[x(t)]\right\} = \quad X(f)\left[1 + \mathrm{sgn}(f)\right], \tag{B.2}$$

where FT designates the Fourier transform operator. Thus:

$$X_a(f) \quad = \quad \begin{cases} 2X(f), & f \geq 0 \\ 0, & f < 0 \end{cases}, \tag{B.3}$$

or, equivalently:

$$X_a(f) \quad = \quad 2u(f)X(f), \tag{B.4}$$

with $u(f)$ the frequency-dependent step function.

The key-point is that $x_a(t)$ can be expressed in the polar form

$$x_a(t) = a_i(t)e^{\mathrm{j}\varphi_i(t)}, \tag{B.5}$$

with the meaning of instantaneous amplitude (IA) (also known as *envelope*) and phase for $a_i(t)$ and $\varphi_i(t)$, respectively. The *instantaneous frequency* is obtained by simple differentiation:

$$f_i(t) \triangleq \frac{1}{2\pi}\frac{\mathrm{d}\varphi_i(t)}{\mathrm{d}t}. \tag{B.6}$$

All the instantaneous quantities refer to $x_a(t)$ and the original signal $x(t)$ as well. The signal $x_a(t)$ can thus be decomposed in two components: an amplitude modulation component $a_i(t)$ and a phase modulation component $\varphi_i(t)$ [implicitly, frequency modulation component $f_i(t)$].

Appendix C

Auto-Correlation Function of an LFM Signal

Due to the importance of matched-filtering in channel estimation, this appendix derives the expression of the auto-correlation function of the particular case of an LFM signal. Let $v(t)$ be a real LFM signal null outside the interval $[0, \mathcal{T}]$, with modulation rate α and instantaneous frequency f_0 at $t = 0$. Its temporal auto-correlation function $\Gamma_{v,t}(\tau)$ can be defined by

$$\Gamma_s(\tau) \quad = \quad \int_{-\infty}^{\infty} v(t)v(t-\tau)\mathrm{d}t. \tag{C.1}$$

Let $v_2(t) = v(-t)$ and let $z_v(t)$ and $z_{v_2}(t)$ be the analytic signals associated to $v(t)$ and $v_2(t)$, respectively. Due to the filtering property of analytic signals[44]:

$$\Gamma_{v,t}(\tau) \quad = v(\tau) * v_2(\tau) = \quad \frac{1}{2}\mathrm{Re}\left[z_v(t) * z_{v_2}(t)\right]. \tag{C.2}$$

It is readily verified that

$$z_v(t) = \mathrm{e}^{\mathrm{j}2\pi\left(\frac{\alpha}{2}t^2 + f_0 t\right)}. \tag{C.3}$$

Inserting $z_v(t)$ into (C.2):

$$\Gamma_{v,t}(\tau) \quad = \quad \frac{1}{2}(\mathcal{T} - |\tau|)\cos\pi(2f_0 + \alpha\mathcal{T})|\tau|\mathrm{sinc}\ \pi\alpha|\tau|(\mathcal{T} - |\tau|). \tag{C.4}$$

In many applications, one is interested only on the IA of $\Gamma_{v,t}(\tau)$, given by

$$a_\Gamma(\tau) = \begin{cases} \frac{1}{2}\left|(\mathcal{T} - |\tau|)\mathrm{sinc}\ \pi\alpha|\tau|(\mathcal{T} - |\tau|)\right|, & \tau \in [-\mathcal{T}, \mathcal{T}] \\ 0, & \tau \notin [-\mathcal{T}, \mathcal{T}] \end{cases} . \tag{C.5}$$

For $\tau \geq 0$, the first zero of $a_\Gamma(\tau)$ is given by

$$z_1 = \frac{\mathcal{T} - \sqrt{\mathcal{T}^2 - 4/\alpha}}{2}. \tag{C.6}$$

The quantity $2z_1$ gives an idea of the resolution of a matched-filter for multiple time-delay attenuation channel identification, when it is driven by an LFM input.